Cape Peninsula
University of Technology

MODELLING AND DEVELOPMENT OF FUEL CELL OFF GRID POWER CONVERTER SYSTEM

by

ATANDA KAMORU RAJI

Thesis submitted in partial fulfilment of the requirements for the degree

Magister Technologiae: Electrical Engineering

in the Faculty of Engineering

at the Cape Peninsula University of Technology

Supervisor: Professor MTE Khan

Bellville
DECEMBER 2008

DECLARATION

I, Atanda Kamoru Raji, declare that the contents of this thesis represent my own unaided work, and that the thesis has not previously been submitted for academic examination towards any qualification. Furthermore, it represents my own opinions and not necessarily those of the Cape Peninsula University of Technology.

_____ _____

Signed **Date**

ABSTRACT

Fuel cell technology is an emerging technology that provides a highly efficient, quiet operation, reliable, and environmentally friendly energy conversion system for stationary, automobile (vehicle), and portable applications. An electrochemical process combines hydrogen fuel and oxygen from air to produce water, and in the process it produces electricity and heat. Fuel cell stationary applications which include residential, office buildings, hospitals, hotels, airports and others have received greater attention for their ability to utilize the heat generated for space and water heating. This combined heat and power (CHP) process increases the energy conversion efficiency greatly which in turn save cost of energy usage.

Different power converter topologies for fuel cell systems residential applications are presented in this thesis for efficiency, cost, component count, input ripple current minimization technique, reliability for comparison analysis. The commercial feasibility of fuel cells rests on the cost of the fuel cell system and operating efficiency and fuel cost.

The proposed power converter topology consists of two front end DC-DC converters. The first front-end DC-Dc converter is tightly controlled while the second is a full bridge four interleaved DC-DC converters. Advantages of the proposed topology are reduced input ripple current, high efficiency, low maintenance cost, smaller size, modularity, redundancy. Design overview as well as simulation results are presented.

Fuel cell simulation test results, including transient response are displayed and analyzed. The concept of interleaving of multiple units of the Dc-Dc converter is proposed. Interleaving enables paralleling multiple units of the converters to achieve a high combined power. This results in using semiconductor power devices of lower current rating, lowering sizes of input and output capacitors and reducing the output ripples. Simulations results are presented that verify the concept of interleaving. Preliminary work to implement interleaving is presented, and future work is recommended.

ACKNOWLEDGEMENTS

I have been very fortunate to have had the guidance and support of Professor MTE Kahn throughout my research. On numerous occasions, it was his experience, suggestions and encouragement that made my progress possible. For this, I would like to express my gratitude to him. His dedication did not stop there; I soon realized that his office door was always open if I had any question, and he did not mind getting his hands dirty in the laboratory if the office answer would not suffice.

Most importantly I would like to thank my family for their continue support throughout the years. Much of my success has been because of their love and encouragement. Last, but certainly not least, I own a tremendous amount of gratitude to my friend, Adewole Adekoya Bolarinwa (Prince) for being there for my entire family during my course of study that separated me away from my dear family. Thank you very much Prince you are indeed a friend in need.

The financial assistance of the National Research Foundation towards this research is acknowledged. Opinions expressed in this thesis and the conclusions arrived at, are those of the author, and not necessarily to be attributed to the National Research Foundation.

DEDICATION

To my immediate family, Adeola Khadijat Raji, Taiye Morufudeen Raji, Kehinde Morufatu Raji and Idowu Rahman Raji pillared by Folasade Latifat Raji

TABLE OF CONTENTS

CHAPTER FOUR: MODELLING AND CONTROL

CHAPTER FIVE: INTERLEAVING AND ANALYSIS

CHAPTER SIX: SYSTEM DESIGN, COMPONENTS SELECTION, AND SIMULATIONS

APPENDICES

List of Figures

List of Tables

CHAPTER 1

INTRODUCTION

1.1 Motivation

The electrical energy required for operating electronics appliances, lights, and heating and cooling systems of our homes consume approximately three times the energy at the power plant to generate that electrical energy. That equates to an energy efficiency of about 33%, which is very low (Marc & Ibrahim, 2003). The remaining 67% is waste heat lost to the atmosphere. Increasing the efficiency of generating electricity would help save consumers money, as well as benefit the conservation of natural resources and decrease emissions associated with fossil fuel combustion (Rand & Dell, 2005).

In recent years, there has been an increase in the use of renewable energy due to the growing concern over the pollution caused by fossil fuel based energy. Renewable energy sources, such as photovoltaic (PV) and fuel cell, can be used to enhance the safety, reliability, and sustainability and transmission efficiency of a power system (Brown, Hendry & Harboorne, 2007).

Fuel cells are expected to play an important role in future power generation. The advantages of using a fuel cell to provide the chemical-to-electrical energy conversion is its high fuel-to-electrical energy efficiency of about 50% depending on the type of fuel cell technology employed (Hellman & Van de Hoed, 2007) including system losses. This can be boosted to as high as 80% by using the heat by-product for water heating and space heating or cooling in a co-generation system (Onovwiona & Ugursal, 2006). However, significant technical challenges remain and the commercial breakthrough of fuel cell is hindered by the high cost of fuel cell components which is decreasing (Puttgen, MacGrego & Lambert, 2002). Fuel cells do not provide the robust source characteristics required to effectively follow the load during significant load steps and they have limited overload-handling capacity.

There are many different power converter system topologies developed already. However, these topologies are not optimally suitable for fuel cells because of unique nonlinear V-I static and dynamic characteristics of fuel cells (Choi, Lee, Choi, Won & Yoo, 2005).

Success in the development of a fuel cell off grid power converter system will open the door to micro utilities development and integration with the grid utility as well as rural

electrification where the cost of extending the national grid to such remote area is very high.

1.2 Research Objectives

The main objective of this thesis is to model and develop a new fuel cell inverter topology with DSP control system incorporating an energy management scheme for residential applications. The proposed inverter topology and its control will be designed to be compatible with a fuel cell power source, which typically exhibits 2:1 voltage variation at its output terminals, as well a slow transient response. Moreover, the proposed configuration will simplify the power control management and will have a possibility to interact with the fuel cell controller. Extensive analyses of fuel cells types based on electrical efficiency, reliability, maintainability, cost, and fuel consumption will be examined for optimum power converter design.

A fuel cell, in conjunction with its reformer (production of hydrogen from hydrocarbon fuels sources), has an output voltage that varies with load and age, has limited overload capacity, has an output voltage range that is always too low in relation to the power it puts out for efficient use, is slow to respond to load change if the fuel supply is adjusted for best efficiency, needs considerable parasitic power for pumps, blowers or for heating at start-up and is slow to start up, will not absorb any power and may not accept any ripple (Lesster, 2000)

An appropriate topology is proposed for a 5 kW fuel cell power converter system with much emphasis on high efficiency, high reliability, good power quality and good energy management system. High reliability means system protection from over voltages, voltage spikes, and disturbances as a result of load transients. The research requires the combination of broad multidisciplinary knowledge in magnetic circuit, power converter and control system.

A fuel cell power converter that takes the nonlinearity nature of the fuel cell output into consideration is modelled and developed for a single-phase residential applications with operating voltage of 230 ± 5% V, 50 ± 0.1 Hz, less than 5% ripple, output power of 5 kW, greater than or equal to 90% efficiency. This system will provide alternative energy source cheaper, environmentally friendly and readily available stand-alone power generator. Experimental analyses of the power converter system response to the

nonlinearity nature of fuel cells system, energy management system optimisation techniques, optimization of performance parameters of Dc-Dc power converter, optimization of performance parameters of inverter, and the overall system reliability, and redundancy test, is investigated.

The proposed inverter system is designed and generally tested by means of computer simulations. Later on, an experimental prototype is built and tested for various operating conditions.

1.3 Limitations

The performance of the developed power converter system can be constrained by the semiconductor devices ratings such as transistor power switches, diodes as well as high frequency transformers used. However, a power converter system is developed to limit the constraints associated with these devices. A control scheme is employed to achieve good regulation of the output voltage. The nonlinearity characteristics of fuel cell can introduce some design trade-off that can affect the system overall performance of the proposed topology. However, close simulation of fuel cell electrical characteristics is employed for the final test of the developed power converter system.

1.4 Statement of the Problem

A fuel cell has an output voltage that varies with load dynamics; the fuel supply is adjusted for best efficiency, will not absorb any power and may not accept any ripple.

The aim of the research is to model and develop a fuel cell off grid converter power system using an appropriate power converter topology that is going to take the nonlinearity nature of the fuel cell output into consideration. An appropriate topology is developed for a 5 kW fuel cell output power converter system with much emphasis on high efficiency, high reliability, good power quality and good energy management system. Success in the development of the system will open the door to micro utilities development and integration with the grid utility as well. High reliability means system protection from over voltages, voltage spikes, and disturbances as a result of load transients is achieved. The research requires the combination of broad multidisciplinary knowledge in magnetic circuit, power converter and control system.

A fuel cell simulator is used to observe the efficiency, reliability, transient loads as well as the steady state analysis of the developed power converter system.

1.5 Sub-Problems

Different topologies have been developed for power converter system but in this research project, a novel power converter topology is modelled and developed for fuel cells application taking the nonlinearity I-V characteristics of fuel cells into considerations. Advancement in fuel cells system technology requires that a high efficiency, reliable power converter system will compliment this gain. Experimental analyses to be conducted include the followings:

- Power converter system response to the nonlinearity nature of fuel cells system.
- System reliability and redundancy analysis.
- Energy management system improvement.
- Optimization of performance parameters of DC-DC converter
- Optimization of performance parameters of inverter

1.6 Organisation of the thesis

Chapter 1 presents the introduction which briefly explains the motivation and research objectives of the project. It concludes with the organisational structure of the whole thesis for quick glance of what the thesis content contains and describes. Chapter 2 highlights the literature review papers prior to the development and commencement of the research project as well as during the project development. This is divided into subheadings for easy identification and assess to related topics such as renewable energy, fuel cell system and cost, fuel cell technology, dc-dc boost converters, modelling and analysis of dc-dc power converters and inverter systems.

Chapter 3 contains a qualitative description of the physical operating principles of fuel cell system used as an electrical energy generator. It also explains fuel cell types, advantages and disadvantages of fuel cell system, application areas and detailed electrical characterisation of a fuel cell system. Chapter 4 details the modelling and control of the fuel cell power converter system. Static and dynamic models of fuel cell system are examined. Chapter 5 details in depth analysis of power converter system interleaving techniques in order to reduce the current ripple which is detrimental to the

life span of a fuel cell system operation. It also explains the advantages, disadvantages and limitations of its implementation. Chapter 6 outlines the system design, components selection of the power converter system as well as the simulation results obtained for the designed values of the system. Hardware development and implementation are highlighted in chapter 7 including heat sink, driver circuits, system set-up etc that are thoroughly examined. Experimental measurements and verifications are carried out and incorporated into chapter 7. Chapter 8 concludes the thesis and provides recommendations for future works.

CHAPTER 2

LITERATURE REVIEW

2.0 Introduction

The inventor of fuel cell technology is Sir William Grove, who demonstrated a hydrogen fuel cell in London in the 1830s. Grove's technology remained without a practical application for 100 years. Fuel cells returned to the laboratory in the 1950s when the United States space program required the development of new power systems. Today, the topic of fuel cells encompasses a broad range of different technologies, technical issues, and market dynamics that make for a complex but potentially promising outlook. Significant amounts of public and private investment are being applied to the development of fuel cell products for both stationary and transportation applications.

Fuel cell systems, currently in the early stages of development, are an entirely different approach to the production of electricity than traditional prime mover technologies. Fuel cells are similar to batteries in that both produce a direct current (Dc) through an electrochemical process without direct combustion of a fuel source. However, whereas a battery delivers power from a finite amount of stored energy, fuel cells can operate indefinitely provided the availability of a continuous fuel source. Two electrodes (a cathode and anode) pass charged ions in an electrolyte to generate electricity and heat. A catalyst enhances the process.

Fuel cells offer the potential for clean, quiet, and efficient power generation. As with most new technologies, fuel cell systems face a number of formidable market entry issues resulting from product immaturity, over-engineered system complexities, and unproven product durability and reliability. These translate into high capital cost, lack of support infrastructure, and technical risk for early adopters. However, the many advantages of fuel cells suggest that they could well become the prime mover of choice for certain applications and products in the future.

2.1 Literature Review

2.1.1 Renewable Energy

Renewable energy is energy derived from resources that are regenerative or for all practical purposes cannot be depleted. For this reason, renewable energy sources are fundamentally different from fossil fuels, and do not produce as many greenhouse gases and other pollutants as fossil fuel combustion.

A stand-alone renewable energy system using hydrogen as the energy storage medium and a fuel cell as the regeneration technology was presented by Lehman and Chamberlin. The system is a 9.2 kW photovoltaic (PV) array coupled to a high pressure, bipolar alkaline electrolyser. In reporting the design, details of component selection, size, and integration, control system logic and implementation, and safety considerations are discussed (Lehman & Chamberlin, 1991).

An integrated renewable energy (RE) system for powering remote communication stations based on hydrogen was developed. The system is based on the production of hydrogen by electrolysis whereby the electricity is generated by a 10 kW wind turbine (WT) and 1 kW photovoltaic (PV) array. The WT power available shows that excess electrical energy produced during the best wind periods can be used to produce hydrogen. They also, showed that a PEMFC stack can respond to fast load switching, through a dc/dc converter, with efficiency better that 42% (Agbossou, Chahine, Hamelin, Laurencelle, St-Arnaud & Bose, 2001).

The prospects for hydrogen as a universal energy-provider was examined and considered the impact that its introduction might have on the present deployment of lead-acid batteries in mobile, stationary and road transportation applications. An overview of energy sustainability and hydrogen economy is given (Rand & Dell 2005).

2.1.2 Fuel Cell Technology

Internal reforming Solid Oxide fuel cells eliminate the requirement for a separate reformer and simplify the overall system design. In addition, the requirement for cell cooling, which is usually achieved by flowing excess air through the cathode is also significantly reduced (Nakagawa & Sagara, 2001).

An overview of the current status of fuel cell technology for mobile and stationary applications of both low and high temperature fuel cells, both on materials and

component level as well as on a system is given (De Bruijin, 2005). Their applications are discussed in relation to their environment benefits. The main hurdles preventing commercial introduction still are too high cost, lack of durability, too high system complexity and lack of enough fuel infrastructure.

2.1.3 Fuel Cells System Cost

Systems analysis for mobile and stationary applications of fuel cell systems are presented as well as economic analysis for different fuel cell systems for stationary applications. In particular, CHP generation based on natural gas as the energy carrier is performed. They found that using the annuity method to calculate the cost of electricity, the cost of electricity is still very high for fuel cell systems. Results of sensitivity analysis show that this is mostly accounted for by the system costs and fuel costs as well as the maintenance costs of these power plants (Lokurlu, Grube, Hohlein & Stolten, 2003).

The economics of producing electricity from proton exchange membrane (PEM) fuel cell systems under various conditions, including the possibility of using fuel cell vehicle (FEV) to produce power when they are parked at office buildings and residences is examined. The analysis shows that the economics of both stationary fuel cell and FCV-based power vary significantly with variations in key input variables such as the price of natural gas, electricity prices, fuel cell and reformer cost and fuel cell system durability levels (Lipman, Edwards & kammen, 2004)

2.1.4 Electrical Properties of Fuel Cells System

This paper describes an analysis of the low frequency ripple current generation, distribution and reduction in a fuel cell system. A case study provides a methodology that can be easily in some architecture powered by fuel cells. The internal resistance of a fuel cell was taken into consideration to explain a natural reduction of the ripple current in a system. An active filter was added to the system, draining the low frequency ripple. A theoretical analysis and experimental results were presented (Novaes & Barbi, 2003).

A model for the dynamic state of anode-supported intermediate temperature direct internal reforming planar Solid Oxide fuel cell stack model, that allows for both co-flow and counter-flow operation which consists of mass and energy balances, and electrochemical model that relates the fuel cell and air composition and temperature to

voltage, current density, and other related fuel cell variables was developed to examine the major source of voltage loss. It was found that cathode activation over potentials represents the major source of voltage loss, followed by anode activation over potentials and ohmic losses under the same operating conditions (Aguiar, Adjiman & Brandon, 2004).

A model for the study of solid oxide fuel cell (SOFC) electrical efficiency was developed (Sidwell & Coors, 2005). The chemically reacting flow model considers the coupled behaviour of fluid mechanics, thermodynamic, and transport of electro active species through the electrolyte. Fuel cells are treated as plug flow tubular reactors with no upstream diffusion. It was concluded that it is possible to exceed 60% electrical efficiency in internally reformed SOFCs. They also concluded that POX (0.408 CH_4, 0.123 O_2, 0.059 H_2O, and balance N_2) may provide adequate efficiency for many SOFC applications.

An optimization model constraint for a characterization of SOFC system electrical efficiency was developed through the combination of stack efficiency profiles and power converter efficiency profiles. It was found that constraints on the rate of change in current density are not important design criteria from an economic perspective (Hawkes, Auguair, Hernandez-Aramburo , Leach , Brandon , Green & Adjiman, 2006).

Inverter input ripple current has been reported to possibly degrade fuel cell performance and reduce its operating life if ripple currents are not adequately controlled causing internal losses and increase distortion of its terminal voltage. A ripple minimization technique without increasing the KVA ratings of the Dc-link filter components is possible (Wajiha, Kulkani & Arefeen, 2006)

2.1.5 Dc-Dc Boost Power Converters

A boost converter (set-up converter) is a power converter with an output dc voltage greater than its input dc voltage. It is class of switching-mode power supply (SMPS) containing at least two semiconductor devices and at least one energy storage element. A boost converter boosts the output voltage by first storing energy by passing currents through an inductor and that energy is then delivered at intervals by a MOSFET regulated by PWM (pulse width modulation) to a capacitor. The charged capacitor will

then supply a higher voltage at lower current to the load. Boost converter can be isolated or non-isolated type.

A power converter control approaches based on neural network technique and fuzzy logic was used to propose a new UPS (uninterruptible power supply).It prevents voltage drop from nonlinear loads, total harmonic distortion (THD) which is better than conventional deadbeat control method (Bor-Ren Lin, 1995).

This paper (Calais, Aglidis & Heinhard, 1999) provides an overview on different multilevel topologies and investigates their suitability for single-phase grid connected photovoltaic systems. Several transformerless photovoltaic systems incorporating multilevel converters are compared regarding issues such as component count and stress, system power rating and the influence of the voltaic array earth capacitance. Advantages of multilevel compared to their counterparts include sinusoidal waveform with low harmonic distortion, thus reducing filter requirement and the need of several sources on the Dc side of the converter makes multilevel technology attractive for photovoltaic applications.

In this paper (Canales, Barbosa, Aguilar & Lee, 2003), a zero-voltage switching (ZVC) three level Dc/Dc resonant converter for high-power operation is analysed at fixed and variable frequencies. The converter operates with wide input voltage variations without penalizing the efficiency. As a result, the converter is suitable for applications in which high efficiency and high power density are required. Experimental results for a 2.7 kW prototype verify the operation of the converter performance as designed.

A new high efficiency transformerless Dc/Dc converter is proposed in this paper (Franco, Pfitscher & Gules, 2003) in which large step-up rations is achieved with low duty cycle. The design structure intergrates a multiphase voltage multiplier that allows high static gain with low voltage stress in all the semiconductors used. The main advantages include, low voltage and current stresses, reduction of the turn-on and turn-off losses, low input voltage and current ripples, high efficiency and design modularity. An experimental result confirms the basic operation of the designed converter and theoretical analysis developed.

A novel single-stage half-bridge series-resonant buck-boost inverter (HB-SRBBI) was proposed (Wang & Chen, 2004). The inverter naturally generates an output ac voltage lower or larger than the input dc voltage depending on the duty cycle and power

switches turn on at zero-current-switching (ZCS). A resonant cell was built in the power stage to build ZCS for turning on the power switches. The active switches are operated at a fixed frequency with sinusoidal PWM technique.

An experimental study of some dynamics phenomena that can occur in current-programmed boost converters and novel hardware implementation, able to show pathways through which the boost converter may enter chaos (Catagna & Grassi, 2005). It was demonstrated that variations of the reference current (related to the control current) and variations of the input voltage can generate periodic, sub harmonics, quasi-periodic and chaotic behaviours.

A current-fed full bridge boost converter with zero current switching (ZCS) based on constant on-time for high voltage application is presented by this paper (Chen, Lin, Liang, Chen & Tseng, 2005). The proposed converter utilizes the leakage inductance and the winding parasitic capacitance resonant tank to achieve zero current switching. In order to achieve zero current switching under wide load range, the turn-on time of the full bridge boost converter is kept constant and the output voltage is regulated via frequency modulation. With careful design of the circuit parameters, the proposed converter can be operated with ZCS under wide load range without the use of series-connected diodes. A laboratory prototype implemented verifies the ZCS performance.

A modified converter for use in photovoltaic system with an output terminal that consisted of a solar array and output capacitor in series is proposed (Park, Kang, Cho, Moon, Nam & Ise, 2006). It also presented an efficient parallel driving scheme that employ phase-shift. Increase output voltage, decrease output voltage ripple, current sharing without an unbalanced problem, increase equivalent switching frequency, smaller capacitance value and lower working voltage of the output capacitor were the advantages achieved

This paper (Basu & Undeland, 2006) explores ways, including the use of SiC diodes, to increase the efficiency and switching frequency of continuous mode boost power factor correction circuits. It also shows how energy specific application would need a unique design solution to optimize the cost and performance of a power factor correction. The large dependence of the electrical and thermal performances of the hard switch continuous mode boost power factor correction topology on the characteristics of the power switching devices is investigated. The performance improvement by way of

decrease components count, increased power density and reduced electromagnetic interference provided by the new generation switching diode is highlighted.

A low-voltage Dc network as an alternative to an Ac network is proposed. The battery and sources are connected to the grid via Dc-Dc power converters, which play the main role in ensuring proper power flow and voltage stability for the network. They showed that a Dc network with distributed generation is very realizable when applying simple Dc-Dc power converters, while standard elements on the generation side as well as on the consumption side are applied. This kind of Dc network needs no central control and no communication between the different elements of the network (Azbe & Mihalic, 2006).

2.1.6 Dc-Dc Converters Modelling

The method proposed (Middlebrook & Cuk, 1976) bridges the gap considered to exit between the state-space technique and the averaging technique of modelling power stages by introduction of state-space averaging modelling. The first approach remains strictly in the domain of equation manipulations while the other technique is based on equivalent circuit manipulations resulting in a single equivalent linear circuit model of the power stage.

A storage energy method can be used (Cheng, 2003) to analysis classical switched mode power converter. It was discovered that the basic topologies behaves according to a special patterns. The same approach has been applied to other converters (Luo & Ye, 2005 & Luo, 1999, 2000). The energy ration defined for the inductor and capacitor clearly indicate that if the reactive components are many or the variation of storage energy is large, the ratio will become large. This should be avoided in practical circuits.

The mathematical modelling of dc-dc power converters is a historical problem that has accompanied dc-dc conversion technology since the 1940s. Traditional modelling is not available for complex structure converters because of the very high-order differential equations involved.(Luo & Ye, 2005) proposed a new model to cover all dc-dc power converters by using the energy stored technique in energy storing components (capacitors and inductors).

2.1.7 Fuel Cells Inverters

Dc-Ac power converters are known as inverters. The function of an inverter is to change a dc input voltage to symmetric ac output voltage of desired magnitude and frequency. The output voltage could be fixed or variable of fixed or variable frequency. The output voltage waveforms of ideal inverters should be sinusoidal. However, the waveforms of practical inverters are non sinusoidal and contain certain harmonics. With availability of high speed power semiconductor devices, the harmonics contents of output voltage can be minimized or reduced significantly by switching techniques (Rashid, 2004, p. 226).

A single-phase three-level pulse width modulation (PWM) Ac-Dc power converter with the function of power factor correction and active power filter is proposed to reduce harmonic currents flowing into the power system and to a nearly sinusoidal current with unity power factor. The circuit topology of the adopted three-level PWM ac/dc converter is based on a conventional two-level full-bridge rectifier and one ac power switch. No additional active filter is needed, since the converter adopted can simultaneously as a power factor corrector and an active filter. The advantages of the proposed three-level converter, instead of a two-level converter, are in implementing a high voltage application using low voltage devices and reducing the voltage harmonic contents (Bor-Ren Lin, 2001).

In (Gpinath, kim, Hahn, Webster, Burghardt, Campbell, Becker, Enjeti, Yeary & Howze, 2002), a fuel cell inverter system that employ a three- terminal push-pull Dc-Dc converter to boost the fuel cell voltage (28V) to ± 200V was designed and developed. Advantages of this design include lower parts count, easy manufacturability, lower cost, protection and diagnostic features that provide safety and convenience for the operator. It also provides flexibility and intelligence incorporated to suit varying system and control requirements.

A fuel cell inverter topology designed by (Krein & Balog, 2002) eliminates the need for a Dc intermediate voltage by using an Ac-link output inverter problems associated with convectional cycloconverter circuits such as high distortion and control complexity. The problems of convectional cycloconverter are eliminated by using a multi-carrier PWM technique (Krein, Geng & Balog, 2002). The resulting converter implements a true PWM cycloconverter. It supports natural commutation, and therefore can be built at the same level of control complexity and with the same filter characteristics as a convectional two-

level PWM inverter. The technique of multi-carrier PWM inverter support additional cost advantages by reducing the power conversion stage to two while providing galvanic isolation at the same time.

In (Nergaard, Ferrel, Leslie & Lai, 2002), a complete design consideration for a fuel cell inverter is presented. It made a good alternative to batteries as an energy storage device in ultracapacitor as used in the inverter topology. Each module consists of a full-bridge phase shifted front-end and a half-bridge inverter. It was concluded from the experiment that the fuel cell time constant is reasonably fast, but it oscillates severely after load transient, the Dc bus bulk capacitor which are normally sized for steady-state ripple need to be increased during dynamic conditions, using ultracapacitor for supplementary energy storage is effective, but the ESR needs to be as small as possible to help alleviate the fuel cell current ripple during load transients. The proposed system is shown to be simple, flexible and can provide redundancy with little or no additional cost.

A new high frequency Dc/Ac inverter for home applications using fuel cell as a source of electrical energy is presented (Mazumdar, Batarseh, Kutkut & Demirci, 2002).t e design is based on a push-pull Dc-Dc converter followed by a full-bridge PWM inverter topology. Due to the simplified power stage and application of DSP-based sinusoidal pulse width modulation technique, output voltage total harmonic distortion (THD) is reduced and a relatively smaller inverter size is achieved. The major area of the design was proper filter circuit so that the output of the inverter is clean and suitable for domestic appliances. The designed inverter is rugged and maintenance free.

A new grid connected inverter for fuel cells system is developed by (Andersen, Klumpner, Kjær, & Blaabjerg, 2002). It consists of a current-fed pus-pull Dc-Dc converter and H-bridge inverter. A new dedicated voltage mode start-up procedure has been developed in order to limit the inrush current during start-up. The push-pull topology is selected in order to decrease the conduction losses in the switches due to the low fuel cell voltage. The inverter has shown to be reliable and to exhibit high efficiency.

This paper (Turkey & Krase, 2002) presents a detailed design procedure in designing a fuel cells system for domestic applications. It discusses the topology used to achieve the objective set for 2001 Future Energy Challenge (FEC), the rationale used in choosing the designed topology, detailed component selection optimized to minimise cost, and

the Dc/Dc and Dc/Ac control strategies used. A 10 kW system was built and tested according to the system design. The developed system exhibits high efficiency.

A new low cost 10 kW inverter systems for fuel cell is proposed. The proposed system consists of an isolated dc-dc converter to boost the fuel cell voltage to $400V_{dc}$ and a PWM inverter with filter to convert the voltage to two split-phase $120V_{ac}$. The dc-dc converter uses phase shifting to control power flow through a transformer with a MOSFET full bridge on the high voltage side and voltage doubler on the low voltage side. A high voltage battery is added after the voltage doubler as transient power for load dynamics. Thus the capacitance of the high voltage side capacitors is minimized and significantly reduces the total cost of the system. One IPM is used to realize the voltage doubler and the dc-dc inverter. Simulation and experimental results were demonstrated (Wang, Peng, Anderson, Joseph & Buffenbarger, 2003).

This paper (Andersen, Klumpner, Kjær, & Blaabjerg, 2003) presents a new high efficiency grid-connected single phase converter for fuel cells. It consists of a two stage power conversion topology. The proposed convert consists of an isolated Dc-Dc converter cascaded with a single-phase H-bridge inverter. The Dc-Dc converter is a current-fed push-pull converter. The inverter is controlled as a standard single phase power factor controller with resistor emulation at the output. The converter is reliable and exhibits a high efficiency over a wide input power range. Experimental results verify that the inverter exhibits a high power factor and low current total harmonics distortion (THD).

This paper (Hernando, Villegas, Fernandez, Sebastian & Corral, 2003) presents the design overview of a Dc-Dc converter for uninterruptible power supply (UPS) applications. The fron-end converter uses a full-bridge phase-shifted topology that implements ZVS technique to decrease the losses. A voltage clamp circuit is used on the high voltage side of the isolated transformer to reduce switching losses because the power diodes operate under hard switch condition. A prototype of the converter and experimental results verify the design.

A new power converter is proposed (Testa, 2003) based on cascade connection of a Dc/Dc and a Dc/Ac converters. The Dc/Dc converter is used to control fuel cell current ripple and regulate the power flow from the fuel cells. It is characterised by only two main switches of low side type, operated with an interleaved control technique which

requires the use of two boost inductor chokes. Such control stragetgy provides input current ripple cancellation, which is very important in fuel cells systems in order to extend the lifespan of the system. A regenerative active clamp circuit is also used in order to prevent high peak voltages on the two main switches, maintaining a high efficiency. The proposed system is cost effective and operates under a wide range of input voltages and load conditions with high efficiency.

The proposed inverter (Wang, Pant, Mohammad, Famouri & Osman Demirce, 2003) provides a solution for the low-voltage and high-current fuel cell source by using power modules that are parallel connected input and series connected output in dc-dc boost stage while improving efficiency and reducing cost. Each module carry a lower load and share the high input current from the power source, reducing the conduction and reducing the need for high power rating components. The proposed inverter takes advantage of a digital controller to provide the advanced and complex control algorithms needed to meet the requirement of the fuel cell, as well as the power management of the overall system. Experimental results conformed to the theoretical analysis and demonstrate the feasibility of the approach.

The developed low cost Solid Oxide fuel cell power conditioning (Smith, Gillion, Urciuoli, Mclandrich, Pepa & Lai, 2003) was designed with a bidirectional charging circuit. A three-phase dc-dc converter is proposed to reduce the device current on each phase leg. Although more phase legs appear to be better of current sharing, the gate drive circuit and control design for more legs becomes troublesome when the phase number increases further. The selected design for the dc-ac inverter uses two half bridges connected as a full H-bridge. Because the dc-dc converter uses two transformer taps, two-regulated output buses are available to avoid unbalance problem. Reduced device current, switching loss, passive component size, weight, improved efficiency, use of non-isolated bidirectional converters for the energy management system were achieved.

The proposed (Lee, Jo & Choi, 2003) power processing unit consists of the front-end dc-dc converter, the dc-ac inverter and the bidirectional dc-dc converter. Practical issues such as component rating calculation, high frequency transformer design, heat sink design, and protection are detailed aiming at the cost and efficiency targets. A low cost controller design is discussed along with current-mode control, output voltage regulation with capacitor balancing and a state of charge (SOC) control for battery management. A

10 kW hardware prototype was built and tested in the steady-state as well as in the transient-state.

A 10 kW Solid Oxide fuel cell power converter for residential use was developed by (Todorovic, Palma, Choi, Dowling, Humphrey, Tarbel, Enjeti & Howze, 2003). Two 2.5 kW high frequency transformer was used to reduce leakage inductance and therefore reduce the duty loss for the dc-dc conversion process. One set of lead-acid batteries is provided on the high voltage dc bus to supply load demands. Efficient and smooth control of the power drawn from the fuel cell and the high voltage battery is achieved by controlling the front end dc-dc converter in current mode. A six-switch (IGBT) inverter is employed to produce 120V/240V, 60Hz ac outputs. The control strategy allows the inverter to adapt to the requirements of the load as well as the power source (fuel cell).

A 5 kW low cost power converter for fuel cell using high frequency magnetic, aggressive modular packaging and integrated control is developed (Bohn & Lorenz, 2003). The 5 kW dc input from the solid oxide fuel cell is boosted from 22 V_{dc} (@ full load) to 400 V_{dc} where an additional 5 kW of power from the 400 V_{dc} transient energy storage battery provides a maximum of 10 kW to the inverter output (120/240 V_{ac} split phase 60 Hz). The control system implemented is modular as well, decoupling the boost converter from the output inverter load transient by incorporating an observer filter capacitor voltage to infer output current. The energy management system is implemented by connecting the battery pack to the dc link to reduce device count. Cost is the core challenge for their project.

A low cost, light weight, efficient and compact solid-state hybrid power sources with an integral power distributed and charge management system was designed and built using standard miniature power regulator integrated circuits with appropriate modifications to implement the necessary controls. The resulting converter not only allows the interconnection of fuel cell systems and batteries having dissimilar operating voltage, but it also imposes a power sharing strategy that elicits peak performance from each part of the device (Blackwelder & Dougal, 2004)

A current-fed phase-shifted full-bridge zero current switching (ZCS) Dc-Dc converter with reverse block insulated gate bipolar transistor (IGBT) which is suitable for fuel cell source is investigated by the team of this paper (Zhu, Xu, Shen & Xi, 2005). From the analysis collaborated with experimental results they concluded that (1) the output

current of the fuel cell in this type of a system is continuous and high frequency component of current is lower (2) the turn off losses of the IGBTs is eliminated by operating the system under ZCS condition (3) the rectifier diodes are naturally turned off so the reverse recovery losses of the diodes is eliminated (4) the double line-frequency current ripple is reduced by adding larger capacitor in the Dc-Dc converter output side.

In (Shi, Pan, Chen, Hu & He, 2005), a new combined converter topology with high current and low voltage suitable for fuel cells is presented to meet the demands of high reliability and high power density. By connecting in parallel two-transistor forward converter modules and power switches simultaneously in the input-end, and connecting in parallel or series the converter in the output-end, the proposed converter has many advantages. Advantages such as natural current-sharing amongst power switches, natural voltage-sharing between output capacitors, risk elimination of direct short-through failure in the input Dc link, low voltage stress on the secondary side diodes, and small sized output and output filters are obtained.

In (Wai, 2005), a new designed topology for fuel cell energy conversion is developed. A current-source sine wave voltage inverter is designed in the sense of voltage-clamping and soft-switching. This enables the use of a smaller inductor in the current source circuit and compression of the voltage stress across switches about the two times of the Dc bus voltage. Advantages include lower distortion, fast dynamic regulating speed and insensitivity to load variations, even under nonlinear load.

A high performance fuel cell converter system is presented to show superior efficiency and high-frequency ripple current elimination using a multiphase Dc-Dc converter and low frequency ripple current elimination using a multi loop control technique (Lai, 2005). Major design issues include cost, efficiency, ripple current, and state operation under load transients are examined. A new V6 converter is introduced to show how the high-frequency ripple reduction can be achieved to allow cost reduction on passive components. An active ripple cancellation technique to show how the low frequency ripple can be eliminated is presented. The proposed technique is very attractive for fuel cell power conditioning system without adding to system volume and cost.

A new family of zero-voltage switching phase shift modulated Dc-Dc converter for a medium to high power solid oxide fuel cell application is presented (Mason & Jain, 2005). Method of minimizing conduction loss while maintaining zero voltage switching

(ZVS) across the entire load range is achieved using a new auxiliary circuits, and new control method, which controls the bridge-to-bridge phase shift to control the peak value of the currents through the auxiliary inductors. This behaviour is termed Adaptive Energy Storage because the energy stored by the auxiliary circuit is only what is needed for ZVS, according to the line and load conditions. The new ZVS-PSM-FB Dc-Dc converter family presented in this paper utilizes adaptive energy storage to minimize conducting current, thereby reducing conduction loss and maximizing efficiency.

In (Sharma & Gao, 2006), a new Dc-Dc converter for fuel cell powered distributed residential poer generation system is proposed and developed. The proposed converter uses the leakage inductance foe energy conversion, which not only mitigates the leakage inductance resultant low efficiency and difficulty in control problem, but also eliminates the need for a separate filter inductor. Elimination of the inductance helps reduce the cost of the Dc-Dc converter. Cost reduction and high efficiency are achieved.

In this paper (Fonts, Turpin, Astier & Meynard, 2006) presents an experimental and modelling of a proton exchange membrane (PEM) fuel cell. A small signal model of the electrochemical generator is developed. This model is the extrapolated in order to predict the high signal fuel cell behaviour. The frequency response to small current ripple is measured and modulated through an impedance spectroscopy. It is shown that a fuel cell stack offers possibilities to filter high frequency current harmonics by the intermediary of its double layer capacitor.

A fuel cell based uninterruptible power supply (UPS) that eliminates the ac-dc and dc-ac converter systems was developed. The designed system eliminates the equipment ac power supply and replaced it with a wide range input voltage, high efficiency dc power supply. An overall efficiency of the UPS can be increased by 50% (Gonzales & Tamizhman, 2006).

2.1.8 Energy Management System

Since the fuel cell responds slowly the power will not match the power output from the cell during transients; there will be a power deficiency or excess. The fuel cell could be damaged if more current is taken than it can supply, so current should never exceed available current. Current demands may be less than available current, but this result in unused fuel being exhausted from the fuel cell. For these two reasons some energy storage was required to sink or source the power difference. Lead acid batteries or super capacitors can be used as a form of energy storage system.

A 1 kVA fuel cell powered, line interactive UPS system that employs modularity design was developed. Due to the absence of batteries, the system satisfies the demand for an environmentally friendly, clean source of energy. No delay time is required to take over the full load when the power disturbances occur due to the fast discharging characteristics of the super capacitor employed (Choi, Howze & Enjeti, 2006).

2.1.9 Environmental Impact of Fuel Cells

From an environmental point of view, fuel cell source type of power generation is a zero-emission process (apart from water of course, if pure hydrogen is used). However, for commercial usage, hydrogen must first be extracted from a hydrocarbon fuel in a process utilizing a fuel reformer.

Typical fuels used in this way are natural gas, methanol, ethanol, diesel and gasoline; these fuels are reformed into hydrogen-rich gas, not pure hydrogen. The fuel reformer not only enables the use of the existing fuels, but more importantly, negates the need for brand new fuel storage and transportation infrastructure.

CHAPTER 3

FUEL CELLS SYSTEM AND TECHNOLOGY

3.0 History of Fuel Cells

The principle of the fuel cell was discovered by German scientist Christian Friedrich Schonbein in 1838 and published in the January edition of the Philosophical Magazine. Based on this work, the first fuel cell was developed by Welsh scientist Sir Williams Robert Grove in 1843. The fuel cell he made used similar materials to today's phosphoric acid fuel cell. It was not until 1957 that British engineer Francis Thomas Bacon successfully developed a 5 kW stationary fuel cell. In 1959, a team led by Harry Ihrig built a 15 kW fuel cell tractor for Allis-Chalmers which was demonstrated across the US at state fairs. This system used potassium hydroxide as the electrolyte and compressed hydrogen and oxygen as the reactants. Later in 1959, Bacon and his colleagues demonstrated a practical five-kilowatt unit capable of a welding machine. In the 1960s, Pratt and Whitney licensed Bacon's U.S. patents for use in the U.S. space program to supply electricity and drinking water (Wikipedia, on-line).

3.1 Fuel Cell Operation

A fuel cell is an electrochemical energy conversion device similar to a battery, differing in that it is designed for replenishment of the reactants; that is, it produces electricity from an external supply of fuel and oxygen as opposed to the limited internal energy storage capacity of a battery. Additionally, electrodes within a battery react and change as the battery is charged, or discharged, whereas in fuel cells electrodes are catalytic and relatively stable (Wikipedia, online)

A fuel cell consists of two electrode sandwiched around an electrolyte. Oxygen passes over one electrode and hydrogen over the other, generating electricity, water, and heat.

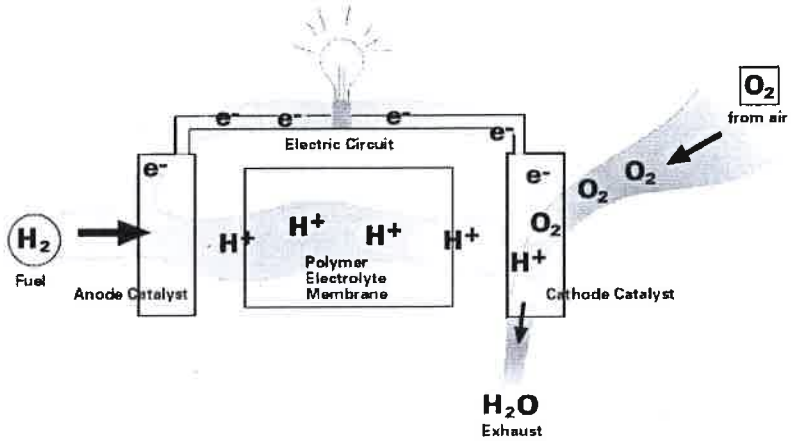

Figure 3.1 Conceptual Reactions of a PEM Fuel Cell

Hydrogen fuel is fed into the anode of the fuel cell. Oxygen (or air) enters the fuel cell through the cathode. The chemical reaction is speeded up by a catalyst, the hydrogen atom splits into a proton and an electron, which take different paths to the cathode. The proton passes through the electrolyte. The electrons create a separate current that can be utilized before they return to the cathode, to be reunited with the hydrogen and oxygen in a molecule of water. Figure 3.1 shows the conceptual operation of a fuel cell.

Anode reactions:

$H_2 + O^{2-} \Rightarrow H_2O + 2e^-$

$CO + O^{2-} \Rightarrow CO_2 + 2e^-$

Cathode reaction:

$O_2 + 4e^- \Rightarrow 2O^{2-}$

Overall reactions:

$H_2 + 1/2\ O_2 \Rightarrow H_2O$

$CO + 1/2\ O_2 \Rightarrow CO_2$

A fuel cell system which includes a fuel reformer can utilize the hydrogen from any hydrocarbon fuel – from natural gas to methanol, and eve gasoline. Since the fuel cell relies on chemistry and not combustion, emissions from this type of a system would still be much smaller than emissions from the cleanest fuel from combustion processes.

3.2 Advantages of Fuel Cells System

- low environmental pollution,
- high efficient power generation,
- fuel diversity (natural gas, LPG, methanol and naphtha),
- reusability of exhaust heat,
- modularity
- faster installation (Ellis el ta, 2001).

3.3 Disadvantages of Fuel Cells System

- High cost of market entry
- No enough support infrastructure
- Production, transportation, distribution and storage of hydrogen is difficult

3.4 Applications of Fuel Cells System

- Stationary electric power
- Distributed generation
- Automotive propulsion
- Space and other closed environment electrical power supply
- Auxiliary power systems
- Derivative applications (portable units)

3.5 Five Main Types of Fuel Cells Technology

Fuel cells are classified primarily by the kind of electrolyte they employ. This determines the kind of chemical reactions that take place in the cell, the kind of catalysts required, the temperature range in which the cell operates, the fuel required, and other factors. These characteristics, in turn, affect the applications for which these cells are most suitable. There are several types of fuel cells currently under development, each with its own advantages, limitations, and potential applications. A few of the most promising types include Alkaline Fuel Cells (AFC), Phosphoric Acid Fuel Cells (PAFC), Proton Exchange Membrane Fuel Cells (PEMFC), Molten Carbonate Fuel Cells (MCFC), and Solid Oxide Fuel Cells (SOFC).

3.5.1 Alkaline Fuel Cells (AFC)

Alkaline Acid Fuel Cells (AFC) uses an aqueous solution of either sodium or potassium hydroxide as the electrolyte. Hydrogen serves as the fuel cell and air or pure oxygen as the reducing agent and have an operating temperature of around 80°C but can be as high as 200°C. The electrodes are made from carbon with platinum electro catalyst which is expensive. AFC found early use in Apollo spacecraft to provide both electricity and drinking water and still is being used for power generation on spacecraft. The use of AFC is limited. Practically only pure hydrogen and oxygen can be used as fuel because carbon dioxide and carbon monoxide are poisons to the cell. The strong alkaline solution also presents corrosion problems. Hence, this type of fuel cell has limited commercial viability. The power density of AFC is in the range of 0.1-0.3 W cm^{-2}. Alkaline fuel cells are available in the kW range (De Bruijin, 2000).

3.5.2 Phosphoric Acid Fuel Cells (PAFC)

Phosphoric Acid Fuel Cells (PAFC) have as its name implies, uses a liquid phosphoric acid as an electrolyte, the acid is contained in a Teflon-bounded silicon carbide matrix and porous carbon electrodes containing a platinum catalyst. The PAFC is considered the "first generation" of modern fuel cells. It is one of the most mature cell types. They also run on hydrogen as the fuel and pure oxygen as the reducing agent. They have an operating temperature of about 200°C. Unlike AFC, they can operate on hydrogen contaminated with carbon dioxide which reduces external fuel cells processing requirements. PAFC are more tolerant of impurities in fossil fuels that have been reformed into hydrogen. They are 85% efficient when used for the co-generation of electricity and heat but less efficient at generation electricity (37-42%). This is only slightly more efficient than combustion-based power plants, which typically operate at 33 to 35% efficiency. PAFC are also less powerful than other fuel cells, given the same weight and volume. As a result, these fuel cells are typically large and heavy. The power density of the PAFC in the range of 0.14 W cm^{-2} (De Bruijin, 2000).

3.5.3 Proton Exchange Membrane Fuel Cells (PEMFC)

Polymer electrolyte membrane (PEM) fuel cells also called proton exchange membrane fuel cells deliver high power density and offer the advantages of low weight and volume, compared to other fuel cells. PEM fuel cells use a solid polymer as an electrolyte and porous carbon electrodes containing a platinum catalyst. They need only hydrogen, oxygen from the air, and water to operate and do not require corrosive fluids like some fuel cells. They are typically fuelled with pure hydrogen supplied from storage tanks or onboard reformers.

Polymer electrolyte membrane fuel cells operate at relatively low temperatures, around 80°C (176°F). Low temperature operation allows them to start quickly (less warm-up time) and results in less wear on system components, resulting in better durability. However, it requires that a noble-metal catalyst (typically platinum) be used to separate the hydrogen's electrons and protons, adding to system cost. The platinum catalyst is also extremely sensitive to CO poisoning, making it necessary to employ an additional reactor to reduce CO in the fuel gas if the hydrogen is derived from an alcohol or hydrocarbon fuel. This also adds cost. Developers are currently exploring platinum/ruthenium catalysts that are more resistant to carbon monoxide.

PEM fuel cells are used primarily for transportation applications and some stationary applications. Due to their fast start-up time, Low sensitivity to orientation, and favourable power-to-weight ratio, PEM fuel cells are particularly suitable for use in passenger vehicles, such as cars and buses (Lipman, Edward & Kammen, 2004).

A significant barrier to using these fuel cells in vehicles is hydrogen storage. Most fuel cell vehicles (FCVs) powered by pure hydrogen must store the hydrogen onboard as a compressed gas in pressurized tanks. Due to the low energy density of hydrogen, it is difficult to store enough hydrogen onboard to allow vehicles to travel the same distance as gasoline-powered vehicles before refueling, typically 300-400 miles. Higher-density liquid fuels such as methanol, ethanol, natural gas, liquefied petroleum gas, and gasoline can be used for fuel, but the vehicles must have an onboard fuel processor to reform the methanol to hydrogen. This increases costs and maintenance requirements. The reformer also releases carbon dioxide (a greenhouse gas), though less than that emitted from current gasoline-powered engines. However, PEM has also been used in portal applications such as computers (Tüber, Zobel, Schmidt & Hebling, 2004).

3.5.4 Molten Carbonate Fuel Cells (MCFC)

Molten carbonate fuel cells (MCFC) are currently being developed for natural gas and coal-based power plants for electrical utility, industrial, and military applications. MCFC are high-temperature fuel cells that use an electrolyte composed of a molten carbonate salt mixture suspended in a porous, chemically inert ceramic lithium aluminium oxide (LiAlO2) matrix. Since they operate at extremely high temperatures of 650°C (roughly 1,200°F) and above, non-precious metals can be used as catalysts at the anode and cathode, reducing costs.

Improved efficiency is another reason MCFC offer significant cost reductions over phosphoric acid fuel cells (PAFC). Molten carbonate fuel cells can reach efficiencies approaching 60 percent, considerably higher than the 37-42 percent efficiencies of a phosphoric acid fuel cell plant. When the waste heat is captured and used, overall fuel efficiencies can be as high as 85 percent.

Unlike alkaline, phosphoric acid, and polymer electrolyte membrane fuel cells, MCFC do not require an external reformer to convert more energy-dense fuels to hydrogen. Due to the high temperatures at which they operate, these fuels are converted within the fuel itself by process called internal reforming, which reduces cost.

Molten carbonate fuel cells are not prone to carbon monoxide or carbon dioxide poisoning-they can even use carbon oxides as fuel-making them more attractive for fuelling with gases made from coal. Although they are more resistant to impurities is than other fuel cell types, scientists are looking for ways to make MCFC resistant enough to impurities from coal, such as sulphur and particulate.

The primary disadvantage of current MCFC technology is durability. The high temperatures at which these cells operate and the corrosive electrolyte used accelerate component breakdown and corrosion, decreasing cell life. Scientists are currently exploring corrosion-resistant materials for components as well as fuel cell designs that increase cell life without decreasing performance.

3.5.5 Solid Oxide Fuel Cells (SOFC)

A solid oxide fuel cell consists of two porous ceramic electrodes, the anode and cathode, separated by a solid ceramic electrolyte. Typical SOFC materials are stabilized zirconium for the electrolyte, Nickel/zirconium cermets for the anode, and doped lanthanum magnate for the cathode (Yamamoto, 2000).

Solid oxide fuel cell operates at high temperatures and atmospheric or elevated pressures, and can use hydrogen, carbon monoxide, and hydrocarbons as fuel and air (oxygen) as oxidant. In this cell, the oxygen ions formed at the cathode migrate through the ion-conducting solid ceramic electrolyte to the anode/electrolyte interface where they react with the hydrogen and carbon monoxide contained in (and/or produced by) the fuel, producing water and carbon dioxide while librating electrons that flows back to the cathode/electrolyte via an external circuit (Ferguson, Fiard & Herdin, 1999). The following chemical equations present the reaction occurring at the electrodes.

Anode reactions:

$H_2 + O^{2-} \Rightarrow H_2O + 2e^-$

$CO + O^{2-} \Rightarrow CO_2 + 2e^-$

Cathode reaction:

$O_2 + 4e^- \Rightarrow 2O^{2-}$ [a]

Overall reactions:

$H_2 + 1/2\ O_2 \Rightarrow H_2O$

$CO + 1/2\ O_2 \Rightarrow CO_2$

SOFC can be classified according to their geometry, operating temperature, relative thickness of PEN (positive-electrolyte/electrode/negative-electrode) components or method of processing the fuel. The operating temperature range of planar anode-supported intermediate-temperature (IT) direct internal reforming (DIR) SOFC is from 823K to 1073K as compared to the 1073-1273K range of high temperature SOFC. The temperature reduction allows IT-SOFC to use a wide range of materials and have a more cost effective fabrication method (Aguair, Adjiman & Brandon, 2004).

Anode-supported SOFC (where the anode is the thickness PEN component and the electrolyte must have high ionic conductivity and small thickness) have been developed to minimize the high Ohmic losses attributed to IT operation. DIR is a possible approach to convert a primary fuel into the hydrogen-rich gas required by SOFC. In this approach, the methane if fed directly to the cell and reforming takes place on the anode, eliminating the need for a separate fuel reformer. It is known that DIR in high-temperature SOFC may lead to steep local cooling effects caused by the endothermic DIR reaction, and can generate large, potentially damaging temperature gradients. However, the lower operating temperature of IT-SOFC has been shown to be beneficial as it naturally reduces the DIR reaction rate. For operation, a SOFC stack must be embedded within a SOFC system incorporating a balance of plant (BOP) to supply air and clean fuel at the appropriating operating conditions, convert the direct current (dc) to alternate current (ac), and remove or process the depleted reactants, products and heat (EG&G Technical Services, 2000; Padulles, Ault & Mcdonald, 2000; John, 1998).

FC REACTANTS AND PRODUCTS

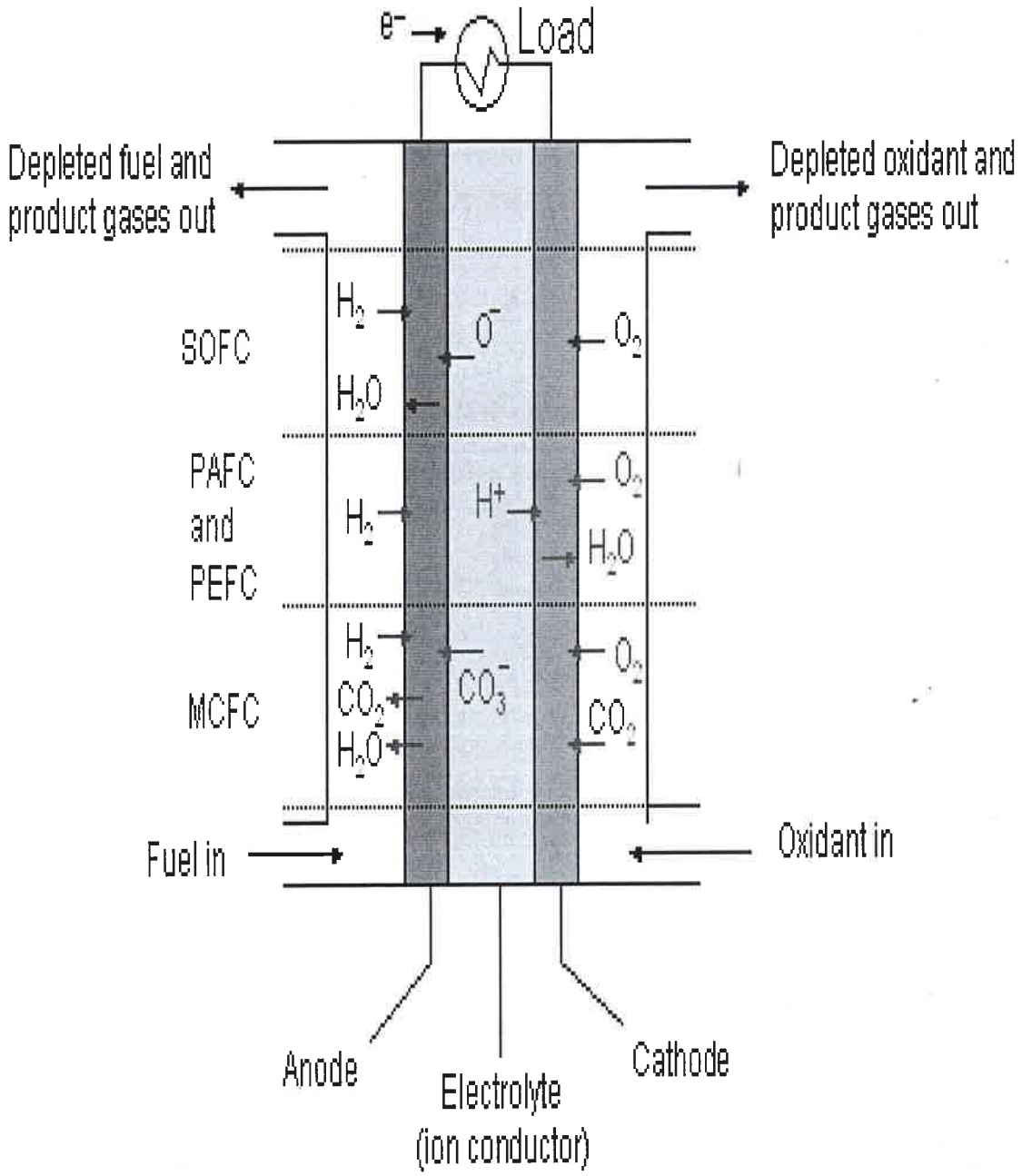

Figure 3.2 Fuel Cells Types and their Reactions

3.6 Electrical Characteristics of Fuel Cells System

The performance of a fuel cell can be expressed by the polarization curve, which describes the cell voltage – load current (V-I) characteristics of the fuel cell that are highly non-linear. Figure 3.3 shows the cell voltage versus current density characteristic of a typical fuel cell system. Optimisation of fuel cell operating points, design of the power conditioning units, design of simulators for fuel cell stack systems, and design of system controllers depend on such characteristics. Therefore, modelling V-I characteristics of fuel cells system is important. A unified mathematical model for both steady-state and dynamic-state was developed by Xue, Cheng and Saatanto (2006).

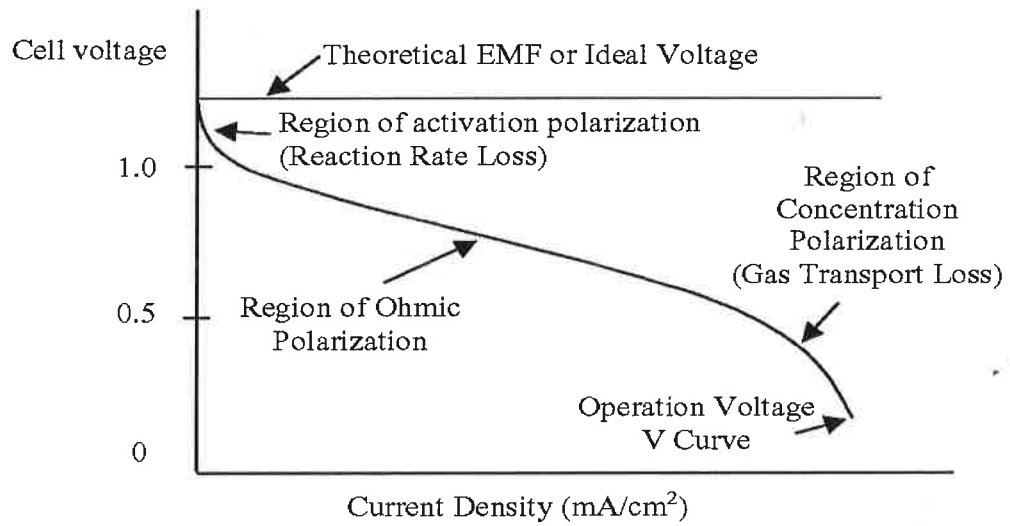

Figure 3.3 Polarization Curve of Fuel Cells System

Several sources contribute to irreversible losses in practical fuel cell. The losses are called polarization, overpotential, or overvoltage, originate primarily from three sources: (1) activation polarization (2) Ohmic polarization (3) concentration polarization. These losses result in a cell voltage for a fuel cell that is less than its ideal potential.

The activation polarization loss is dominant at low current density. At this point, electronic barriers have to be overcome prior to current and ion flow. Activation losses show some increase as current increases. Ohmic polarization loss varies directly with current, increasing over the whole range of current because all resistance remains essentially constant. Gas transport losses occur over the entire range of current density,

but these losses become prevalent at high limiting currents where it becomes difficult to provide enough reactants flow to the cell reaction sites.

These distinguished regions can be observed from figure 3.3 above. Regions of activation polarization, Ohmic polarization, and concentration polarization are clearly depicted in the figure. Each of the regions is explained as follows:

Region of Activation polarization: Activation polarization is present when the rate of an electrochemical reaction at an electrode surface is controlled by sluggish electrode kinetics. In order words, activation polarization is directly related to the rates of electrochemical reaction. There is a close similarity between electrochemical and chemical reactions in that both involve an activation barrier that must be overcome by the reacting species. The activation losses can be obtained by Tafel equation:

$$V = A\ln\left(\frac{i}{i_o}\right) \qquad 3.1$$

Where A is a constant, V is the overvoltage, I is the current density, i_o is the current density at which the voltage begins to drop to zero.

Region of Ohmic polarization: Ohmic losses occur because of resistance to the flow of ions in the electrolyte and resistance to flow of electrons through the electrode materials. The dominant Ohmic losses, through the electrolyte, are reduced by decreasing the electrode separation and enhancing the ionic conductivity of the electrolyte. Because both the electrolyte and fuel cell electrode obey Ohm's law, the Ohmic losses can be expressed by the equation

$$\eta_{ohm} = iR \qquad 3.2$$

Where I is the current flowing through the cell and R is the total cell resistance, which includes electronic, ionic, and contact resistance.

Region of concentration polarisation: As a reactant is consumed at the electrode by electrochemical reaction, there is loss of potential due to the inability of the surrounding

material to maintain the initial concentration of the bulk fluid. That is, a concentration gradient is developed. Several processes may contribute to concentration polarization: slow diffusion in the gas phase in the electrode pores, solution/dissolution of reactants/products into/out of the electrolyte, or diffusion of reactants/products through the electrolyte to/from the electrochemical reaction site. At practical current densities, slow transport of reactants/products to/from the electrochemical reaction site is a major contribution at higher currents when the fuel and oxidant are used at higher rates and the concentration in the gas channel is at a minimum. The voltage drop due to concentration polarization can be expressed as

$$V = S_s^{'} - mI_m e^{ni_m} \qquad 3.3$$

Where I_m=I-I_d, V_s' and I_d are the coordinates of the point where V-I characteristics starts to deviate from being linear (start of mass transport action), and m and n are mass transfer parameters. While I_d is the limiting at which the fuel is used up at a rate equal to its maximum supply rate, other constants depend on the fuel cell and its operating condition.

It has been shown that one cannot arbitrarily increase the operating voltage to increase the electrical efficiency of fuel cells. Peak electrical power is a compromise between fuel utilization and operating voltage, which are antagonistic. High open circuit voltage is not necessarily a good indicator of high electrical efficiency (Roderick & Coors, 2005).

Inverter input ripple current has been reported to possibly degrade fuel cell performance and reduce operating life of fuel cells if ripple currents are not adequately controlled (Rekha & Radman, 2007), however analysis and minimization technique have been developed for designing reliable fuel cell power systems (Shireen el ta, 2006).

- has an output voltage that varies with load and age,
- has limited overload capacity,
- has an output voltage range that is always too low in relation to the power it puts out for efficient use,
- is slow to respond to load change if the fuel supply is adjusted for best efficiency,
- needs considerable parasitic power for pumps, blowers or for heating at start-up,

- is slow to start up,
- will not absorb any power and
- may not accept any ripple (Lesster, 200).

3.7 Comparison between Fuel Cells Technology

The fuel cell types described in previous subchapters have significantly different operating regimes. As a result hardware materials, fabrication technique, and system requirements differ. These distinctions result in individual advantages and disadvantages that govern the potential of the various cells to be used for different applications.

The PEMFC, like the SOFC, have a solid electrolyte. In contrast to the SOFC, the PEMFC cell operates at a low temperature of approximately 80°C. This result in a capability to bring the cell to its operating temperature quickly, but the rejected heat cannot be used for cogeneration or additional power generation. The PEMFC can operate at very high current densities compared to other fuel cells technology. However, heat and water management issues may limit the operating power density of a practical system. The PEMFC have problem with carbon monoxide poisoning of the catalyst but increasing the temperature can solve this problem to some extent.

The most advantageous characteristics of the AFC include its excellent performance on hydrogen and oxygen compared to other fuel cells technology due to its active oxygen electrode kinetics and its flexibility to use a wide range of electro catalyst. Disadvantage of AFC is that the strongly alkaline electrolytes (NaOH, KOH) absorb carbon dioxide, which ultimately reduces electrolyte conductivity. This means that impure hydrogen cannot be used as a fuel, and air has to be free of carbon dioxide prior to use as the oxidant in the AFC.

The PAFC cathode's slow oxygen reaction rate cause lower cell performance than the AFC and the cell still requires hydrocarbon fuels to be reformed into a hydrogen-rich gas. The PAFC system efficiency improved because of its higher operating temperature and simple fuel conversion (no membrane and attendant pressure drop). Also the need for scrubbing carbon dioxide from the processed air is eliminated.

Two high-temperature fuel cells (SOFC and MCFC), have two major advantages over low-temperature types. First, they can achieve high electrical energy conversion

efficiency which makes them particularly attractive for efficient stationary power generation. Second, the high operating temperatures allow direct internal processing of fuel s such as natural gas. This reduces the system's complexity compared with low-temperature power plants, which requires hydrogen generation in an additional process step. The PAFC and PEMFC units tend to use precious metal catalysts, while catalysts of the MCFC and SOFC units are typical nickel based, which tremendously reduces the cost. In addition, higher-temperature fuel cells can electrochemically react with hydrogen as well as other fuels (e.g. Carbon monoxide and methane). Table 3.1 summarizes the characteristics of five main types of fuel cells technology discussed in this thesis (EG&G Technical Services, 2002)

Table 3.1 Characteristics of Five Main Types of Fuel Cell Technology

	PEMFC	AFC	PAFC	MCFC	SOFC
Type of Electrolyte	H^+ ions (with anion bound in polymer membrane)	OH^- ions (typically aqueous KOH solution)	H^+ ions (H_3PO_4 solution)	CO_3^{2-} ions (typically molten $LiKaCO_3$ eutectics)	O^{2-} ions (stabilized ceramics matrix with free oxide ions)
Typical Construction	Plastic, Metal, or Carbon	Plastic, Metal	Carbon, Porous Ceramics	High Temperature Metals, Porous Ceramics	Ceramics, High Temperature Metals
Internal Reforming	No	No	No	Yes, Good Temperature Match	Yes, Good Temperature Match
Operational Temperature	65-85°C	90-260°C	190-210°C	650-700°C	750-1000°C
Oxidant	Air to Oxygen	Purified Air to Oxygen	Air to Enriched Oxygen	Air	Air
DG System Level Efficiency, % HHV	25 to 35%	32 to 40%	35 to 45%	40 to 50%	45 to 55%
Primary Contaminate Sensitivity	CO, Sulphur, and NH_3	CO, CO_2, and Sulphur	CO<1%, Sulphur	Sulphur	Sulphur

The ideal performance of a fuel cell depends on the electrochemical reactions that occur between different fuels and oxygen as summarized in table 3.2 under the pressure of 1 atm (EG&G Technical Services, 2002).

Table 3.2 Ideal Voltage as a Function of Cell temperature under 1 atm pressure

Temperature	25	80	100	205	650	1000
Cell Type		PEMFC	AFC	PAFC	MCFC	SOFC
Ideal Voltage	1.23	1.17		1.14	1.03	0.91

Low-temperature fuel cells (PEMFC, AFC and PAFC) require noble metal electro catalysts to achieve practical reaction rates at the anode and cathode, and hydrogen is the only acceptable fuel. With high-temperature fuel cells (SOFC and MCFC), then requirements for catalysis are relaxed, and the number of potential fuels expands. While carbon monoxide poison a noble metal anode such as platinum in low temperature fuel cells, it compares with hydrogen as a reactant fuel cells where non-noble metal catalysts such as nickel can be used.

3.8 Conclusion

Fuel cells can convert a remarkably high proportion of the chemical energy in a fuel to electrical energy. With the efficiencies approaches 60%, even without co-generation, fuel cell power plants are nearly twice as efficient as convectional power plants. Unlike large steam plants, the efficiency is not a function of the plant size for fuel cell power plants. Small-scale fuel cell plants are just as efficient as small ones, whether they operate at full load or not. Fuel cells contribute significantly to the cleaner environment; they produce dramatically fewer emissions, and their by-products are primarily hot water and carbon dioxide in small amounts. Because of their modular nature, fuel cells can be placed at or near load centres, resulting in savings of transmission network expansion.

CHAPTER 4

MODELLING AND CONTROL

4.1 Introduction

This chapter describes the models and control of fuel cells system and dc-dc power converter. Both dynamic and static models of fuel cells system are provided for analysis and simulation purposes. Analysis of a dc-dc power boost converter is provided for both continuous and discontinuous conduction modes. The control scheme to achieve adequate regulation is examined and appropriate control laws are developed.

4.2 Fuel cells

The non-linearity voltage-current characteristics of fuel cell system make it not an ideal voltage source. Their electrical characteristics cannot be completely ignored during the modelling process. The output voltage of a typical fuel cell system varies with loads and fuel flow rate.

The output voltage variation of the fuel cell results in an input variation to the inverter. This means that the inverter should not only have good audio susceptibility, but also resilient to large signal changes in input voltage. Depending on the fuel cell stack, the hydrogen flow rate may change according to the load in attempt to operate the fuel cell in its most efficient region. This change in hydrogen flow may involve mechanical valves and other relative slow processes, which are controlled on the fuel cell side. Therefore, the response of the fuel cell may be slow to change in inverter load, and it may require some communication from the inverter.

4.2.1 Fuel Cells Modelling

From the electrical point of view, the simplest approach to model a fuel cell system is to assume that its characteristics are completely linear. Then the fuel cell can be viewed as an ideal voltage source with a series resistance proportional to the gradient of the middle region of the fuel cell voltage-current curve. An ideal diode can be added to prevent current from flowing into the fuel cell stack, as shown in figure 4.1. This model is accurate enough through the majority of the operating region of the fuel cell and is a very good approximation. If the fuel cell has a slow response time as most fuel cell

system do, a small capacitor is added to give the voltage source a time constant as shown in figure 4.2.

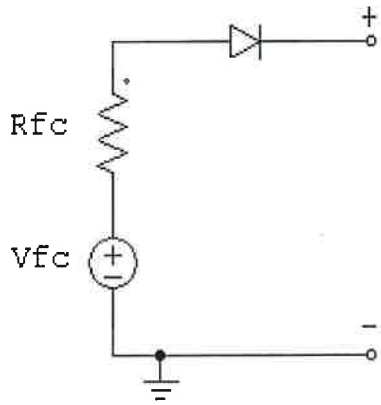

Figure 4.1 First Order Model of Fuel Cell Model without Delay

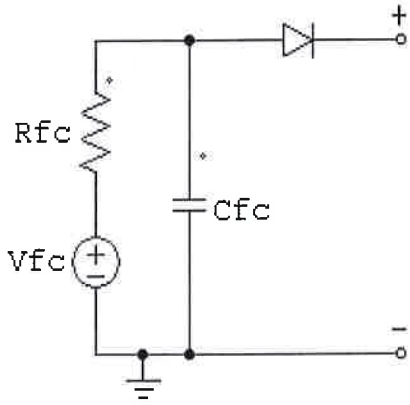

Figure 4.2 First Order with Delay

A more accurate electrical model of a fuel cell can be developed (G Fontes, C Turpin, S Astier & T A Meynard, 2007). The non-linear model requires current feedback and uses conditional equations to determine the output voltage. Other parameters such as temperature, pressure and hydrogen levels can be incorporated into the cell model (Haiping Xu, Li Kong & Xuhui Wen, 2004). A block diagram version of this model is shown in figure 4.3

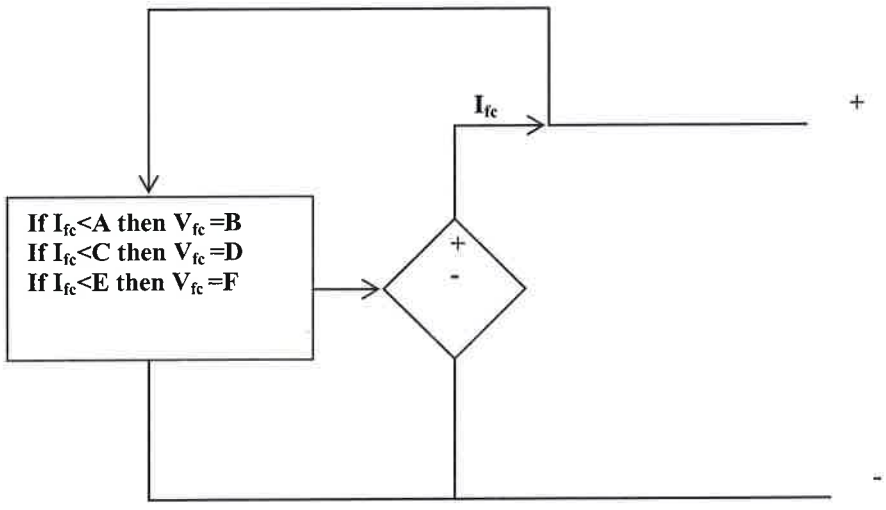

Figure 4.3 Higher Order Model of Fuel Cell

4.3 Non-Isolated Dc-Dc Boost Converter Modelling

The method used in this project for modelling the Dc-Dc converter bridges the gap that exist between the state-space technique which rely on the domain of equation manipulations and averaging method which is based on equivalent circuit manipulations. The formal method primary advantage is in the unified description of all power converter stages regardless of the topology while the latter method provides the designer the distinct advantage of physical insight into the behaviour of the original switched circuit. State-space averaged modelling technique offers the advantages of both methods. The basic dc-dc conversion function of switching converters is achieved by switching between two linear networks consisting of ideally lossless storage elements, inductances and capacitors. In practice, this function may be obtained by use of transistors and diodes which operates as synchronous switches. The general equations for steady-state (dc) and dynamic performance (ac) as well as important transfer functions can be developed.

Figure 4.4 below is a boost converter that produces an output voltage that is always greater than the input supply. The switching dc-dc converter only operates in two distinct

stages described as ON state and OFF state because it is assumed to be operating in the conduction mode. These two stages are shown in figures 4.5 and 4.6.

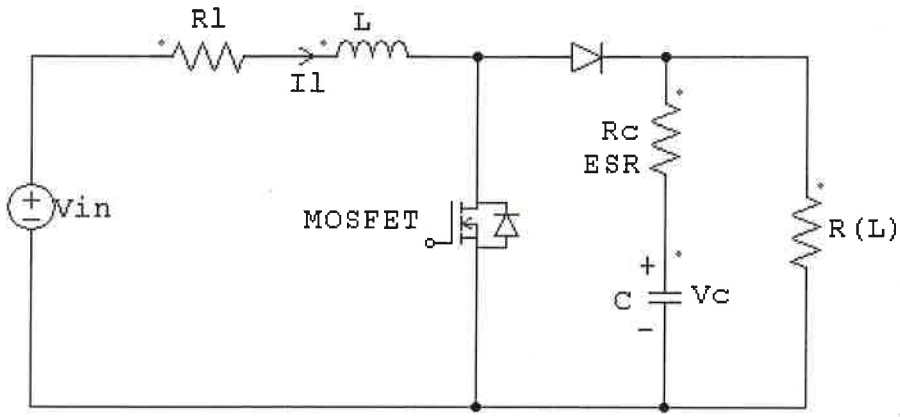

Figure 4.4 Non Isolated Dc-Dc Boost Converters Topology

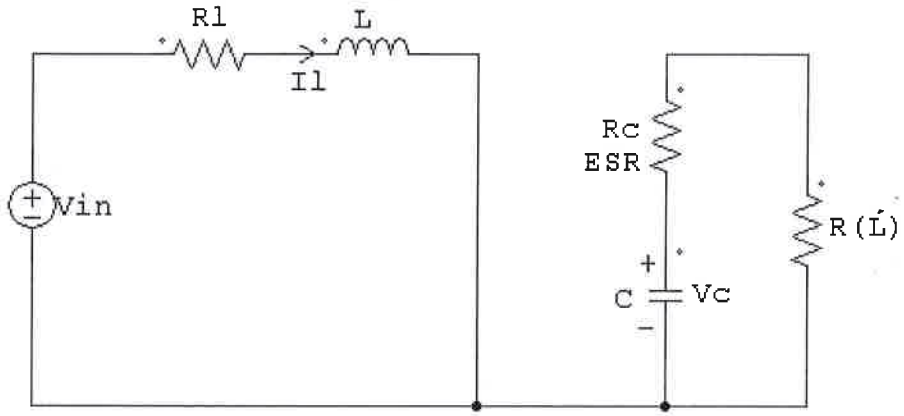

Figure 4.5 ON State of a Non Isolated Dc-Dc Boost Converter Topology

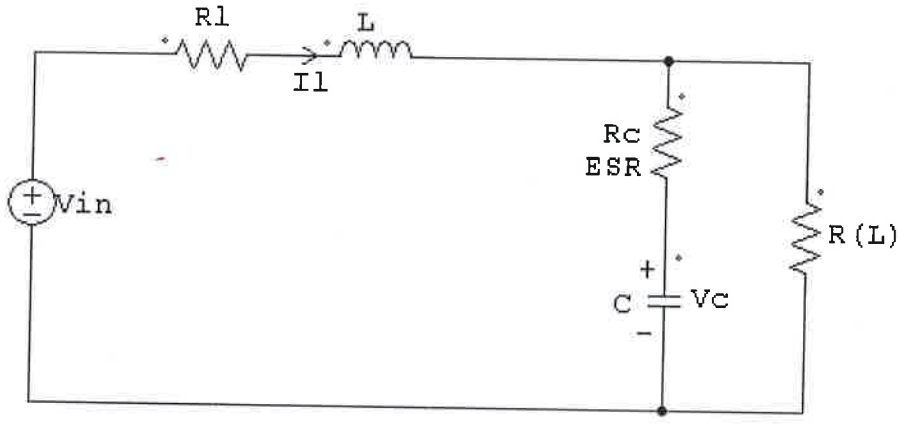

Figure 4.6 OFF State of a Non Isolated Dc-Dc Boost Converter Topology

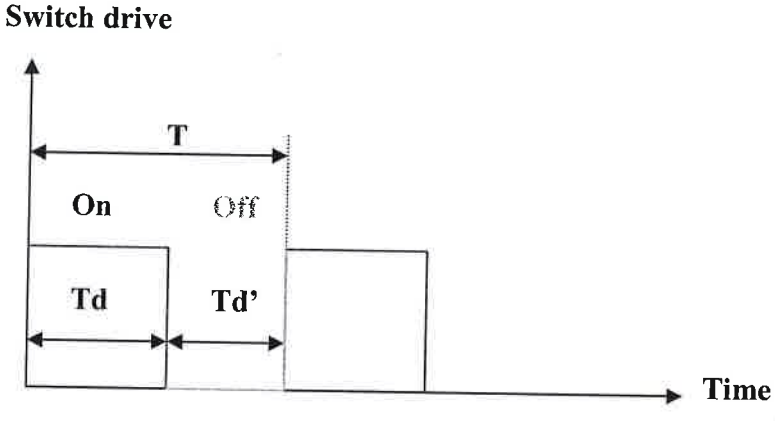

Figure 4.7 ON and OFF Time Durations

4.3.1 Ideal Dc-Dc Boost Converter Analysis

Analysis of the circuit is carried out based on the following assumptions. The circuit is ideal. It means that when the switch is ON, the voltage drop across it is zero and the current through it is zero when it is open. The diode has zero voltage drops in the conducting state and zero current in the reverse-bias mode. The time delays in switching on and off the switch and the diode are assumed to be negligible. The inductor and the capacitor are assumed to be lossless.

The responses in the circuit are periodic. It means especially that the inductor current is periodic. Its value at the start and end of a switching cycle is the same. The net increase

in inductor current over a cycle is zero. If it is non-zero, it would mean that the average inductor current should either be gradually increasing or decreasing and then the inductor current is in a transient state and has not become periodic.

It is assumed that the switch is made ON and OFF at a fixed frequency and let the period corresponding to the switching frequency is T. Given that the duty cycle is d, the switch is on for a period equal to DT, and the switch is off for a time interval equal to (1 - D)T. The inductor current is continuous and is greater than zero.

The capacitor is relatively large. The RC time constant is so large, that the changes in capacitor voltage when the switch is ON or OFF can be neglected for calculating the change in inductor current and the average output voltage. The average output voltage is assumed to remain steady, except when the change in output voltage is calculated. The source voltage VS remains constant.

4.3.2 Inductor Current with Switch Closed

When the switch is closed, the equivalent circuit that is applicable is shown in Fig. 4.5. The source voltage is applied across the inductor and the rate of rise of inductor current is dependent on the source voltage Vin and inductance L. The differential equation describing this condition is:

$$L\frac{di_l}{dt} = Vin(t) \qquad 4.3.1$$

If the source voltage remains constant, the rate of rise of inductor current is positive and remains fixed, so long as the inductor is not saturated. Then equation (4.3.1) can be expressed as:

$$\frac{\Delta i_l}{\Delta t} = \frac{Vin(t)}{L} \qquad 4.3.2$$

The switch remains ON for a time interval of DT in one switching cycle and hence DT can be used for t. The net increase in inductor current when the switch is ON can be obtained from equation (4.3.2) to be:

$$\Delta I_l = \frac{Vin(t)}{L} \times (dT) \qquad 4.3.3$$

4.3.3 Inductor Current with Switch Open

When the switch is open, the circuit that is applicable is shown in Fig. 4.6. Now the voltage across the inductor is equation 4.3.3 if the output voltage is Vo.

$$v_l = Vin - Vo \qquad 4.3.4$$

Given that the output voltage is larger than the source voltage, the voltage across the inductor is negative and the rate of rise of inductor current, described by equation (4.3.3), is negative. Hence if the switch is held OFF for a time interval equal to (1 - D) T, the change in inductor current can be computed as shown in equation (4.3.6)

$$\frac{di_l}{dt} = \frac{Vin - Vo}{L} \qquad 4.3.5$$

$$\Delta I_l = \frac{Vin - Vo}{L} \times (1 - D)T \qquad 4.3.6$$

The change in inductor current reflected by equation (4.3.6) is a negative value, since Vo > VS. Since the net change in inductor current over a cycle period is zero when the response il(t), the sum of net changes in inductor current expressed by (4.3.4) and (4.3.6) should be zero. That is,

$$\frac{Vin}{L} \times DT + \frac{Vin - Vo}{L} \times (1 - D)T = 0 \qquad 4.3.7$$

On simplifying equation (4.3.7), we get that

$$Vo = \frac{Vin}{1 - D} \qquad 4.3.8$$

It has been stated that when $i_l(t)$ is periodic, the net change in inductor current over a cycle is zero. Since change in inductor current is related to its volt-seconds, the net volt-seconds of the inductor have to be zero. The expression for the net volt-seconds can be obtained from equation (4.3.6) and it can be seen that the numerator of equation (4.3.7) should be zero. That is,

$$Vin \times DT + (Vin - Vo) \times (1 - D)T = 0 \qquad 4.3.9$$

The value of d varies such that 0 < D < 1 and it can be seen from equation (4.3.8) that output voltage is greater than the source voltage, and hence this circuit is called the boost converter. The output voltage has its lowest value when D = 0 and then the output voltage equals the source voltage. When d approaches unity, output voltage tends to infinity. Usually d is varied in the range 0.1 < D< 0.9. Figure 4.8 depicts the graphical relationship between the conversion ratio and duty cycle.

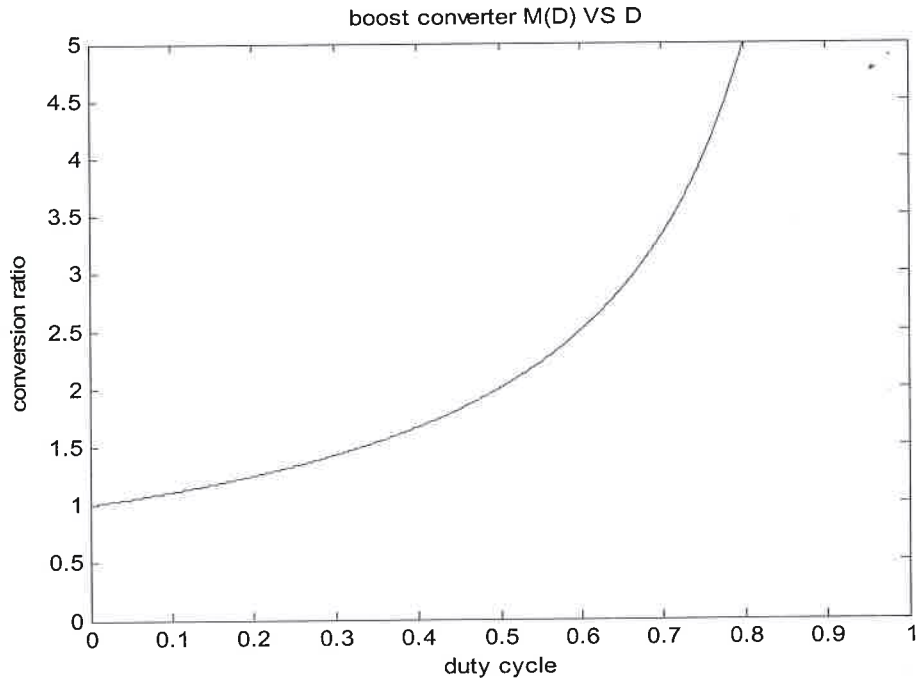

Figure 4.8 A Graphical Relationship Between Conversion Ratio and Duty Cycle of a Boost Converter.

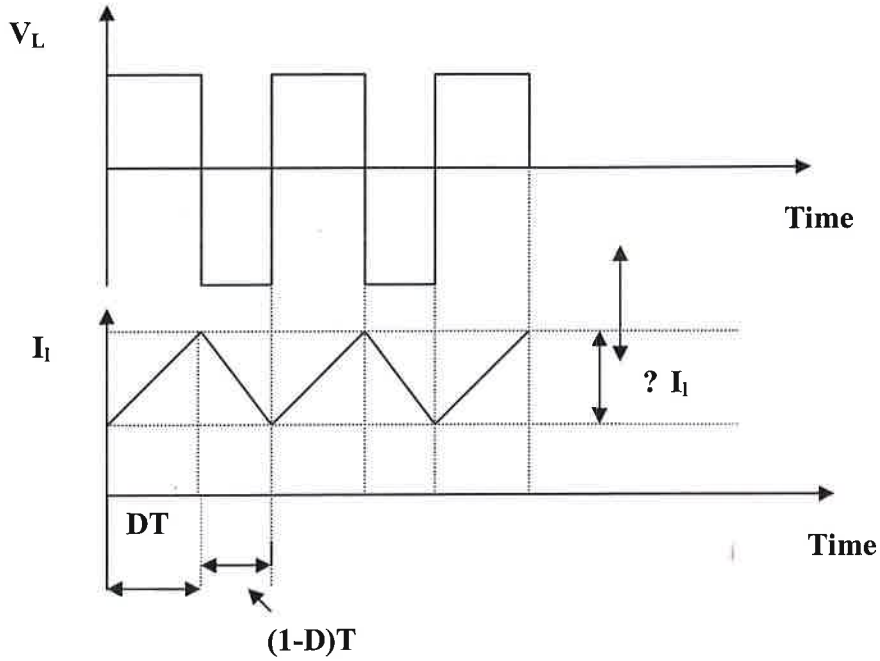

Figure 4.9 Waveforms of Inductor Voltage and Inductor Current.

The waveforms of inductor voltage and inductor current are shown in Fig. 4.9. These waveforms are drawn assuming that both the output and the source voltage remain steady. These waveforms illustrate how the inductor voltage is related to its current.

4.3.4 Output Voltage Ripple with Switch Closed

In this sub-section, the change in output voltage is calculated. It needs to be emphasized that the peak-to-peak ripple in output voltage is quite small for a well-designed circuit. For the inductor, the net change in inductor current over a cycle is zero when $i_l(t)$ is periodic. For the capacitor, the net change in capacitor voltage over a cycle is zero when it is periodic. When the switch is closed, the equivalent circuit in Fig. 4.5 shows that the boost converter is split into two sub-circuits, with the loop currents decoupled from each other. When the switch is closed, the output voltage is sustained by the capacitor. During this period, the capacitor discharges part of its stored energy and it re-acquires this energy when the switch is open. When the switch is open, part of

the inductor current charges the capacitor since the inductor current usually remains larger than the current through the load resistor. From Fig. 4.4,

$$i_c = C\frac{dVo(t)}{dt} \qquad 4.3.10$$

When the current through a capacitor charges it up, its rate of rise of capacitor voltage is positive since the capacitor voltage is increasing. When the switch is open, the capacitor is discharging its energy with its voltage falling and the current through the capacitor is then a negative value. The output voltage remains positive and hence the output current is positive and it is the negative of the capacitor current, as can be seen from Fig. 4.4. Since the change in output voltage is quite small, it can be assumed that the load current remains constant at its average value and equation (4.3.10) can be now expressed as:

$$i_{c(t)} \approx -\frac{Vo}{R} \qquad 4.3.11$$

When the capacitor current is constant, its voltage changes linearly with time. Here the period for which the switch is closed is DT and the DT can be used in place of ?and the peak-to-peak ripple in output voltage expressed as ∇o is then:

$$_{\Delta vo} = i_c \times (DT) = -\frac{Vo}{R} \times (DT) = -\frac{dVo}{fR} \qquad 4.3.12$$

Equation (4.3.12) yields the value of the peak-to-peak ripple in output voltage. In equation (4.3.12), 1/f replaces T since T is the reciprocal of switching frequency.

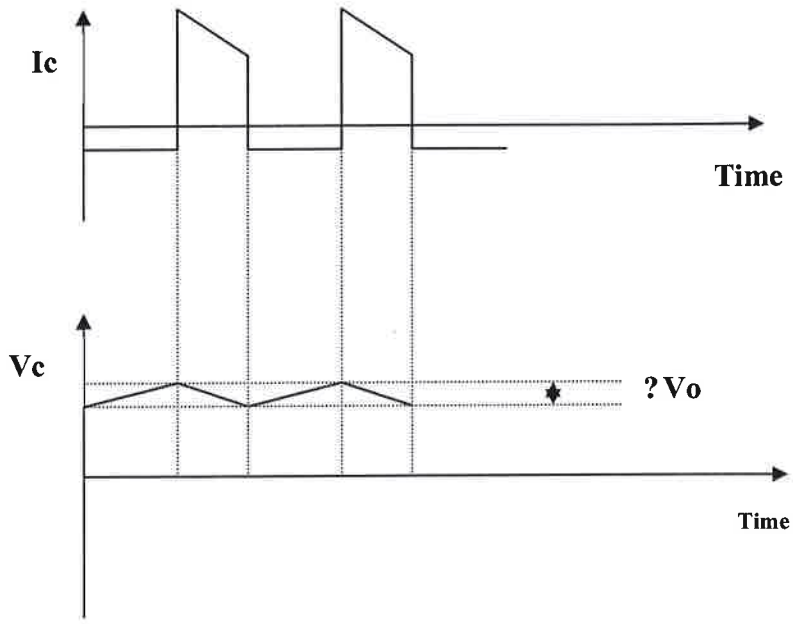

Figure 4.10 Waveforms of Capacitor Current and Capacitor Voltage.

Figure 4.10 shows how the capacitor current and voltage vary over a cycle. The ripple in output voltage is exaggerated in Fig. 4.10, whereas in practice it would be much smaller. If the output voltage is drawn to scale, the ripple in output voltage would not be noticeable.

4.3.5 Average Inductor Current Expression

The average inductor current can be found out by equating the power drawn from the source to the power delivered to the load resistor. Again the ripple in output voltage is ignored and it is assumed justifiably that the output voltage remains steady at its average value. Power Po absorbed by load resistor is then:

$$P_o = \frac{(Vo)^2}{R} \qquad 4.3.13$$

It can be seen from the circuit in Fig. 1 that the current drawn from the source flows through the inductor. Hence the average value of inductor current is also the average

value of source current. Let the average inductor current be IL. Then power Pin supplied by the source is then:

$$P_{in} = Vin \times I_l \qquad 4.3.14$$

After equating equations (4.3.13) and (4.3.14), we get the average inductor current as:

$$I_l = \frac{(Vo)^2}{Vin \times R} \qquad 4.3.15$$

Since load current Io is:

$$I_o = \frac{Vo}{R} \qquad 4.3.16$$

Using equations (4.3.8) and (4.3.16), equation (4.3.15) can be re-presented as:

$$I_l = \frac{Io}{1-D} \qquad 4.3.17$$

Since 0 < D < 1, it can be seen from equation (4.3.17) that $I_l > Io$.

4.3.6 Continuous Conduction Mode

The analysis thus so far is based on the assumption that the current through the inductor is continuous. The inductor current varies over a cycle, varying between a minimum value and a maximum value. The minimum and maximum values can be expressed in terms of its mean value and its change as expressed in equation (4.3.3). That is,

$$I_{l,\max} = I_l + \frac{\Delta I_l}{2} \qquad 4.3.18$$

and

$$I_{l,\min} = I_l - \frac{\Delta I_l}{2} \qquad 4.3.19$$

It is shown in Fig. 4.11 how the maximum and the minimum inductor current can be obtained. It is also shown that as the load resistor becomes greater, the average inductor current reduces, but the peak-to-peak ripple in inductor current does not change. It has to be so and expression for ?Il in equation (4.3.3) does not indicate any term reflecting the load resistor.

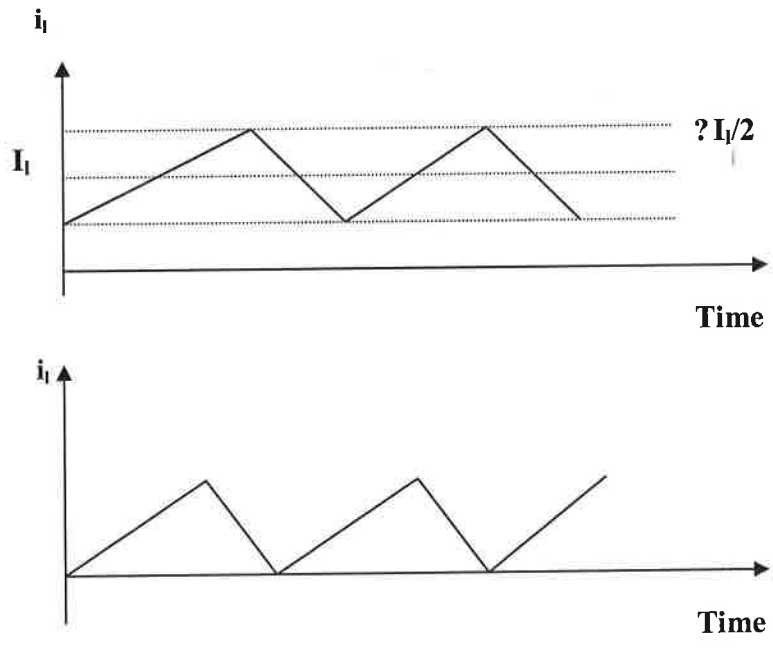

Figure 4.11 Inductor Currents for Continuous Conduction Mode and Boundary Condition Mode.

For continuous conduction,

$$I_l > \frac{\Delta I_l}{2} \qquad 4.3.20$$

At the boundary of continuous and discontinuous conduction,

$$I_l = \frac{\Delta I_l}{2} \qquad 4.3.21$$

Another expression for IL is now obtained. Substituting for Vo in equation (4.3.15) the expression in equation (4.3.8), we obtain that

$$I_l = \frac{Vin}{(1-D)^2 \times R} \qquad 4.3.22$$

Substituting for IL from the equation above and for ΔL from equation (4.3.3), equation (4.2.18) becomes:

$$I_{l,\max} = \frac{Vin}{(1-D)^2 \times R} + \frac{(DT)Vin}{2L} \qquad 4.3.23$$

and

$$I_{l,\min} = \frac{Vin}{(1-D)^2 \times R} - \frac{(DT)Vin}{2L} \qquad 4.3.24$$

From equations (4.3.23) and (4.3.24), the condition for continuous conduction is:

$$\frac{Vin}{(1-D)^2 \times R} > \frac{(DT)Vin}{2L}, or$$
$$f > \frac{Rd(1-D)^2}{2L} \qquad 4.3.25$$

Expressions (4.3.25) can be interpreted as follows, assuming that only one of the four parameters is varied at a given time with the other three parameters remaining unchanged.

The circuit tends to become discontinuous,

- if the switching frequency f is decreased, or
- if the duty cycle D is reduced, or
- if the load resistance increases, or
- if the inductance used has lower value

4.3.7 Discontinuous Conduction Mode

When the conduction is discontinuous, the voltage across the inductor is zero for part of the cycle since there is no current through the inductor. Let D_1T be the time for which the switch is ON in one cycle and let D_2T be the period for which the diode conducts. The waveforms relevant to the inductor when the conduction is discontinuous are shown in Fig. 4.12. Since the conduction is discontinuous,

$$D_1 + D_2 < 1 \qquad 4.3.26$$

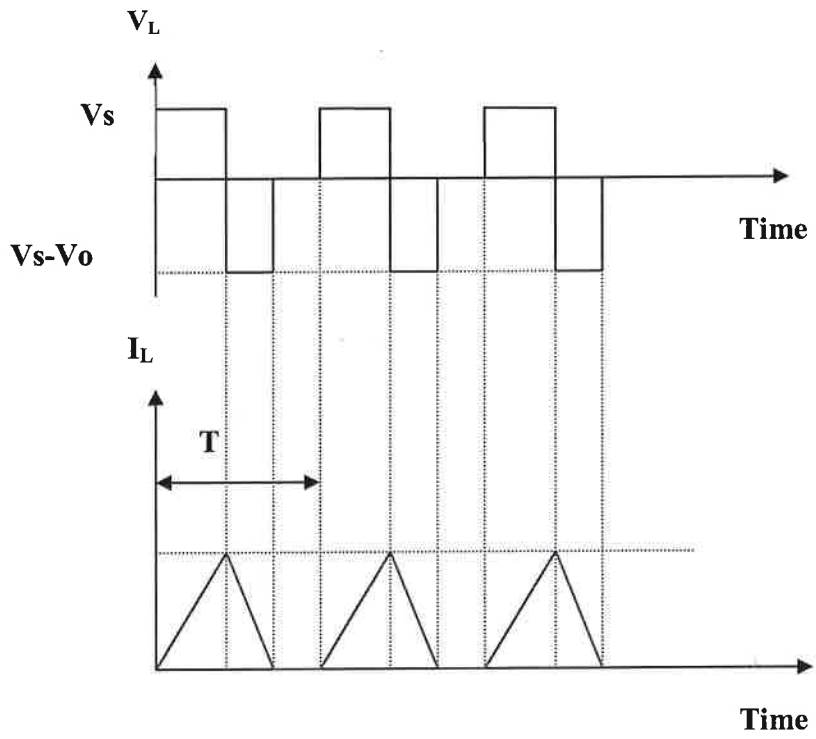

Figure 4.12 Inductor Voltage and Inductor Current for Discontinuous Conduction Mode

An expression for the output voltage can be obtained in terms of source voltage, duty cycle D1 of the switch and duty cycle D_2 of the diode. Since the net change in inductor current is zero over a cycle, the net volt-seconds area associated with the inductor is zero. From Fig. 4.12,

$$Vin \times D_1 T + (Vin - Vo) \times D_2 T = 0 \qquad 4.3.27$$

On simplifying, an expression for Vo can be obtained. Then

$$Vo = Vin \times \frac{(D_1 + D_2)}{D_2} \qquad 4.3.28$$

The value of d1, the duty cycle of the switch, is usually known, but the period for which the diode conducts is an unknown quantity depending on the other circuit parameters. The value of D2 can be determined in several ways. Here it is determined using the power balance between the input and output. When the circuit is ideal, the input power equals output power. Let the average source current be IS and the average output current be Io. Then

$$Vin \times I_s = Vo \times I_o \qquad 4.3.29$$

Using equation (4.2.28), we get that

$$I_s = I_o \times \frac{(D_1 + D_2)}{D_2} = \frac{Vo}{R} \times \frac{(D_1 + D_2)}{D_2} = \frac{Vs}{R}\left(\frac{D_1 + D_2}{D_2}\right)^2 \qquad 4.3.30$$

The average source current be I_S can be obtained from Fig. 4.12. The average source current is the same as the average inductor current. Let the peak inductor current be ?IL and the period for which this current flows is ($D_1T + D_2T$). This period is the base of the triangle that defines the inductor current. The average inductor current is obtained as the area of this triangle divided by the cycle period. We have that

$$I_s = \Delta I_l \times \frac{(D_1 + D_2)}{2} \qquad 4.3.31$$

Equating equations (4.3.30) and (4.3.31),

$$\Delta I_l \times \frac{(D_1 + D_2)}{d_2} = \frac{Vs}{R}\left(\frac{D_1 + D_2}{D_2}\right)^2 \qquad 4.3.32$$

From equation (4.3.3),

$$\Delta I_l = \frac{D_1 T V_s}{L} = \frac{D_1 Vs}{fL} \qquad 4.3.33$$

Substituting for ?I_l from equation (4.3.33) in equation (4.3.32), we get that

$$\frac{D_1}{2fL} = \frac{(D_1 + D_2)}{R \times (D_2)^2} \qquad 4.3.34$$

Equation (4.3.34) can be re-written as:

$$(D_2)^2 = \frac{2fL}{R \times D_1} \times (D_1 + D_2) \qquad 4.3.35$$

Solving for d_2,

$$d_2 = \frac{fL}{R \times D_1} \times \left[1 + \sqrt{1 + \frac{2R(D_1)^2}{fL}}\right] \qquad 4.3.36$$

Equation (4.3.36) states how d_2 varies as a function of R, d_1, f and L. Once D_2 is known, V_o can be obtained from equation (4.3.28).

It is possible to get an expression for V_o as a function of R, d_1, f and L. For this, we equate the average load current with the average diode current. The average output current can be obtained from the average output voltage and the load resistor. The average diode current is:

$$I_{D,avg} = \Delta I_l \frac{D_2}{2} \qquad 4.3.37$$

Using the expression for ?I_L from equation (4.3.33), and replacing the L.H.S. by the average load current,

$$\frac{Vo}{R} = \frac{VinD_1D_2}{2fL} \qquad 4.3.38$$

Hence we obtain that

$$d_2 = \frac{2fL}{RD_1} \times \frac{Vo}{Vs} \qquad 4.3.39$$

By substituting for d_2 from equation (4.3.36) in the above equation, we can get an expression for Vo/VS. Alternatively, equation (4.3.28) can be re-written as:

$$\frac{Vo}{Vs} = 1 + \frac{D_1}{D_2} \qquad 4.3.40$$

Using the expression for d_2 from equation (4.3.39) in equation (4.3.40),

$$\frac{Vo}{Vs} = 1 + \frac{R(D_1)^2}{2fL \times \left(\frac{Vo}{Vs}\right)} \qquad 4.3.41$$

That is,

$$\left[\frac{Vo}{Vs}\right]^2 - \frac{Vo}{Vs} = \frac{R(D_1)^2}{2fL} \qquad 4.3.42$$

Solving for the ratio of output to source voltage and taking the positive root of the expression on the R.H.S. of equation (4.3.42),

$$\frac{Vo}{Vs} = \frac{1}{2} \times \left[1 + \sqrt{1 + \frac{2R(D_1)^2}{fL}}\right] \qquad 4.3.43$$

Equation (4.3.43) states how (Vo/VS) varies as a function of R, D_1, f and L

The critical resistance at a given duty cycle can be expressed as

$$R_c = \frac{2fL}{D_1 \times (1 - D_1)^2} \qquad 4.3.44$$

4.4 Isolated Dc-Dc Boost Converter Analysis

The second stage Dc-Dc boost converter is required to step-up the regulated 60V output voltage of the first stage Dc-Dc boost converter to a nominal voltage of 350V, as shown in figure 4.13. The full-bridge type is a topology of choice with which a phase-shift PWM technique can be implemented.

The phase shift control can achieve zero voltage, reducing the losses in the switch and therefore increasing system efficiency. High frequency transformers are employed to allow the 60V output voltage of the first stage converter to be boosted to 350V for the Dc link to the inverter and for its smaller size.

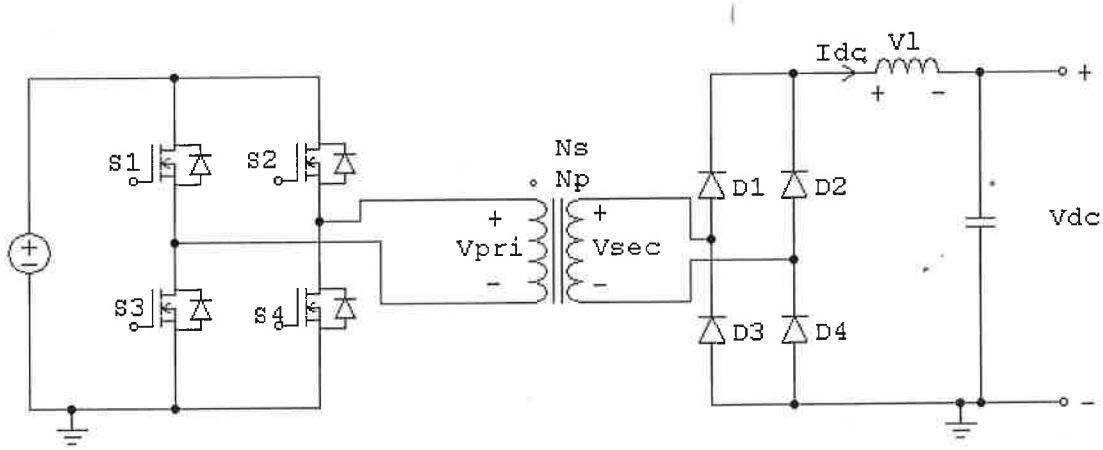

Figure 4.13 Schematic Diagram of Second Stage Dc-Dc Boost Converter

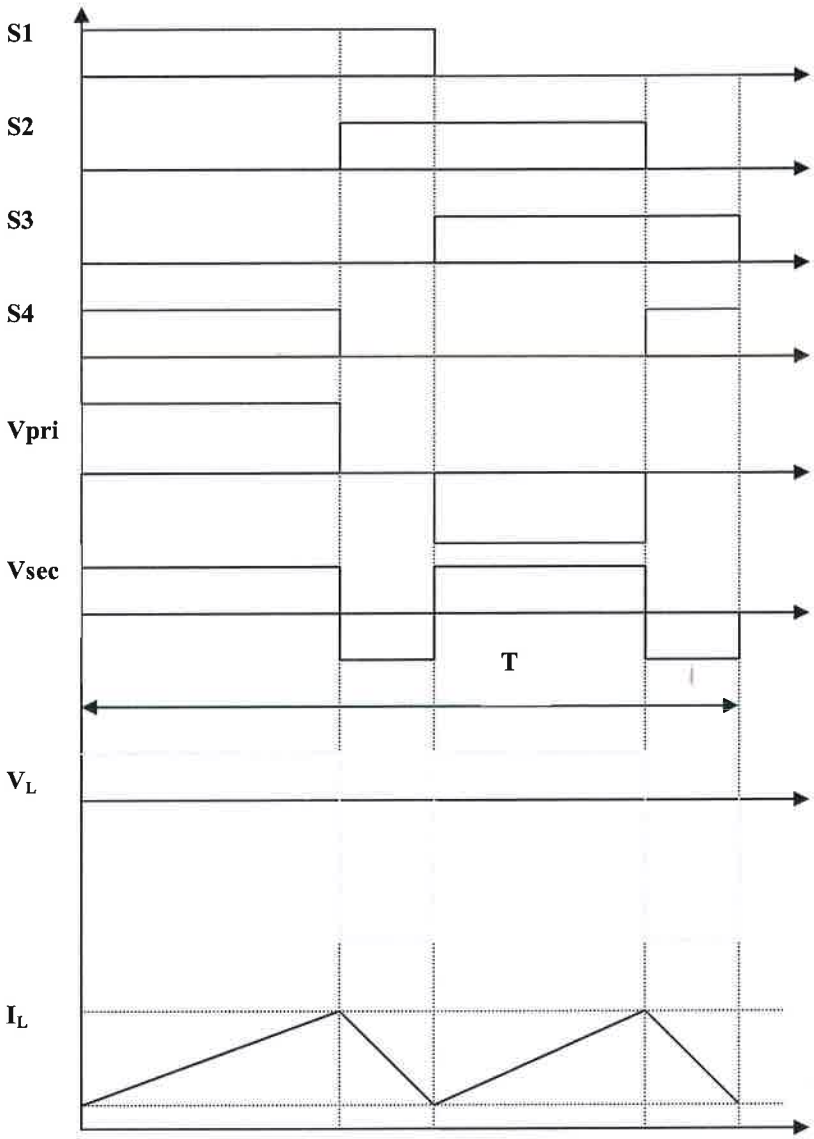

Figure 4.14 Switching waveforms, Primary and Secondary Voltages, load voltage and current waveforms

Four interleaved Dc-Dc boost converters was connected in parallel in parallel-input parallel-output configuration. Four high frequency transformers connected in parallel supply the four parallel connected diodes bridges. Each of the transformers is rated one quarter of the total power converter rating. This configuration reduces the leakage inductances and therefore reduces the duty cycle. The reduce duty loss also reduces turns ratio of the transformer. This reduces the voltage rating of diodes in the secondary

side of the second stage boost converter and current rating of MOSFETs in the primary side. Figure 4.14 shows the main waveforms of the second stage Dc-Dc converter.
From the inductor voltage V_L equation for the second-volt of the inductor can be expressed as

$$(Vin \times \frac{Ns}{Np} - V_{dc}) \times DT = V_{dc} \times \left(\frac{T(1-D}{2}\right) \quad 4.3.45$$

Therefore, the duty cycle of the proposed second stage Dc-Dc boost converter is obtained by

$$D = \frac{N_p \times V_{dc}}{2 \times N_s \times V_{in}} \quad 4.3.46$$

4.5 Control Scheme

In general switching converters can be controlled by one of the following methods

- Varying the frequency of switching, while keeping the on and off time durations constant.
- Varying the on and off durations of the switch while keeping the frequency constant.
- Varying both the on and off durations of the switch as well as the frequency of switching.

Variation in the switching frequency makes it difficulty to filter the ripple components in the input and output waveforms of the converter. Thus methods involving frequency variations are not commonly used. Figure 4.15 depicts a block diagram of PWM showing relevant building blocks that can be used in switching power converter. The most common method of controlling the on and off durations of the switch in a power converter is called Pulse Width Modulation (PWM). In PWM control scheme, the switch control signal is generated by applying a gain to the difference or error, between the actual output voltage and the desired output voltage. This method can very easily be

implemented to generate a regulated output voltage. Figure 4.16 shows the generation of PWM signal.

The frequency of the repetitive waveform with a constant peak, which is shown to be a saw tooth, establishes the switching frequency. This frequency is kept constant in a PWM control and is chosen to be a few kilohertz range. When the amplified error signal, which is varies very slowly with time to the switching frequency, is greater than the saw tooth waveform, the switch control signal becomes high, causing the switch to turn on. Otherwise the switch is off. In terms of V (control) and the peak of the saw tooth waveform V_{st} in figure 4.16, the switch duty ration can be expressed as

$$D = ton/T = V\ control/V_{st} \qquad 4.3.47$$

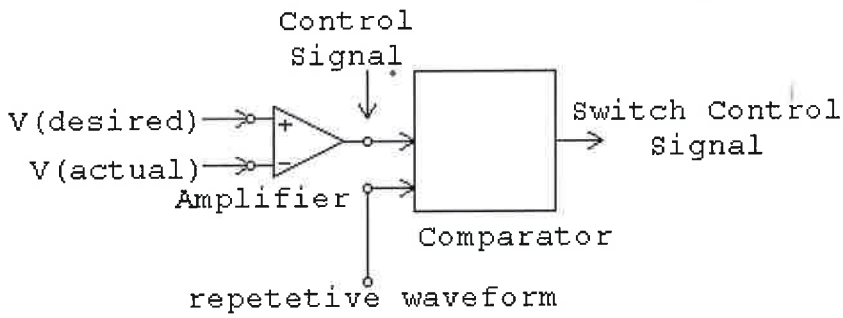

Figure 4.15 Pulse Width Modulation Block Diagram

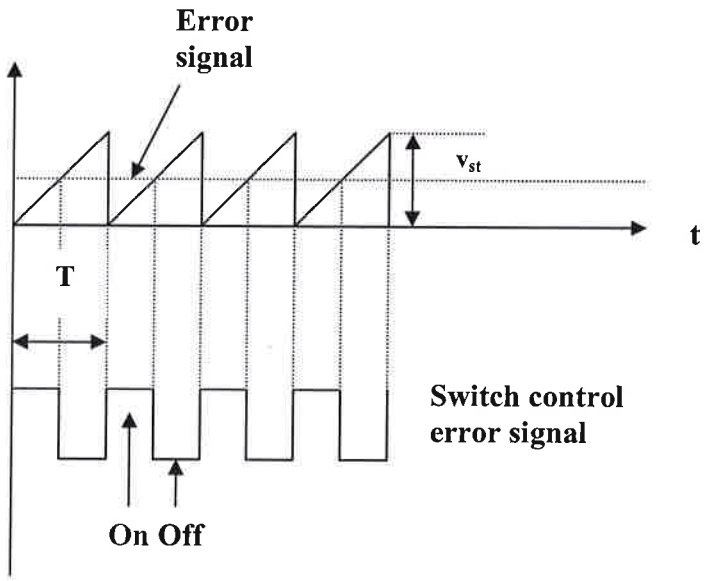

Figure 4.16 Pulse Width Modulation Comparator Signals

Another method of generating PWM signals is called Current Mode Control, whereby a second loop is used to control the inductor current. There are several different ways in which this can be done, the most common being constant frequency control whereby the switch is turned on at a constant frequency. To achieve this, the error signal from the loop compensator is used as a reference to be compared with the peak current signal and a sawtooth waveform. This means that the error voltage now determines the output current, not the voltage. The advantage of this approach is simple. Since it compares current, it is unaffected by device parasitics. This means that it can be used in paralleling of converters by setting the same error voltage to each converter hence resulting in equal current sharing.

Both these methods of control are most commonly and traditionally implemented using analogue techniques. However, due to fairly difficult fine-tuning of the control loops to allow for converter parasitics and ensuring stability, there are significant advantages in controlling converters digitally. This can be done using microcontrollers, digital signal processing (DSP) chip or Application Specific Integrated Circuits (ASICs).

The advantages of digital control are vast since the control schemes can easily be developed in software. PID control loops can be tested and adjusted quickly to suit its

application with the possibility of added control features such as current limiting and sharing, under-voltage and over-voltage protection, etc. Digital controllers are also generally more reliable and less sensitive to temperature fluctuations.

4.5.1 Proportional Integral Control

The feedback loop of proposed converter is implemented in the simulation using Proportional Integral (PI) control method. The PI feedback control method adds positive corrections, removing the error from a system's controllable variable as shown in figure4.10. PI control method consists of two actions-the proportional action and the integral action. The proportional action involves multiplying the error with a negative constant (proportional gain) and adding the product to the controlled quantity. The principle of proportional action requires that the amount of change in the manipulated variable vary directly with the size of the error that is the proportional gain dictates the sensitivity of the correction action. The integral action involves integrating the error over a period of time and then multiplies with a negative constant (integral gain) and adding the product to the controlled quantity. Therefore, this action averages the measured error over a period of time to find the process output's average error from the desired value. Integral action brings the controlled variable back to the set point in the presence of a sustained upset or disturbance that is integral action acts to eliminate steady state error.

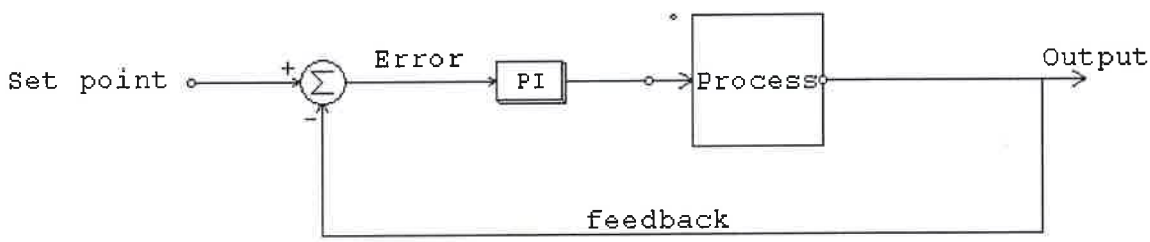

Figure 4.17 PI Control Scheme

4.5.2 Closed Loop Control Using PWM

Under this section, the closed-loop control of the ideal circuit is considered. For the boost converter, the output voltage increases as the duty cycle of the switch increases and vice versa, hence the PWM circuit can be used. The block diagram is shown in Fig. 4.17. A more detailed block diagram is shown in Fig. 4.18.

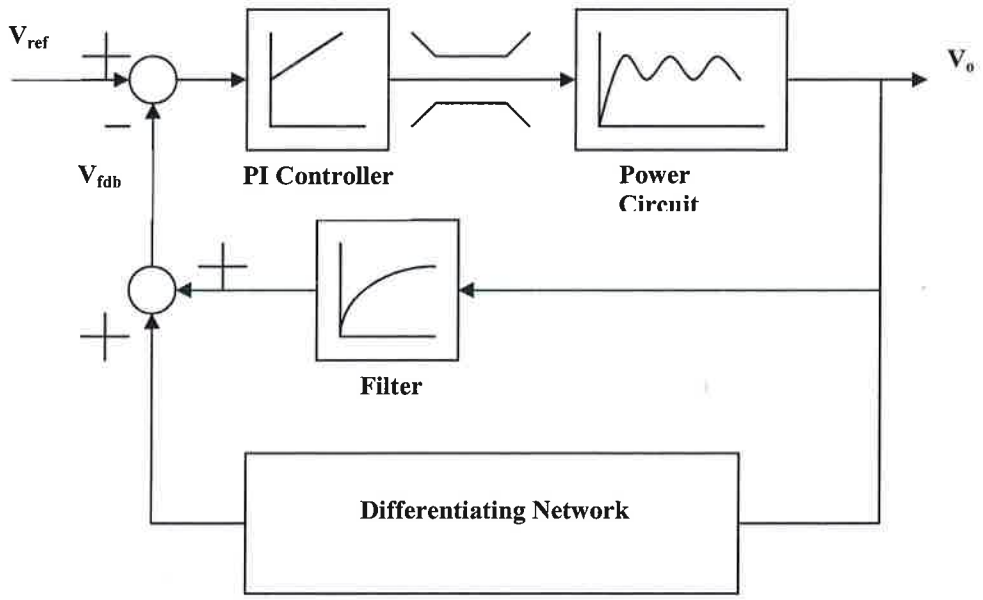

Figure 4.18 Block Diagram with a PI Controller

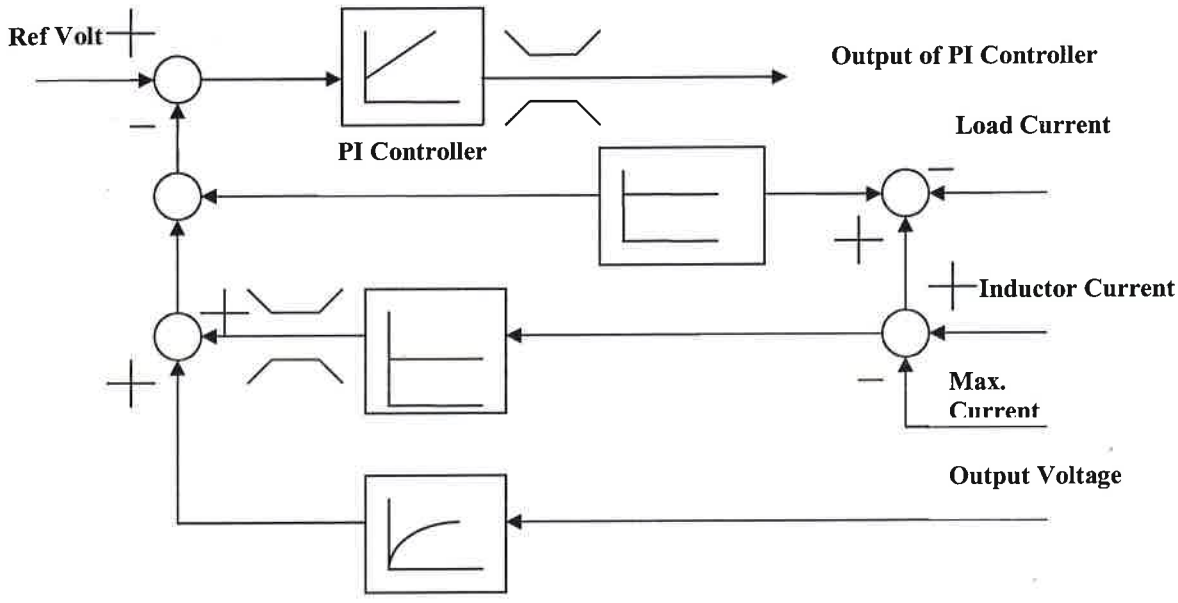

Figure 4.19 Feedback Arrangement

The transfer function of the circuit in open loop is obtained as outlined below by using an approximate method. Even though it is difficult to justify the approximation, it is presented. The output voltage is expressed by equation (2.4.8). Let the quiescent duty cycle be assumed to be D and let the small increment to duty cycle be d. Then equation (2.4.8) can be presented as:

$$\frac{Vo}{Vin} = \frac{1}{1+(D+d)} = \frac{1}{1-D} \times \frac{1}{1-\frac{d}{1-D}} \qquad 4.3.48$$

If d<< (1-D), then the above equation can be approximated using the binomial expansion and retaining only the first two terms. That is,

$$\frac{Vo}{Vin} = \frac{1}{1+(D+d)} = \frac{1}{1-D} \times \left[1+\frac{d}{1-D}\right] \qquad 4.3.49$$

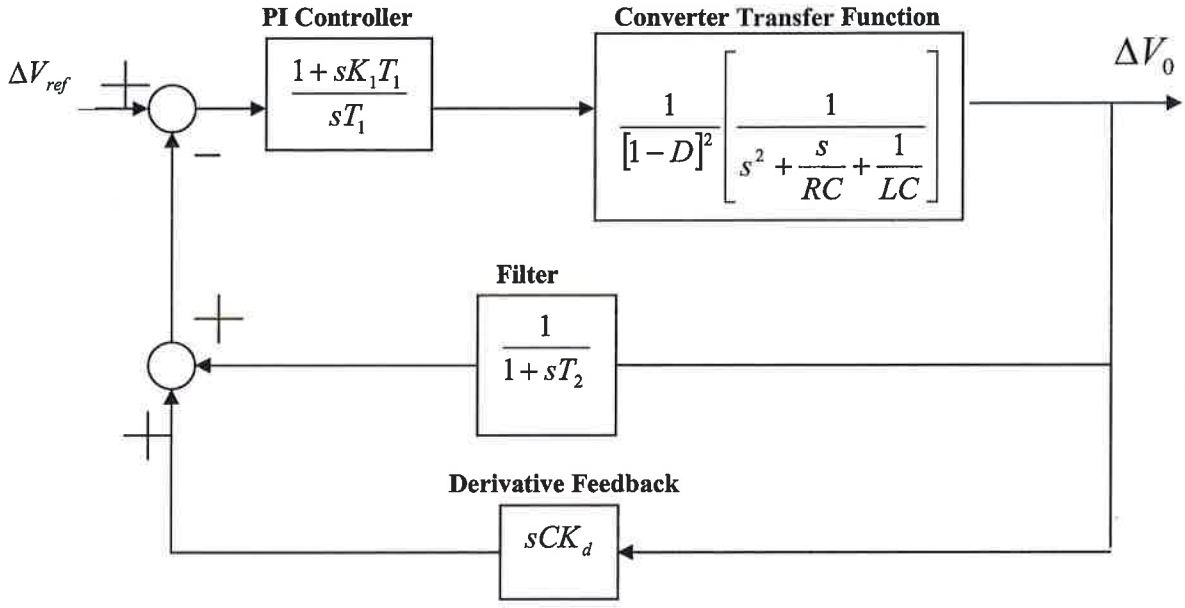

Figure 4.20 Control Scheme Block with Transfer functions

The change in output, denoted as ?Vo, can be expressed as

$$\Delta Vo = \frac{1}{1+(D+d\ )^2} \times \frac{Vin}{s^2+\frac{s}{RC}+\frac{1}{LC}} \qquad 4.3.50$$

The transfer function can then be obtained as:

$$\frac{\Delta Vo(s)}{\Delta Vref(s)} = \frac{G(s)}{1+G(s)H(s)} \qquad 4.3.51$$

where G(s) is

$$G(s) = \frac{1+sK_1T}{sT} \times \frac{1}{(1-D)^2} \times \frac{Vin}{s^2+\frac{s}{RC}+\frac{1}{LC}} \qquad 4.3.52$$

and H(s) is

$$H(s) = sCK_d + \frac{1}{1+sT} \qquad 4.3.53$$

The design of the controller is based on the block diagram in Fig. 4.19. The difference between the inductor current and the load current is the capacitor current and the current through the capacitor is proportional to the derivative of the capacitor voltage and the derivative feedback is obtained as shown. .

For the simulation of the power circuit using PWM, closed loop scheme used is shown in Fig. 4.20. As long as the inductor current is less than the maximum current, the feedback signal is the sum of the output voltage filter output and a derivative signal obtained from the inductor current and the load current. When the inductor voltage exceeds the set maximum value, the feedback signal contains an additional element proportional to the amount by which the inductor current exceeds the maximum current. The output of the PI controller determines the duty cycle.

Figure 4.21 Boost Converter Controller Board

Figure 4.22 System Controller Board

4.6 Power Inverter System Modelling

Inversion is the conversion of the Dc power to Ac power at a desired output voltage or current and frequency. A static semiconductor inverter circuit performs this electrical energy inverting transformation. The term voltage-fed and current-fed are used in connection with the output from the inverter circuits.

A voltage-source inverter (VSI) is one in which the Dc input voltage is essentially constant and independent of the load current drawn. The inverter specifies the load voltage while the drawn current shape is dictated by the load. A current-source inverter (CSI) is one in which the source, hence the load current is predetermined and the load impedance determines the output voltage. The supply current cannot change quickly. This current is controlled by series dc supply inductance which prevents sudden changes in current. The load current magnitude is controlled by varying the input Dc voltage to the large inductance; hence inverter response to load change is slow. Being a current source, the inverter can survive an output short current thereby offering fault ride-through property. Voltage control may be required as needed in this project, to

maintain a fixed output voltage when the dc link bus voltage regulation is poor, or to control power to a load. The inverter output can be single-phase, three-phase or multi-phase. Variable output frequency may be required for Ac motor drives speed control where, in conjunction with voltage or current control, constant motor flux can be maintained.

Different inverter topologies have been studied and developed for many years. Inverters can be found in variety of forms, including full bridge or half bridge, single phase or three phase, current source (CSI) or voltage source (VSI), and two-level or multilevel (Calais, Agelidis & Meinhardi,1999) Historically, more emphasis has been placed on the design of three phase inverters, especially for application like motor drives, active filters, and interruptible power supply. These same applications can be applied to single-phase inverters. Single-phase inverters that require a Dc-Dc front-end, similar to the one described in this thesis, have also been developed for photovoltaic energy conversion systems (Park, Kang, Cho, Moon, Nam & Ise, 2006; Yuvaraja, Dachuan & Shanguang, 2004)

The half bridge inverter is not used in practice mainly due to two reasons, both having to do with the neutral connection between the two bus capacitors as shown in figure 4.23. Both switches S1 and S2 are operated complementarily. It is generally desirable to use only one bus capacitor instead of two, in which case the neutral connection would not exist.

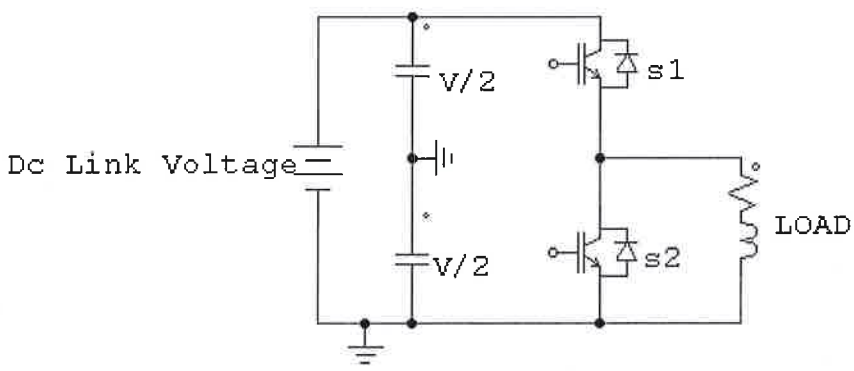

Figure 4.23 Half- bridge Inverter with Mid-point

Firstly, having two identical bus capacitors in series reduces the effective bus capacitance by a factor of two. Hence to achieve a desired bus capacitance one must

purchase two bus capacitors of twice the size, which is economically unattractive. Having two bus capacitors in series is typically desirable only when it is necessary to achieve the desired voltage rating of the application.

Secondly, having a neutral connection between the two bus capacitors forces the load current to flow through these capacitors. In this situation the impedance of the bus capacitors would have to be sized to minimize the resulting AC voltage across them. If our load requires DC currents, this will become impossible to achieve. Hence for single-phase applications we often use the full-bridge inverter.

The push-pull inverter is efficiently used for low power applications. A full-bridge inverter system which is capable of operating efficiently for high power applications is used in this project because it is designed for residential power system of 5kW. The operation of such system is explained with aid of figure 4.24.

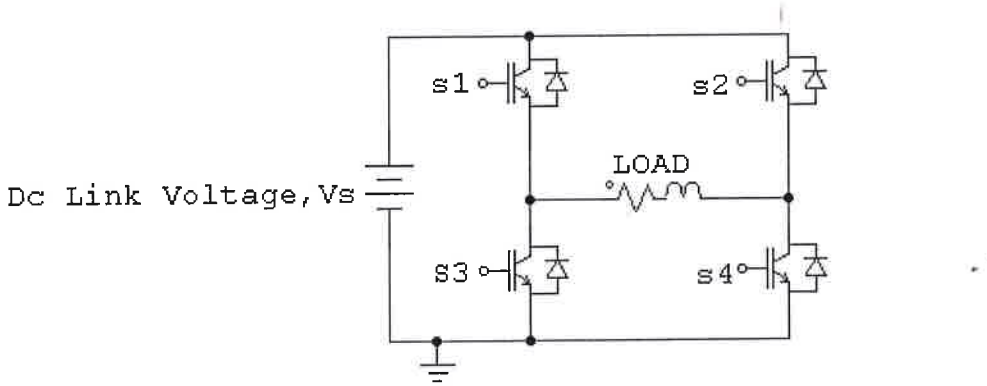

Figure 4.24 H-Bridge Inverter

Inverter output waveforms (either voltage or current) are usually rectilinear in nature and as such contain harmonics which may lead to reduced load efficiency and performance. Load harmonics reduction can be achieved by either filtering, selected harmonics-reduction chopping or pulse-width modulation. To achieve a better efficiency for the project both filtering and sine wave pulse-width modulation (SPWM) is used.

Figure 4.25 depicts the schematic diagram of the bridge inverter that is sine wave pulse-width modulated (SPWM) with 0.85 amplitude modulation index and 30 KHz switching frequency. Figures 4.26 and 4.27 show the output current waveform and FFT obtained. The output current contains very pronounced 50Hz sine wave and very low decreasing

harmonics currents. A low pass filter with a cut-off frequency of 1000 kHz was considered for the output filter so that the size of capacitor and inductor are reduced.

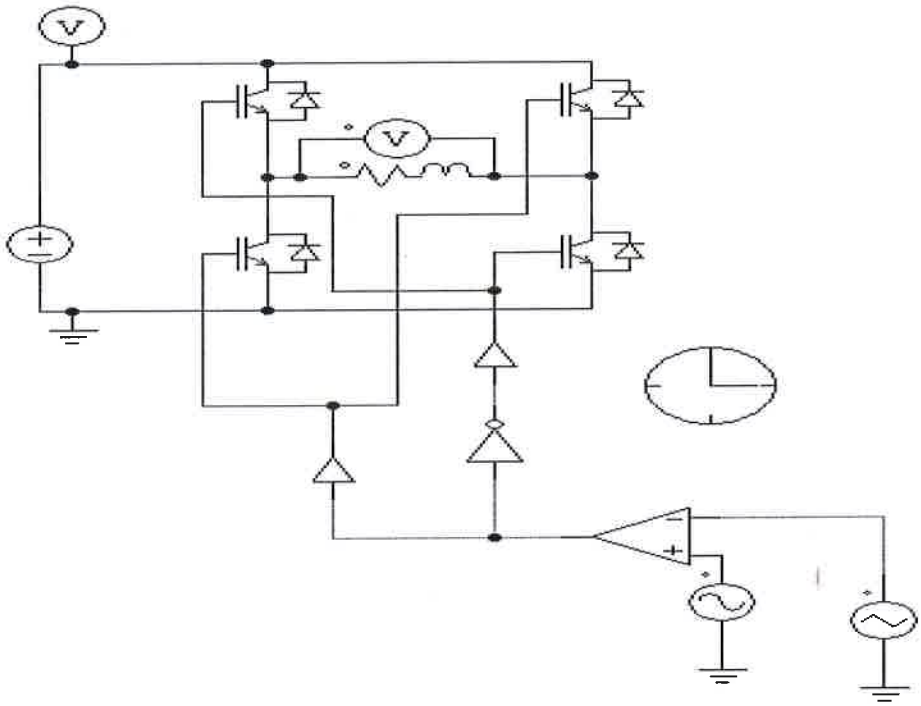

Figure 4.25 SPWM Bridge Inverter with inductive load

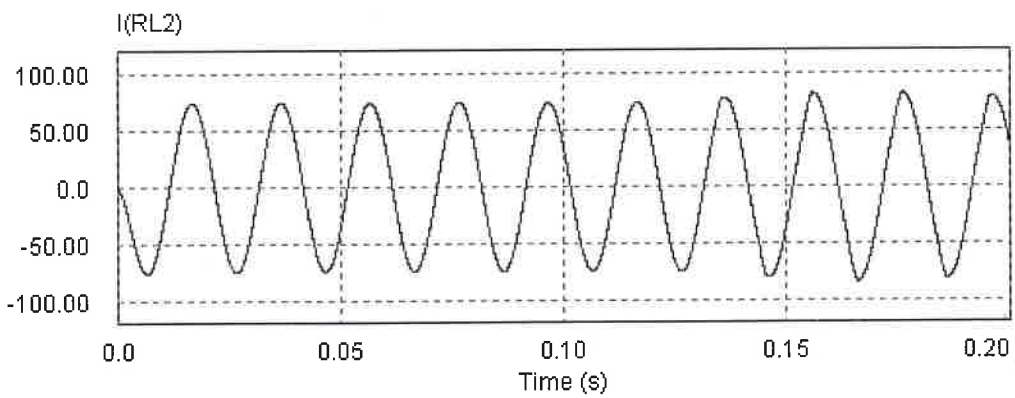

Figure 4.26 Inverter Output Current

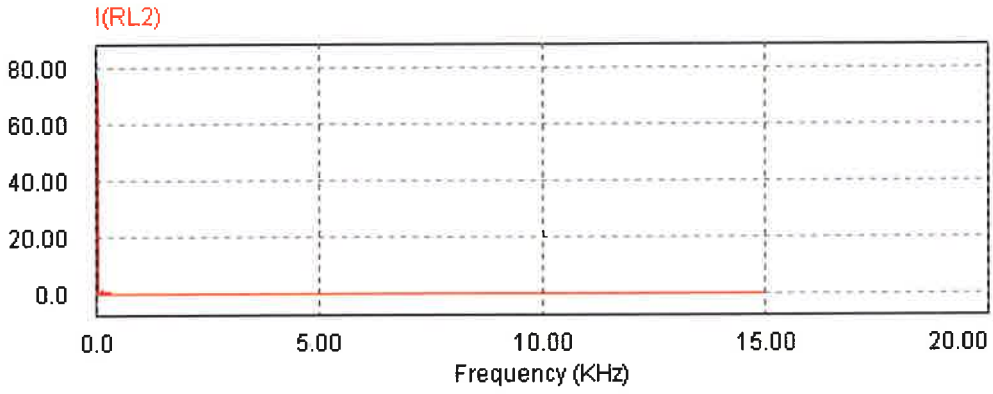

Figure 4.27 Fast Fourier Transform of Inverter Output Current

Control techniques for inverters are quite abundant and include options such as analog versus closed loop, and stationary versus rotating reference. The control design for single-phase inverter can actually be more complicated than that for three-phase inverters, because it is difficult to apply coordinate transformation to single-phase systems. Control methods include deadbeat to state feedback and some involving sensing current and voltage sensor. The control scheme employed for this work is a DSP sine wave pulse-width modulated because of its low cost, highly integration, protection, easy of development advantages (L Leung, D Alfano, 2006).

The developed control board is shown in figure 4.28. The board PCB layout was developed with Eagle PCB software.

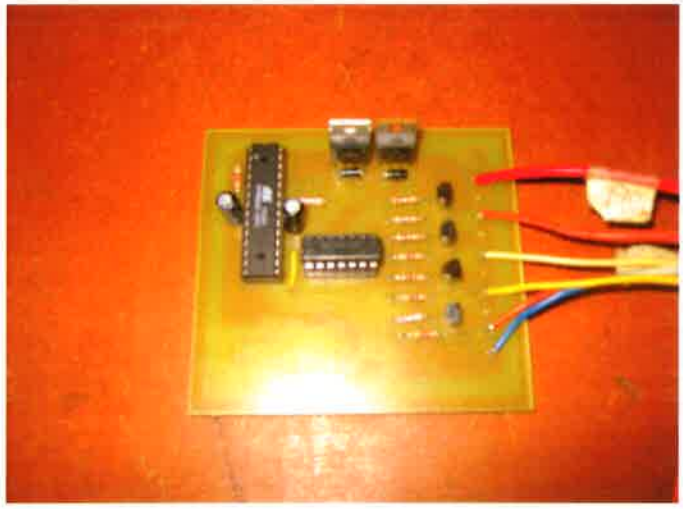

Figure 4.28 SPWM Control Circuit Board

Figure 4.29 shows the Semikron inverter stack with switched, heat sink incorporated togethe.

Figure 4.29 Semikron Inverter Stack

The control signals to the four switches of the inverters are shown in the figure. This sine wave pulse-width modulated signal is operated with 30 kHz switching frequency. The circuit diagram of SPWM is figure 4.210

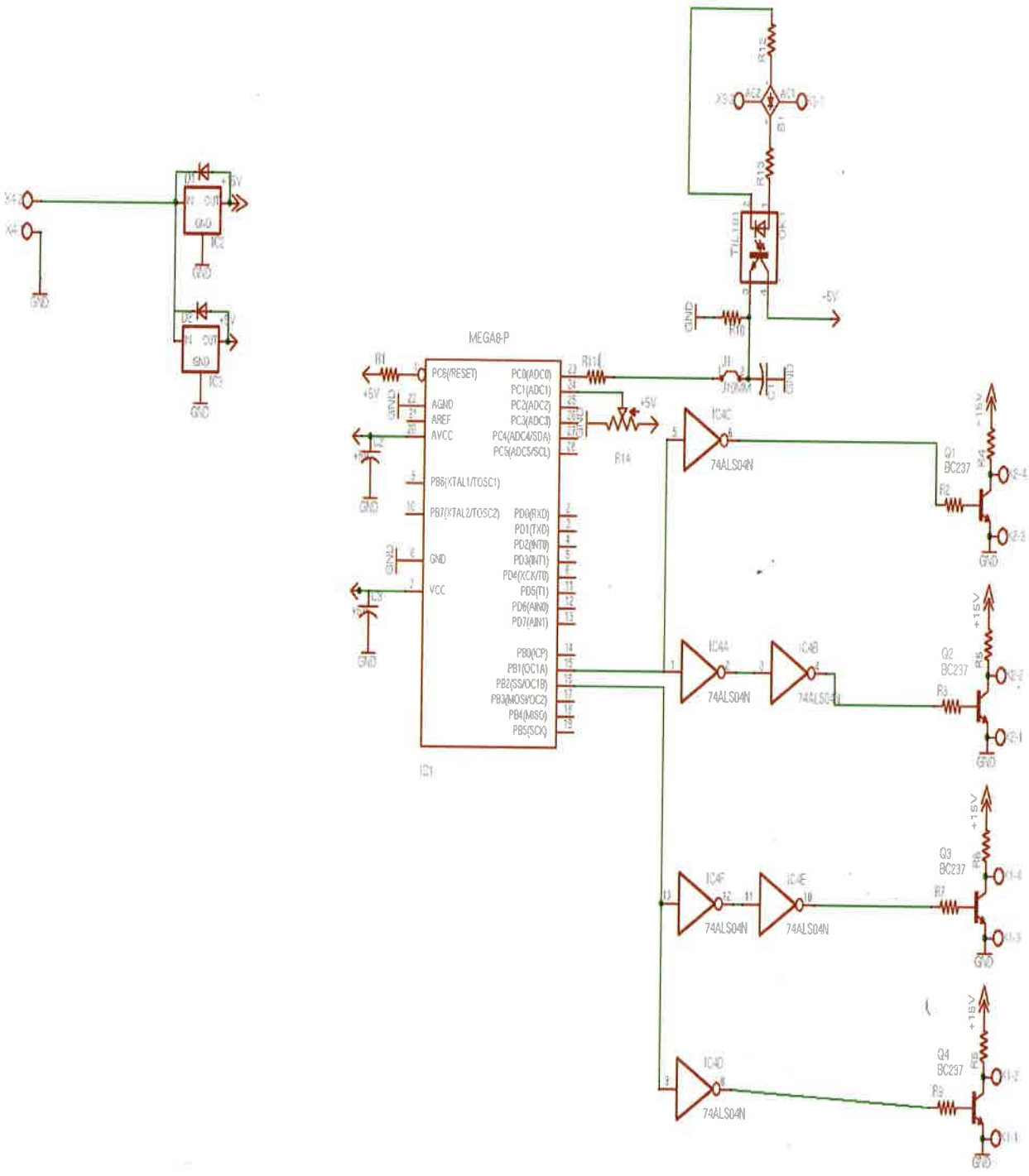

Figure 4.210 Control Schematic Circuit Diagram

CHAPTER 5

CONVERTERS INTERLEAVING AND ANALYSIS

5.1 Introduction

Interleaving of power converters involves paralleling n (>1) individual power converter unit to provide n times the power of each individual converter. The aim of interleaving power converters is to divide the current flowing through the semiconductor switches (by a factor of n), thereby reducing conduction losses and enabling use of lower rated silicon devices. Paralleling semiconductor switches, rather paralleling the entire units also results in dividing the current flowing through each switch, but it does not reduce the input and output ripple.

Interleaving n Dc-Dc converter units introduces 360/n phase displacement between high frequency ripples generated by two adjacent phases. The overlap of these displaced or phase-shifted ripples makes their sum flatter. The frequency of the total ripple is n multiple of the frequency of each phase, and the amplitude of the combined ripple is reduced (Shin, Park, Chang & Choi, 2005).

An interleaved Dc-Dc power converter for fuel cell applications reduces the ripple amplitude of the high frequency input current, which also helps avoid high frequency interaction inside the fuel cell stack and prolongs the fuel cell lifetime.

5.2 Interleaving Concept and Advantages

Interleaving power converters refers to paralleling of multiple switching converters for which the switching frequency is identical, but for which the switching instants are sequentially phased over equal fractions of the switching period (Wei Chen, 1999). Paralleled converters are synchronized to have the same switching frequency to eliminate beat frequency noise at both the input and output terminals (Tofoli & Gallo, 2005).

The benefit of interleaving power converters can best be understood using a simple graphical waveform analysis. Consider two boost converters in parallel, switched 180° out of phase as shown in figure 5.1. Paralleling of converter stage such as this would usually only occur in high power application such as in this project, where the device ratings were the limiting factor, however, the advantages of interleaved switching reach far beyond that. As can be observed in figure 5.2, the two resulting inductor currents are

summed at the output. Figure 5.2 was obtained from Psim simulation environment with values for inductors L1, L2 equal 100μH each and output capacitor C equals 700μF with power output of 5000 kW .Since they are switched out of phase, the current cancel each other out resulting in much smaller output currents at double the switching frequency, reducing the filtration requirements significantly. The result of the simulation when one boost converter is implemented in the Psim environment with input inductor value of 220μH and output capacitor value of 1000μF as designed in chapter 4 is depicted in figure 5.4

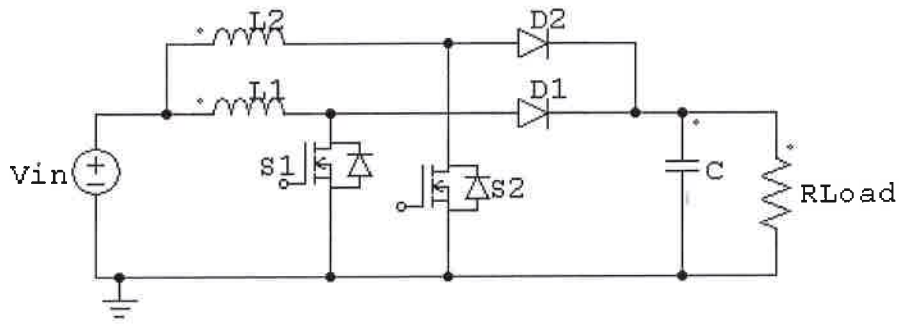

Figure 5.1 Schematic Diagrams of Two Interleaved Boost Converter System

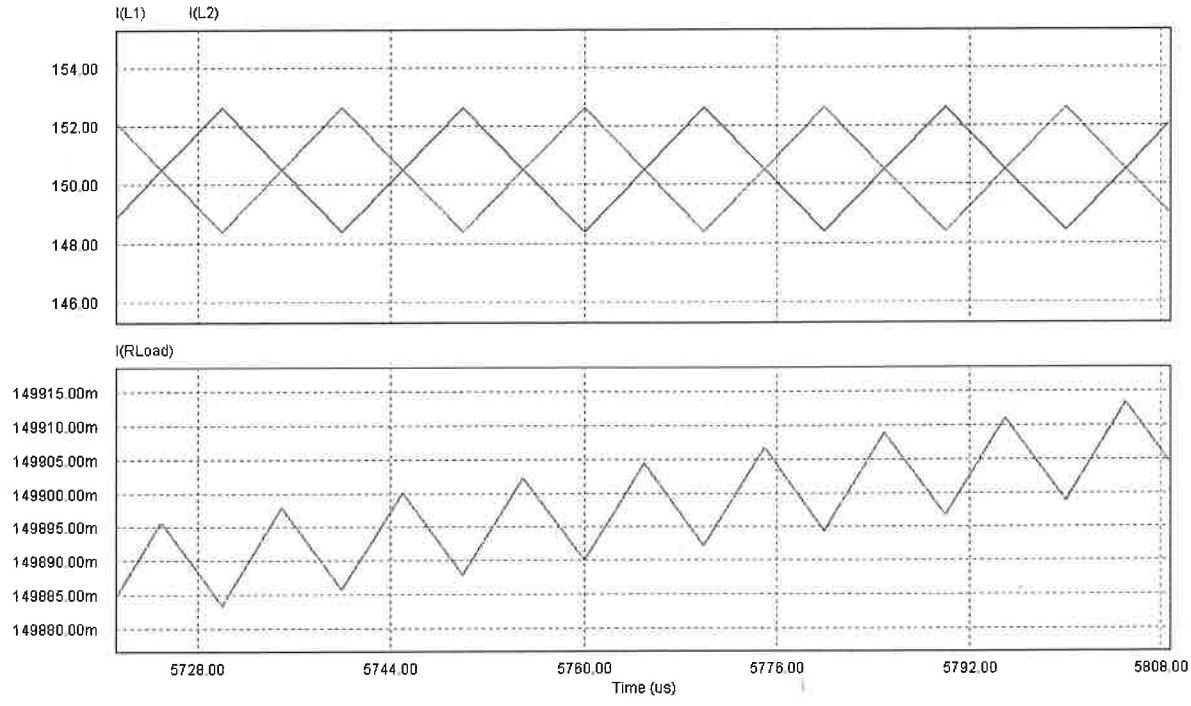

Figure 5.2 Two Interleaved Boost Converter System Waveforms

Obviously, this offers huge advantages that result in higher power conversion efficiencies, reduction in physical size and ultimately lower costs. Higher efficiency can be obtained due to an effective increase in switching frequency without an increase in switching losses as well as reduced losses from the ESR of the filter capacitors due to lower levels of ripple current. The size and costs are reduced since the reduction in filtration requirements are occurs both at the input and output.

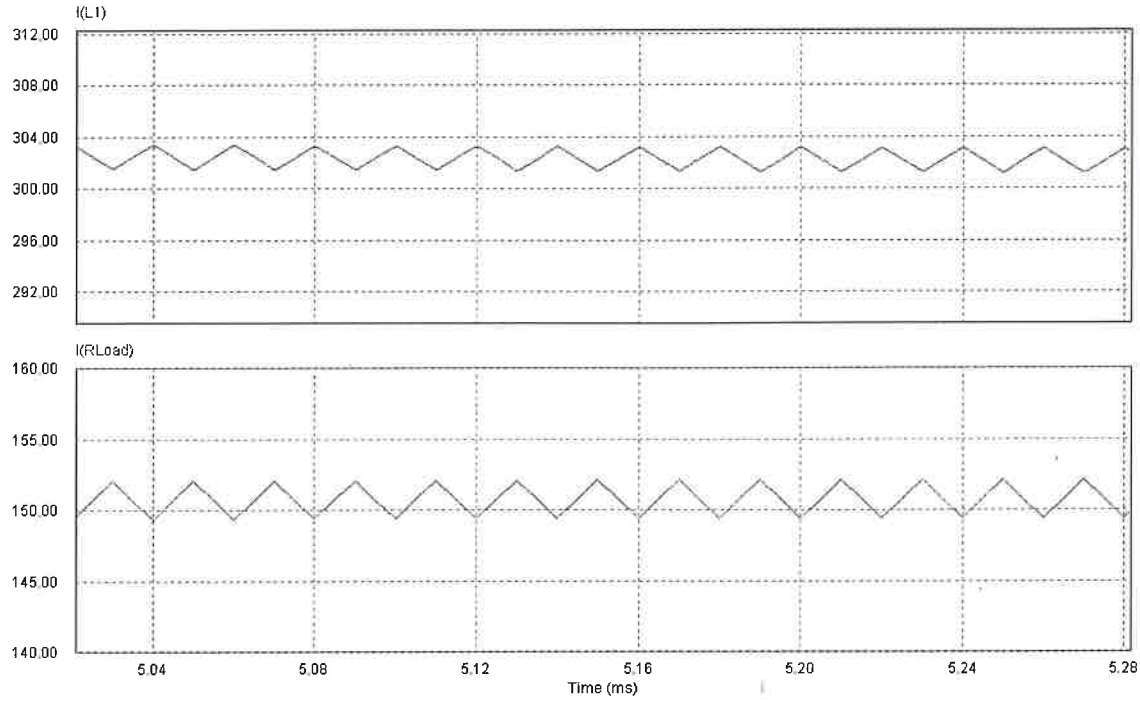

Figure 5.3 A Single Boost Converter System Waveforms

Off course, this concept works not for only two paralleled converters, but for as many converters as is practical or required. However, there exist a set number of converters that maximizes the benefits. In the above example, it can be noted that if the duty cycle was 50%, the individual inductor currents would combine and fully cancel each other out, resulting in zero current ripple. However, if the number of the converters were increased to, say four, then the output ripple cancellation would be 25%, 50% and 75%. It is clear that an optimum phase number exist and need to be evaluated over complete operating duty cycle range. This is further explained in the following section.

Another point to be made is that since output current cancellation occurs, the ripple of each converter can be increased by using smaller inductors. However, when the number of phases is large, the average per-unit current decreases even though the allowable per-unit ripple grows. This makes it very difficult to keep the converters operating in Continuous Conduction Mode and still operating with significant inductor ripple.

5.3 Output Ripple Current Cancellation

The phase relationship of figure 5.2 shows how ripple current cancellation at the output works. Because of the 180° phase difference between the two converters, the two inductor ripple currents in the two-phase converter tend to cancel each other, resulting in a smaller ripple flowing into the output capacitor. The frequency of the output ripple current is double of output ripple is doubled as well. All of these factors contribute to a smaller output capacitor for the same ripple voltage requirement.

Total current cancellation can occur for any number of phases depending on the duty cycle that they are operation at. The degree of cancellation at other duty cycles can be calculated by dividing the total of the summation of ripple currents at any operating point by the ripple current of one phase. It has been shown that the resultant current is given by the formula below.

$$\Delta I_o = \frac{NV_oT}{L_f} \frac{\prod_{i=1}^{N}\left|\frac{i}{N}-D\right|}{\prod_{i=1}^{N-1}\left(\left|\frac{i}{N}-D\right|+\frac{1}{N}\right)}, N = 2,3,4..... \qquad 5.1$$

Where

N = number of phases

T = switching period

D = the duty cycle.

V_o = Dc output voltage

ΔI_o = Ripple current

L_f =output inductor

The current ripple in a single is given by when N=1

$$\Delta I_o = \frac{V_oT(1-D}{L_f}, forN = 1 \qquad 5.2$$

Hence, by dividing the two, the ratio of ripple cancellation is obtained. This can be plotted as in figure 5.4, so that the optimum choice of number of converters can be made intuitively and quickly.

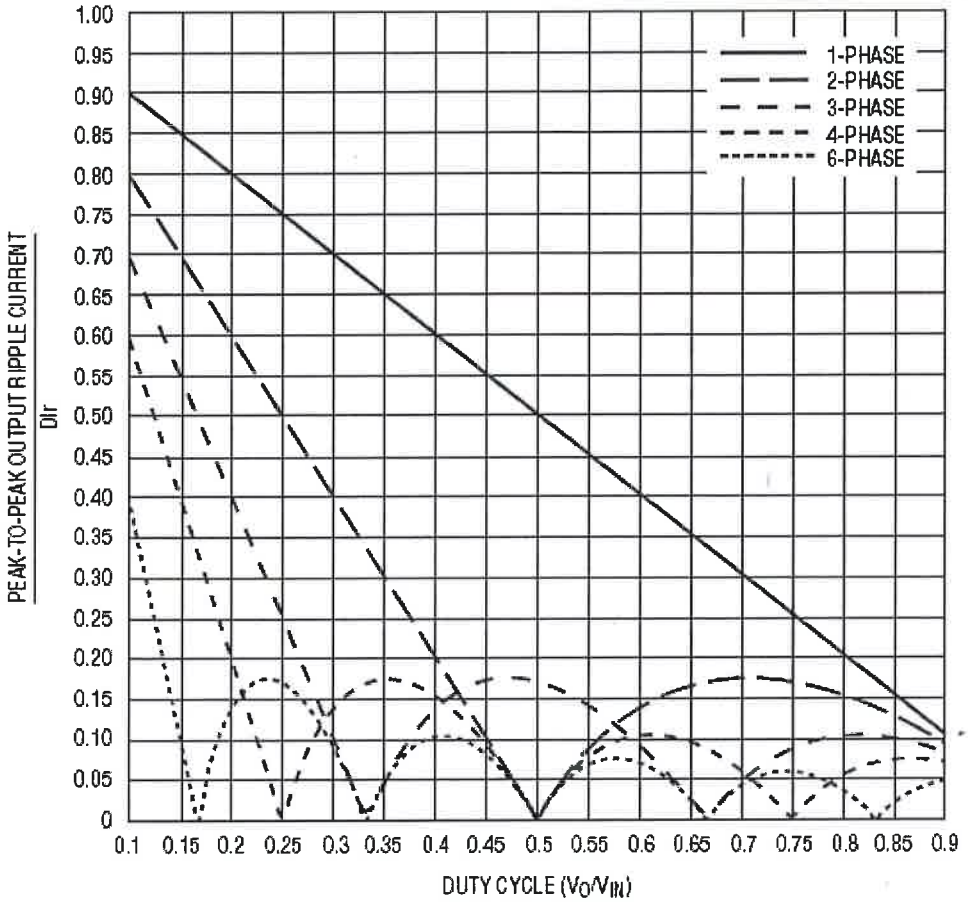

Figure 5.4 Influences of Phase Number and Duty Cycle on Output Ripple Cancellation

5.4 Load Transient Response Analysis

The influences of interleaved converters on the load transient performance are numerous. First, the reduced output ripple voltage allows more room for voltage variations during load transient because the ripple voltage will consume a smaller portion of the total error budget. With the same number of capacitors on the output terminals of the power converter, the sum of the overshoot and undershoot can be reduced drastically. Second, the reduced ripple inductor allows the use of lower

inductors. This speeds up the output current slew rate of the power converter. Consequently, an interleaved converter helps improve the load transient response of the power converter.

5.5 Input Ripple Current Cancellation Analysis

A similar analysis can be performed on the input currents as to the output currents. The result is fairly different due to the different waveforms on the input ripples. However, the principles are the same and near total cancellation can occur. Total cancellation can never be achieved due to the output ripple superimposed on the input ripple. The operating points where ripple cancellation are greatest are the same points as for the output current cancellation. An equation expressing RMS input ripple current developed [3] which when normalized against the total load current can be plotted against duty cycle as depicted below in figure 5.5

$$I_{i(RMS)} = \sqrt{\left(D-\frac{k}{N}\right)\left(\frac{k+1}{N}-D\right)\times I_o^2 + \frac{Nc^2}{12ND^2}\left(\frac{V_o(1-D)T}{L_f}\right)\left[(k+1)^2\left(D-\frac{k}{m}\right)^3 + k^2\left(\frac{k+1}{m}-D\right)^3\right]}$$

5.3

Where k=FLOOR (N.D), N= 1,2,3...

The FLOOR(X) function provides a greatest integer that is smaller than or equal to X.

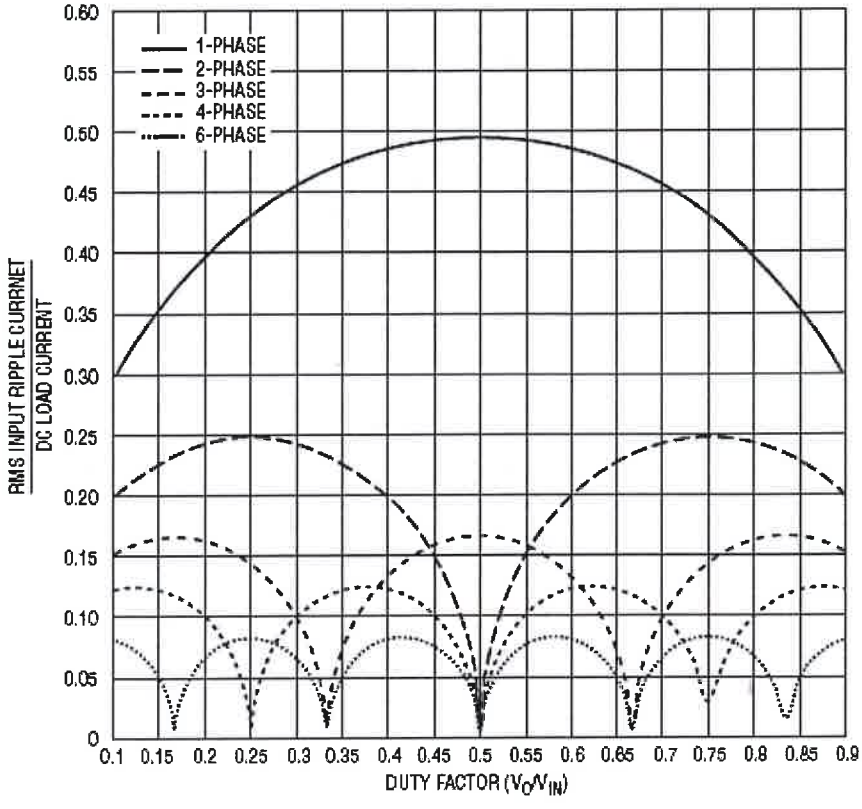

Figure 5.5 Influences of Phase Number and Duty Cycle on Input Ripple Cancellation

5.6 Current Sharing

Whenever converters are paralleled whether interleaved or not, current sharing between converters becomes a problem. Due to parasitics and component tolerances, some converters may draw more current than others. If this starts to occur the temperature in that converter will rise leading to a further increase in current. This continues until a fuse blows or components either fail or saturate. To balance the thermal stress in each component, paralleled converters must share the load current.

The current haring can be easily achieved by implementing peak current mode control. In current mode control converter, the load current is proportional to the error voltage in the voltage feedback loop. If the paralleled converters see the same error voltage, they will source equal currents. This current-sharing scheme will prevent an individual module

from suffering excessive current stress in steady state and during line or load transient conditions.

Even though the use of digital controllers provide perfect matching of duty cycles for different phases, current sharing is very difficult to achieve without specific current sharing control. As a result, converter currents must be accounted for within the PID control loops.

5.7 Control Scheme of Interleaved Converters

The control of interleaved converters is much the same as that of a single phase converter. As mentioned previously in chapter 4, a control signal was compared to a sawtooth waveform to generate a PWM signal. Exactly the same concept is used in interleaved conversion except that the control signal is compared to number of phase shifted sawtooth waveforms. The comparison of each sawtooth waveform to the control signal generates the equally phase shifted PWM signals. Simulation result for four interleaved boost converter is shown in figure 5.6.

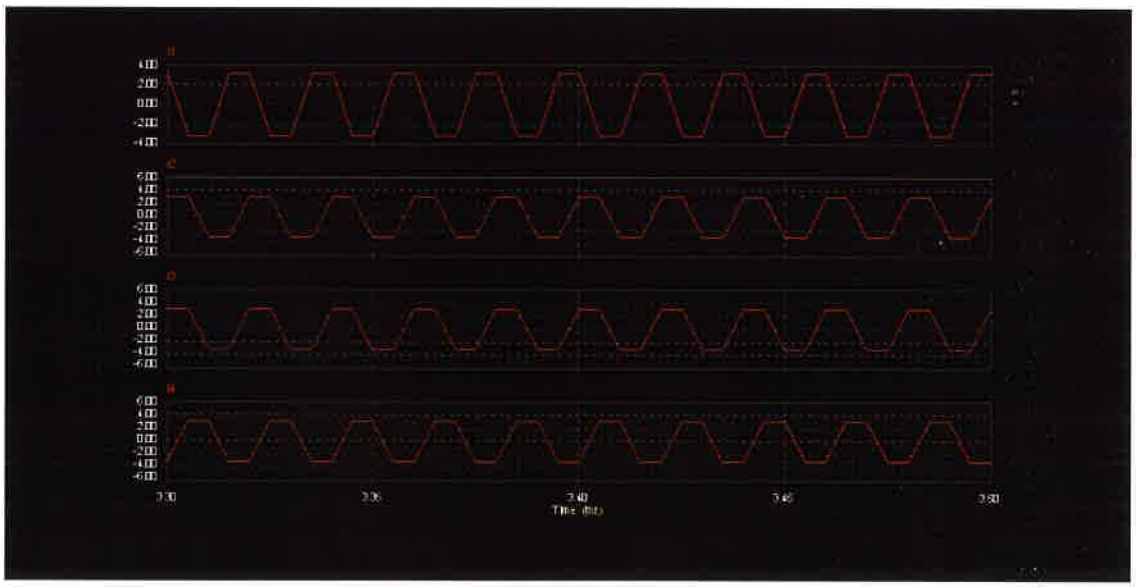

Figure 5.6 Output Currents through each of the Four Interleaved Boost Converter

CHAPTER 6

SYSTEM DESIGN, COMPONENTS SELECTION, AND SIMULATIONS

6.1 Fuel Cells Power Converter System Model

The figure 6.1 below shows a block diagram of the proposed 5 kW fuel cells power converter system. The input Dc voltage varies in a wide range from 21V to 42V and the output Ac voltage is maintained at 230±5%V, 50±0.1% Hz.

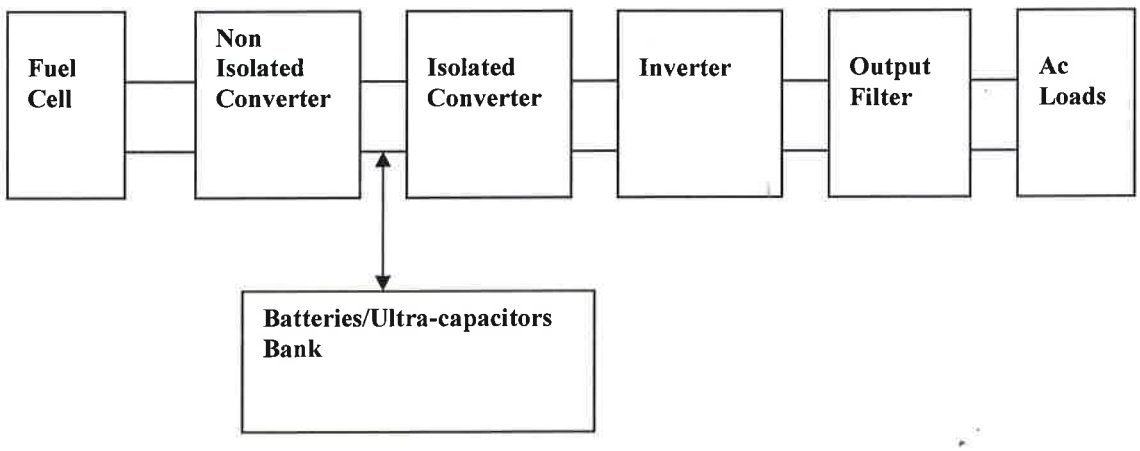

Figure 6.1 Block Diagram of the Fuel Cells Power Converter System

The input Dc voltage from the fuel cells is first stepped up to a regulated 60V Dc bus using a high frequency non isolated Dc-Dc boost converter. The 60V non isolated Dc-Dc boost converter is then converted to 400V by means of the second stage Dc-Dc boost converter with four high frequency isolated transformers. The output of this second stage converter is finally inverted by using a PWM driven inverter stage to supply load at 230V, 50Hz. An output filter is connected to the inverter output to produce a low Total Harmonics Distortion (THD) Ac waveform. Ultra-capacitors or batteries bank is floated on the 60V Dc bus to supply electrical energy as a backup energy storage system as required by the project. The second stage Dc-Dc boost converter consists of four interleaved converters to reduce the output ripple content, reduce the size of the Dc link capacitor, reduce device stresses, increase efficiency, and introduce redundancy.

The efficiency of the high frequency transformer in the second stage boost converter depends on the stability of the primary input voltage. The transformer needs to be designed to accommodate the lowest voltage levels for the expected output voltage level. During the normal operation, the nominal input voltages are typically much higher than the minimum value and the transformer does not operate optimally if the isolated transformer is not preceded by the non isolated Dc-Dc boost converter. The fuel cells power converter system in the project overcomes this by regulating the input voltage of the second stage converter at 60V during the normal system operation. Therefore, the isolated Dc-Dc boost converter can operate in open loop, thus simplifying the control of the entire system. However, since the second stage boost converter consists of four interleaved converters, there is a need for current mode control to ensure that current is evenly distributed amongst the interleaved converters. Additionally, since the input voltage of the isolated Dc-Dc boost converter is higher, the current ratings of the switches can be much lower, which, together with the lower transformers turn ratio, reduces the overall cost of the system and increase the efficiency.

6.2 Design Overview and Components Selection

6.2.1 Dc-Dc Boost Converters Inductors

The selection of inductors is driven by the output current amplitude, the allowable output ripple content and the switching frequency.

First-Stage Dc-Dc Converter Inductor.

This section details the design of the first stage Dc-Dc boost converter with the following Requirements

Input power = 5 kW

Minimum input voltage = 21V

Maximum input voltage = 42V

Output voltage = 60V

Switching frequency = 30 kHz

Permissible ripple current, ΔI_L = 40%

Power loss budget >= 200W

The minimum current flows through the inductor when the fuel cells output voltage is 42V, thus the minimum current is obtained as

$$I_{in-\min} = \frac{5000}{42} = 119.05A \quad 6.1$$

The maximum current flows through the inductor when the fuel cells output voltage is 42V, thus the maximum current is obtained as

$$I_{in-\max} = \frac{5000}{21} = 238.10A \quad 6.2$$

$$D_{\max} = 1 - \frac{V_{in-\min}}{V_{out}} = 0.65 \quad 6.3$$

$$D_{mim} = 1 - \frac{V_{in-\max}}{V_{out}} = 0.30 \quad 6.4$$

$D_{\max}$, $I_{in-\max}$ and if the ripple current ΔI_L =40% of $I_{in-\max}$ = 95.24A range were used to design the inductor as follows,

From equation 4 in chapter 4

$$V_l = L\frac{\Delta I_l}{\Delta t} \quad 6.5$$

$$\Delta t = TD_{\max} = 3.33\times10^{-5}\times0.65 = 2.17\times10^{-5}\ \text{sec} \quad 6.6$$

$$L \geq \frac{V_{in-\max}\Delta t}{\Delta I_L} = \frac{42\times2.17\times10^{-5}}{95.24} \quad 6.7$$

$$L \geq 9.55\mu H \quad 6.8$$

Inductor of 20μH is selected from a manufacturer considering margins for transients, flux fluctuations and prevention of discontinuous conduction mode operation.

Figure 6.2 A Single Stage Boost Converter

6.2.2 Open-loop Simulation of the First Stage Dc-Dc Power Converter

The schematic circuit diagram of the designed first stage Dc-Dc boost converter is shown in figure 6.3 in the open-loop configuration. Simulations for different input voltages, minimum and maximum duty cycle were conducted.

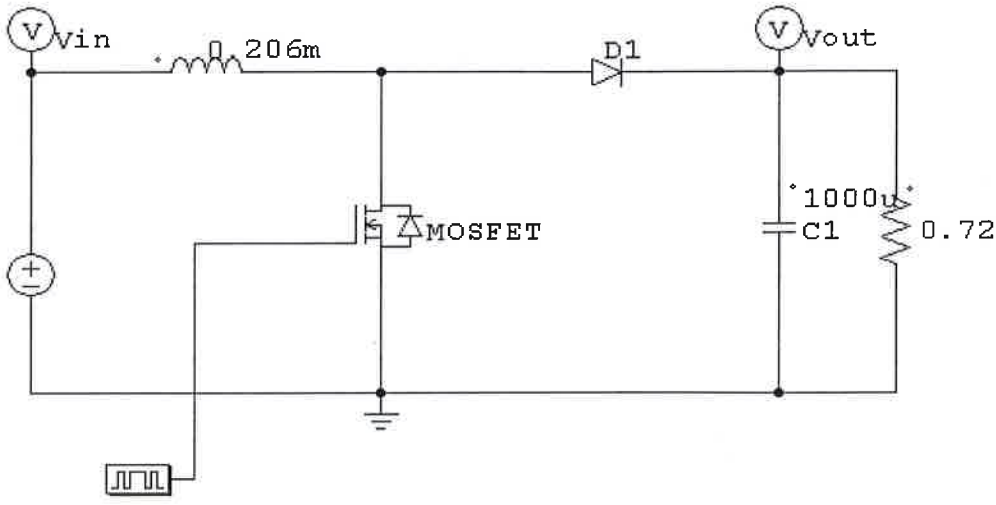

Figure 6.3 Schematic PSIM Simulation Diagram of the 1st Stage DC-DC Boost Power Converter for the Open loop Control System Analyses.

The steady-state is achieved after 3.75ms for an input voltage of 42V, duty cycle of 0.3 at maximum power delivery of 5000W as shown in figure 6.4. A faster steady-state of 5ms is achieved with an input voltage of 21V, duty cycle of 0.63 when delivering maximum power of 5000W as depicted in figure 6.5. These two sets of simulation results described the two extreme cases maximum input voltage at minimum duty cycle and minimum input voltage at maximum duty cycle which put a lot of stresses on the power semiconductor switches.

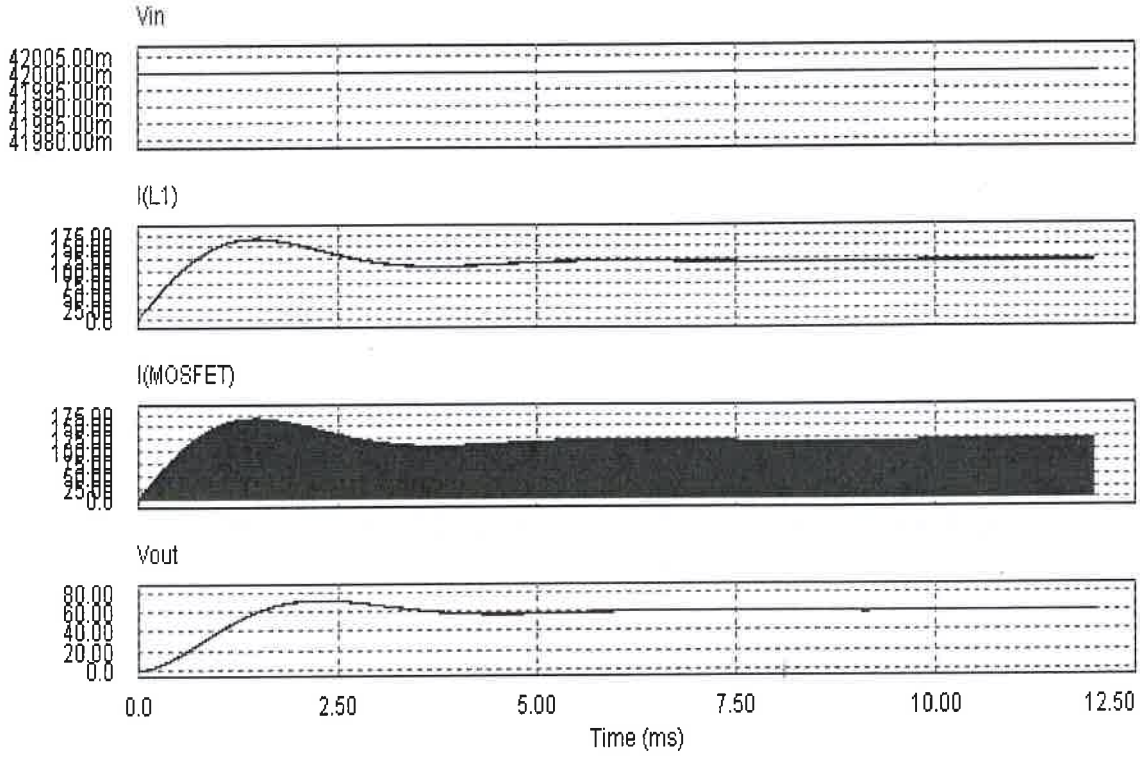

Figure 6.4 Open Loop Simulation of 1st stage Dc-Dc Converter for V_{in_max}=42V and D_{min}=0.3 at Maximum Power Delivery of 5000 kW.

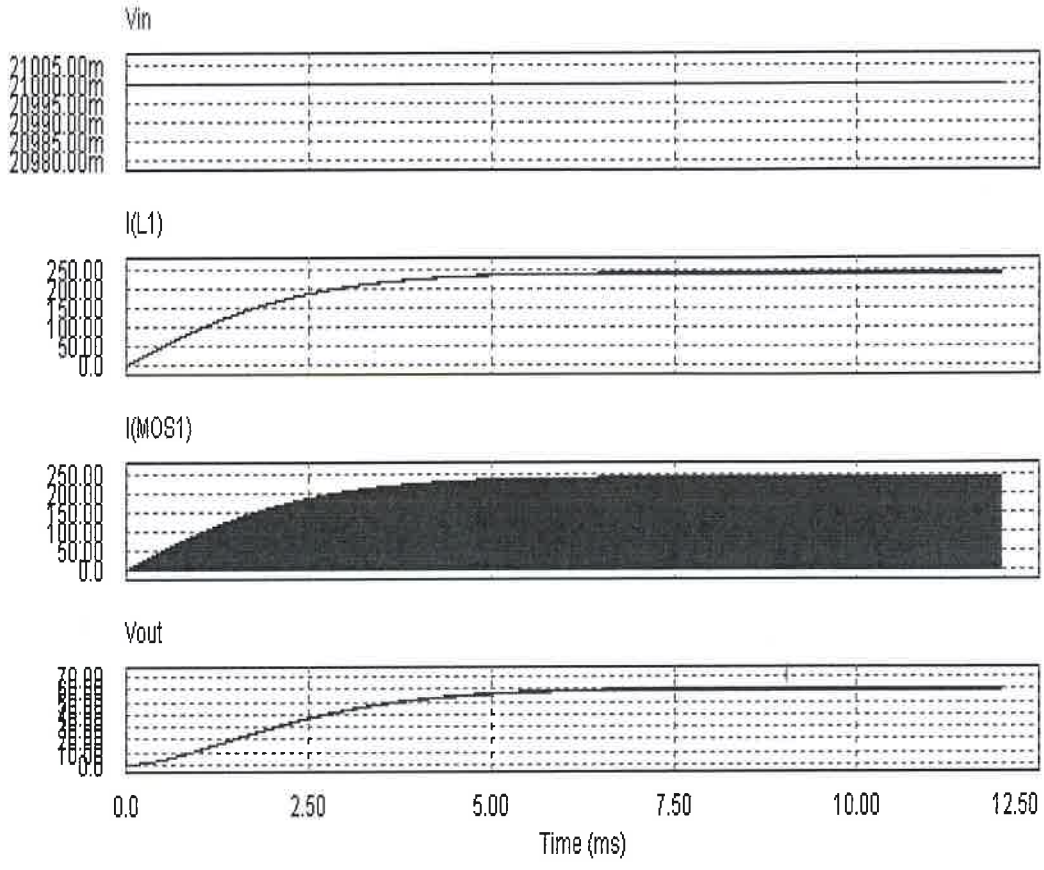

Figure 6.5 Open Loop Simulation of 1st Stage Dc-Dc Converter for V_{in_min} = 21V and D_{min}=0.63 at Maximum Power Delivery of 5000 kW.

6.2.3 Closed-loop Simulation of the First Stage Dc-Dc Power Converter

The schematic circuit diagram of the designed first stage Dc-Dc boost converter is shown in figure 6.6. Chosen closed-loop parameters for the simulation produce satisfactory transient response. Input voltages of 21V, 32v and 42V for maximum load of 5000W were simulated. Slower time response was obtained for an input voltage of 21V (figure 6.7), faster time response for an input voltage of 42V (figure 6.8) while a moderate time response was obtained for a nominal input voltage of 32V (figure 6.9)

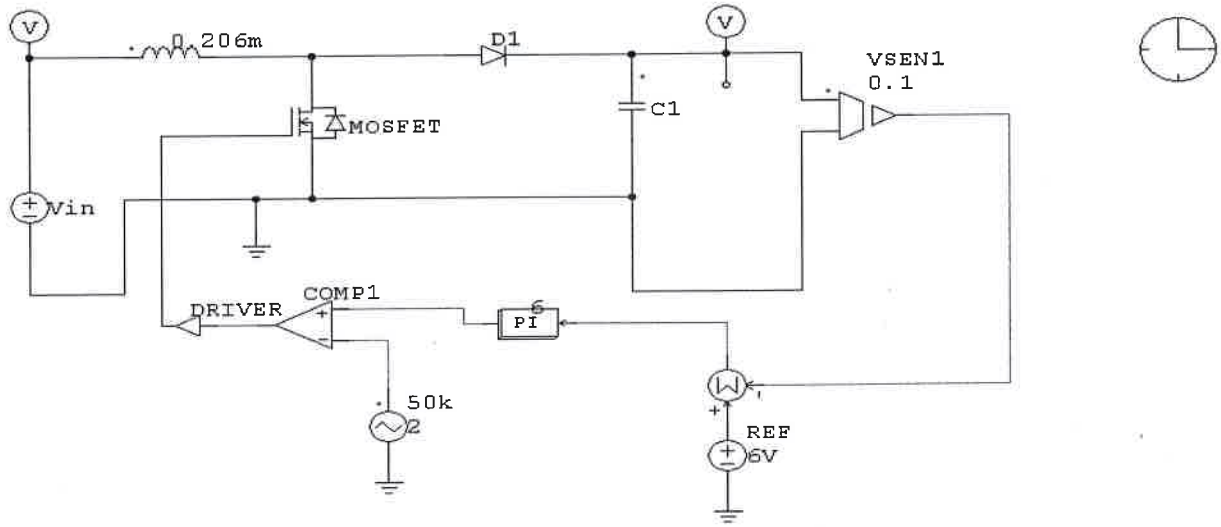

Figure 6.6 Schematic PSIM Simulation Diagram of the 1st Stage DC-DC Boost Power Converter for the closed loop Control System Analyses.

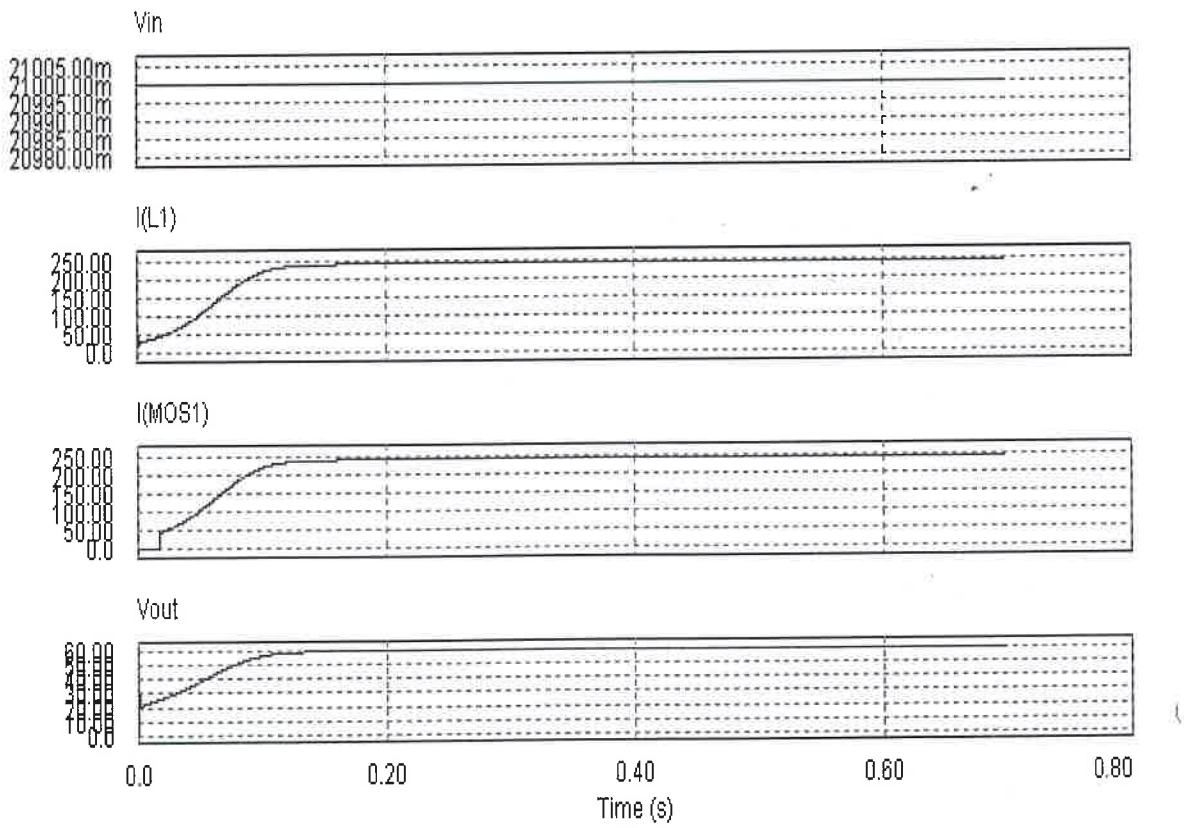

Figure 6.7 Closed Loop Simulation of 1st Stage Dc-Dc Power Converter for V_{in_min} = 21V at Maximum Power Delivery of 5000 kW.

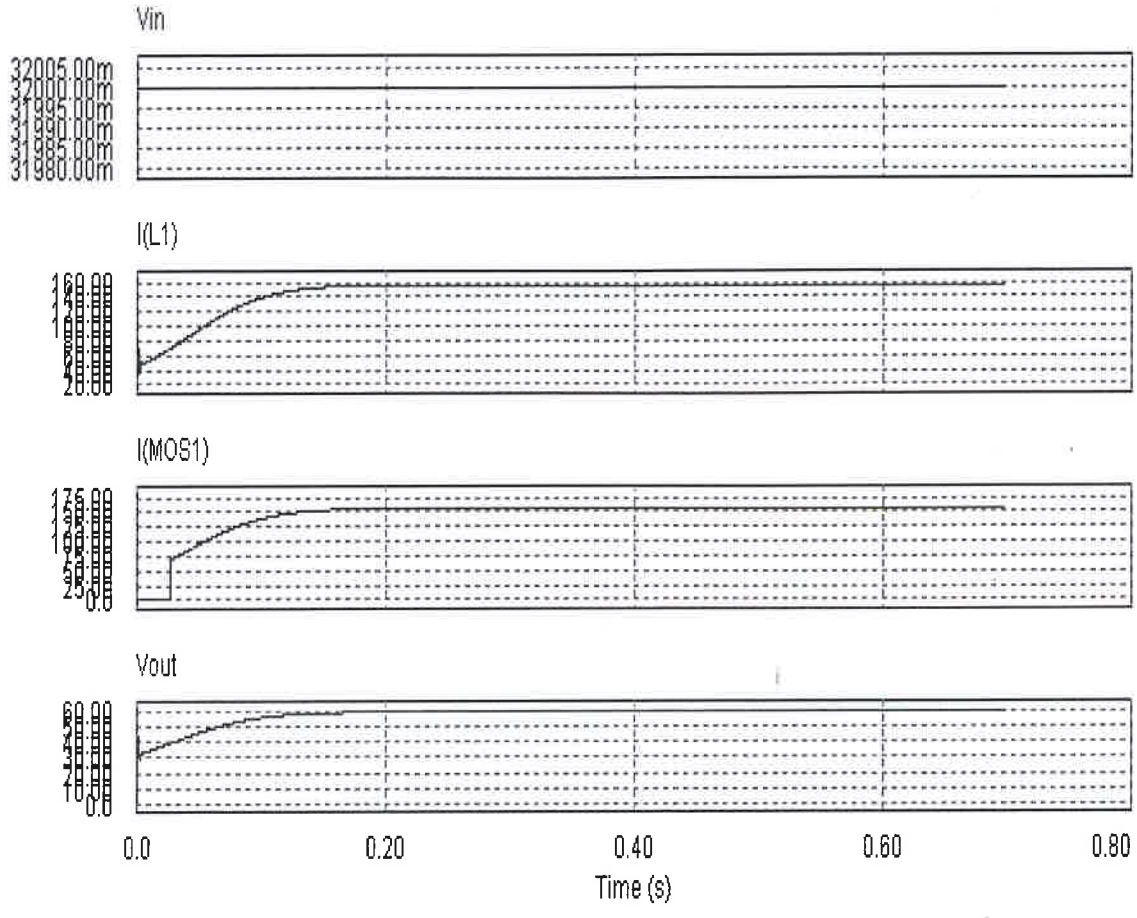

Figure 6.8 Closed Loop Simulation of 1st Stage Dc-Dc Power Converter for $V_{in\_nominal}$ = 32V at Maximum Power Delivery of 5000 kW.

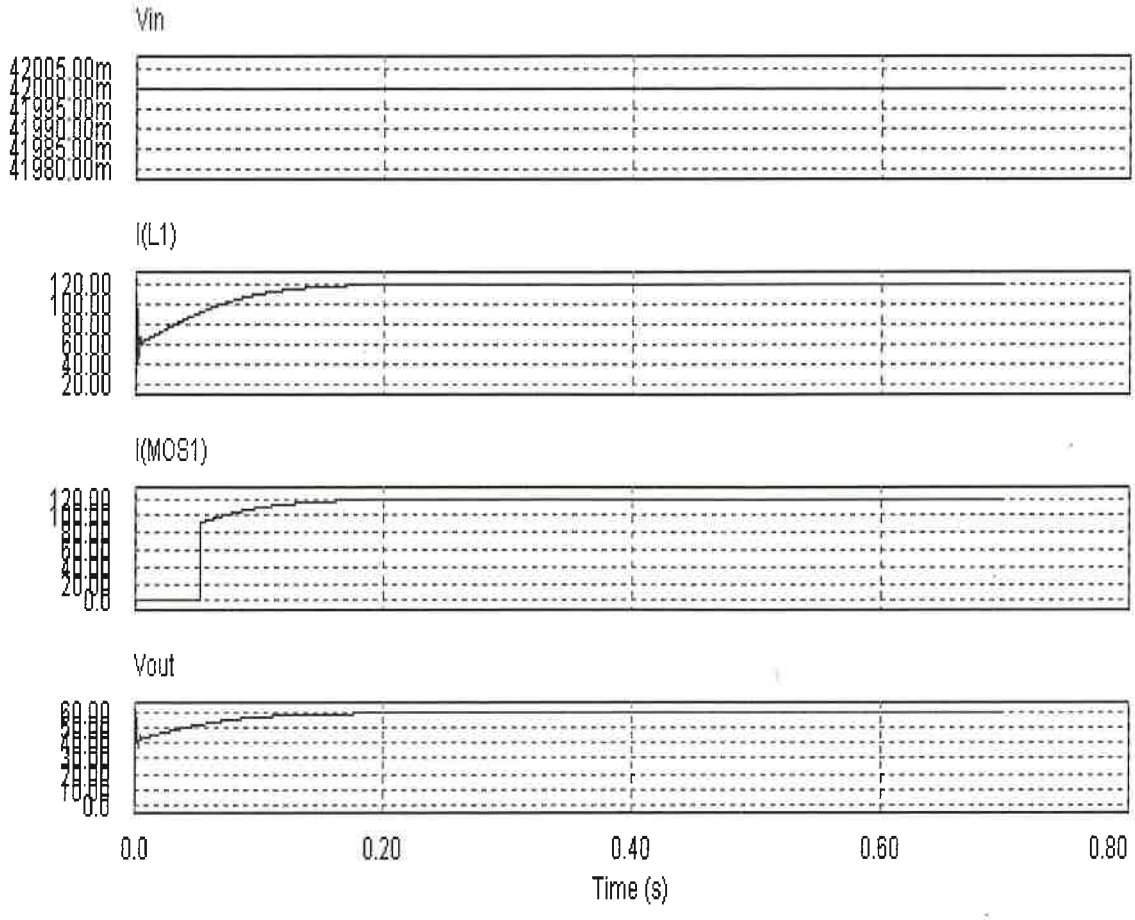

Figure 6.9 Closed Loop Simulation of 1st Stage Dc-Dc Power Converter for V_{in_max} = 42V at Maximum Power Delivery of 5000 kW.

6.2.4 Dc-Dc Boost Converter Capacitor

In switching power converter, the function of the capacitor is store electrical energy. The output capacitance for a boost power converter is selected to limit output voltage ripple to an acceptable specification as stated in chapter 4. The series impedance of the capacitor and the power stage output current determines the output voltage ripple. The three elements of capacitor that contribute to its impedance and voltage ripple are equivalent series resistance (ESR), equivalent series inductance (ESL), and capacitance of the capacitor.

If the ripple voltage $\Delta V_c = 2\%$ of $V_{out} = 60V$ and output power is 5000W then,

$$I_{out} = \frac{p_{out}}{V_{out}} = \frac{5000}{60} = 83.33A \qquad 6.13$$

and

$$\Delta V_c = 1.2V \qquad 6.14$$

$$C \geq \frac{I_{out} \times \Delta t}{\Delta V_c} \qquad 6.15$$

$$C \geq \frac{83.33 \times (1-0.3) \times 3.33 \times 10^{-5}}{1.2} \qquad 6.16$$

$$C \geq 1620\mu F \qquad 6.17$$

For continuous inductor current mode operation and assuming there is enough capacitance such that the ripple due to the capacitance can be ignored, the ESR needed to limit the ripple voltage is given as

$$ESR \leq \frac{\Delta V_0}{\left(\frac{I_{\max}}{1-D_{\max}} + \frac{\Delta I_L}{2}\right)} \qquad 6.18$$

Substituting the followings into equation 6.18

$\Delta V_o = 1.2V, I_{in-\max} = 238.10A, D_{\max} = 0.65$, and $\Delta I = 2.39A$, we have

$$ESR \leq 1.26m\Omega \qquad 6.19$$

Ripple current flowing through a capacitor's ESR causes power dissipation in the capacitor. This power dissipation causes a temperature increase internal to the

capacitor. Excessive temperature can seriously shorten the expected life of a capacitor. Capacitors have ripple current ratings that are dependent on ambient temperature and should not be exceeded.

For continuous inductor current mode operation, the RMS value of the ripple current flowing in the output capacitance is given by

$$I_{c(RMS)} = I_o \times \sqrt{\frac{D_{\min}}{(1-D_{\min})}} \qquad 6.20$$

Substituting $D_{\min} = 0.3$,

$$I_{c(RMS)} = 83.33 \times \sqrt{\frac{0.3}{(1-0.3)}} \qquad 6.21$$

$$I_{c(RMS)} = 54.53A \qquad 6.22$$

Selection criteria are

Type: Low-impedance aluminium electrolytic

$I_{c(RMS)} \geq 54.53A, ESR \leq 1.26m\Omega, V_{c(rated)} \geq 60V, LowESL$, and $C \geq 1620\mu F$

6.2.5 Second-Stage Dc-Dc Converter Inductor

During time 0 <t< (DT/2), the inductor voltage becomes,

$$V_L = Vin \times \frac{Ns}{Np} - V_{dc} \qquad 6.9$$

$$D = \frac{Ns \times V_{dc}}{2 \times Np \times V_{in}} \qquad 6.10$$

Therefore, according to equation (6.10), the duty ratio ranges from 0.37 to 0.46 to regulate the Dc link voltage of 400V when the input to second stage boost converter is between the output of the first stage boost converter (60V) and the energy storage system (48V).

This inductance can be obtained by combining equations (6.9) and (6.10) to obtain

$$L = \frac{(1-2D)\frac{Ns}{Np} \times Vin \times D}{\Delta I \times f_s} \qquad 6.11$$

Assuming a permissible ripple current on the inductor to be 50% of the maximum current at the Dc link or 3.125A peak to peak, the inductance can be calculated using equation 6.11 to be L=127μH. The peak inductor current can also be calculated as

$$I_{L,peak} = I_{dc} + \frac{1}{2}\Delta I = 4.69A \qquad 6.12$$

From figure 4.14, the RMS value of the inductor can also be calculated as,

$$I_{L,rms} = 3.79A \qquad 6.13$$

Inductor of 250μH is selected from a manufacturer

6.2.6 MOSFETs Switches and Diodes

The selection of MOSFETs was determined by the current requirements and the voltage rating as well as closely comparing their $R_{DS(on)}$ and switching characteristics. Lower voltage ratings and higher current capabilities tend to drive the conduction losses through reduced $R_{DS(on)}$ values, however, the switching losses are increased due to large gate charges and parasitic capacitances. Thus, a compromise must be made between low conduction losses or low switching losses.

6.2.5.1 First Stage Dc-Dc Boost Converter

The voltage ratings of diodes and MOSFETs are calculated based on the moment at which the fuel cell outputs a maximum voltage of 42V at a minimum duty cycle of D_{min}= 0.3. The current rating of diodes and MOSFETs are calculated based on the moment at which the fuel cell supplies a maximum current of 230.10A at a maximum duty cycle of D_{max}=0.65

When the fuel cell voltage is 42V, the output voltage of the 1st Dc-Dc boost converter becomes 60V; therefore, the peak voltage of a diode is 60V. The voltage rating of the power diode is taken as 100V having considered safety margin. An ultra-fast recovery diode is chosen to lower the switching loss due to the high frequency operation (50 kHz). As the diode only conduct when the MOSFET switch is off, the average current rating of the diode can be obtained as

$$I_{D,av} = I_{dc} \times \sqrt{(1 - D_{\min})} \qquad 6.23$$

$$I_{D,av} = 67.72A \qquad 6.24$$

The peak value of the diode is identical to the peak value of the inductor. Then,

$$I_{D,peak} = I_{dc} + \frac{1}{2}\Delta I_l \qquad 6.25$$

$$I_{D,peak} = 239.20A \qquad 6.26$$

For the rectifier diodes, the secondary winding voltage becomes 420V when the primary winding voltage is 60V if a transformer turn ratio of 1:7 is assumed. Therefore, the peak voltage of the rectifier diode is 420V. A safety margin should be considered due to the ringing phenomenon at the secondary winding of the high frequency transformer. The voltage rating of the diode is determined to be 600V. An ultra-fast recovery diode is chosen to lower loss due to high switching frequency operation (50 kHz). As the diodes

always conduct quarter of a switching cycle, the average current rating of the diodes can be obtained by,

$$I_{D,av} = \frac{1}{4} \times I_{DC} = 3.125A \qquad 6.27$$

The peak current of the diodes are identical to the peak current of the inductor. Then,

$$I_{D,peak} = I_{L,peak} = 4.69A \qquad 6.28$$

An ultra-fast power diode with a rating of 600V, 10A was selected from a manufacturer. Power MOSFETs were selected as a switching device for the first and second Dc-Dc boost converters because they operate optimally under low voltage and high current condition coupled with their easy paralleling capability. The peak voltage of the first converter stage MOSFET is 60V which is the voltage across the drain and source of the MOSFET when it is not conducting. Considering safety margin due to voltage spikes, the device voltage rating over 100V should be acceptable. The maximum current of 230.10A flows through the MOSFET when the fuel cells voltage is 21V at the maximum duty cycle of 0.65.

For the second stage boost converter, by multiplying the average current and peak current values of the secondary winding side of the transformer by the transformer's turn ratio (1:9), the average and peak values of the MOSFETs are calculated as 28.13A and 42.21A respectively. Considering safety margin, MOSFETs with ratings of 100V, 75A were selected from a manufacturer.

6.2.7 Energy Storage Device Design

In order to operate the fuel cell efficiently, the flow rate of hydrogen must be adjusted with changes in electrical load. Depending on the type of fuel cell system, this flow change can be a very slow process and have time constant in the 30 seconds range. Therefore, some type of supplementary energy storage is typically needed.

Batteries are common choice and can be a good one if high voltage battery configuration is used. This high voltage string of batteries can be placed across the regulated with little or additional circuitry. However, large number of cells in series can

be expensive and often leads to unbalance issues. Additionally, battery placement on the high side does not provide the auxiliary power necessary to start-up the fuel cell ancillary system. A low voltage battery configuration is more desirable, but requires additional circuitry to ensure safe operation. If the low voltage batteries are interfaced with the high side, a bi-directional Dc-Dc converter is needed. The low voltage battery string could be placed on the low side and controlled with semiconductor switches or contactor. However, batteries generally have a short lifetime and often require some type of battery management system, which can be quite costly.

An interesting alternative to batteries is the use of ultrcapacitors, which have a wider voltage range than batteries and can be directly paralleled across the input bus. Ultrcapacitors have a specific energy density less than that of a battery, but a specific power greater density greater than a battery, making them ideal for short (up to several seconds) pulses of power. Certain ultracapacitors (unsymmetrical electrochemical) can hold charge over extended periods of time, so act like a battery. However, unlike batteries, these ultracpacitors have a short charge time and much longer lifetime. The energy storage options are summarized in Table 6.1 below

Table 6.1 Energy Storage Comparison

Energy Storage	Voltage/Location	Advantage/s	Disadvantage/s
Battery	12V, Any side	• Minimum number of batteries	• Require bi-directional dc-dc converter
Battery	400V, High side	• Allow smaller size dc-dc converter • Stable high-side dc bus voltage • No additional circuitry	• Lack of start-up and support for fuel cell ancillary system • Large number of batteries, low life-expectancy due to unbalance cell voltage
Battery	48V, Low Side	• Minimum number of batteries	• Require additional circuitry for protection and a full power dc-dc converter
Ultracapacitor	48V, Low side	• No additional circuitry • No maintenance	• Availability and cost

A high side battery bank is used for the experiment. Battery bank of eight batteries is used to provide 192V open circuit voltage with rated output power of 5000W. Only eight of the sixteen batteries showed in figure 6.9 are used for the experimental work.

Figure 6.9 196V Battery Bank as Supplementary Energy Supplies

6.2.8 Thermal Management

To calculate the required heat sink for each of the MOSFET, the power loss within the device must first be calculated. The main source of power loss is through conduction, which is simply calculated by I^2R. The maximum RMS current required to flow through the top or bottom MOSFET would occur when the duty cycle is at a maximum for any MOSFET. Hence the worst case is considered when making switch selection.

6.2.9 High Frequency Transformer

The system requires that four isolated converter are interleaved together for the added advantages mentioned in chapter 4. Each of the transformers is designed for 1.25 kW as follows:

Core material

Ferrite is an ideal core material for transformers and inductors in the frequency range 20 kHz to 3 MHz, due to the combination of low cost and core losses. Ferrite core is chosen as a material of a high frequency transformer.

Core size

The power handling capacity of a transformer core can be determined by the area product W_aA_c, where is W_a the available core window area, and A_c is the effective core cross-sectional area. The project made used of the procedure for core size selection provided by (Magnetic Co).

The area product is given by,

$$W_a A_c = \frac{P_{dc} \times C \times 10^8}{4 \times e \times B \times f_s \times K} \qquad 6.29$$

where P_{dc} is the output power, C is the current capacity, e is the transformer efficiency, B is the flux density, f_s is the switching frequency and K is winding factor. Table 6.2 lists popular ferrite shapes available today and their comparative ratings under different considerations. As depicted in the table, selection depends on many factors, and there is no one correct answers for all situations; in most cases, the choice is a compromise (Magnetic Co).

Table 6.2 Ferrite Core Comparative Geometry Considerations

	Pot Core	Double Slab Core	E Core	EC, ETD Cores	PQ Core	EP Core	Torroid
Core Cost	High	High	Low	Medium	High	Medium	Very low
Bobbin Cost	Low	Low	Low	Medium	High	High	None
Winding Cost	Low	Low	Low	Low	Low	Low	High
Winding	Good	Good	Excellent	Excellent	Good	Good	Fair
Assembly	Simple	Simple	Simple	Medium	Simple	Simple	none
Mounting flexibility*	Good	Good	Good	Fair	Fair	Good	Poor
Heat dissipation	Poor	Good	Excellent	Good	Good	Poor	Good
Shielding	Excellent	Good	Poor	Poor	Fair	Excellent	good

*hardware is required for clamping core halves together and mounting assembled core on a circuit board or chassis.

The core type of choice is 'EER' core, then

$$C = 5.07 \times 10^{-3} cm^3 / Amp \qquad 6.30$$

The transformer efficiency is assumed to be 90%. The winding factor is K= 0.3 (primary side only). The flux density B is assumed to be 2000(gauss). Then, the W_aA_c product is calculated as follows

$$W_a A_c = \frac{1.25 \times 10^3 \times 5.07 \times 10^{-3} \times 10^8}{0.9 \times 4 \times 0.3 \times 25 \times 10^3 \times 2000} \qquad 6.31$$

$$W_a A_c = 11.74 cm^4 \qquad 6.32$$

Using the core selection table by area product distribution (refer to appendix A), the core of 47054-EC was selected. Magnetic data for the selected core is shown in appendix B.

Number of turns

Once a core is chosen, the calculation of primary and secondary turns and their wire sizes are readily accomplished. The number of primary turns is given by,

$$Np = \frac{V_p \times 10^8}{4 \times A \times B \times f_s} = \frac{60 \times 10^8}{4 \times 2000 \times 2.79 \times 25000} \qquad 6.33$$

$$Np = 10.75 turns \qquad 6.34$$

Here Vp is the peak primary voltage and A is the cross sectional area of the core, which are given in appendix B. Considering duty loss of 20% at the secondary winding of the transformer originating from the leakage inductance, the final numbers of turns for primary and secondary windings are determined to be

$$N_P : N_S = 11 : 90 \qquad 6.35$$

Wire size

The wire size of the transformer windings is calculated based on the RMS value of the winding current. Since the winding current is 1.414 times larger than the switch current at each side of the transformer, the RMS values of the primary and secondary winding currents can be calculated to 30A and 3.125A, respectively. Then, at 500 circular mils per RMS ampere, the required number of circular mils is obtained by,

Primary circular mil requirement = 500.Irms =15000 6.36

Secondary circular mil requirement =500.Irms =1563 6.37

Hence, the wire sizes AWG 5 and AWG 14 are selected from AWG table (see Appendix C) for the primary and secondary wires respectively.

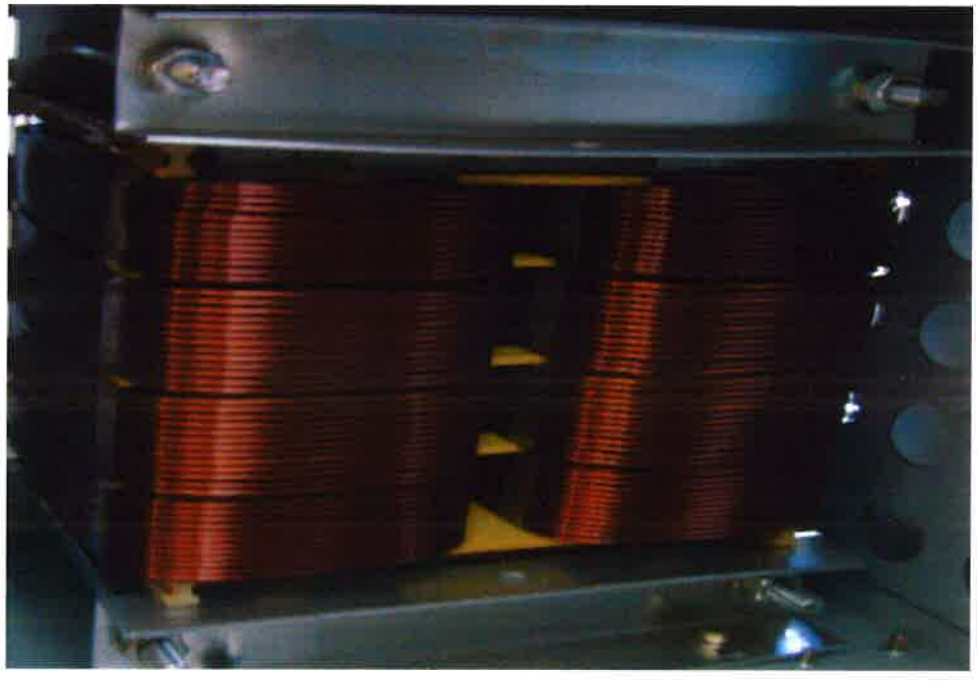

Figure 6.11 High Frequency Transformer.

6.2.10 DC link capacitor

For a worst case, 5 kW at a displacement factor of 0.7 is considered, then the output VA becomes,

$$VA_{out} = \frac{5000}{0.7} = 7142.86VA \qquad 6.38$$

The full load current is given by,

$$I_{a,rms} = \frac{7142.86}{230} = 31.06A \qquad 6.39$$

For the sake of simplicity, the output current i_a is assumed to consist of only fundamental ($I_{a,1}$) and third harmonic ($I_{a,3}$). Further assuming $I_{a,3}$=0.7 $I_{a,1}$ (which is typical of a single phase rectifier type non linear load) since this is a typical case of single phase rectifier type nonlinear load,

$$I_{a,rms} \cong \sqrt{I_{a,1}{}^2 + I_{a,3}{}^2} = 1.22\, I_{a,1} \qquad 6.40$$

Therefore, the fundamental RMS value of the output current becomes,

$$I_{a,1} = \frac{31.06}{1.22} = 25.46A \qquad 6.41$$

The most dominant component of the Dc link capacitor current i_{c1} is the fundamental frequency current, the RMS value of which equals

$$I_{c1,1} \cong I_{a,1} = 25.46A \qquad 6.42$$

For permissible voltage ripple ΔV_{c1} less than 5% or 20V, capacitance can be obtained by,

$$C_1 \geq \frac{I_{c1,1}}{\omega \Delta V_{c1}} = \frac{25.46}{2 \times \pi \times 50 \times 20} \geq 4052\mu F \qquad 6.42$$

The peak voltage rating of the Dc link capacitance becomes,

$$V_{c1,peak} = V_{DC} + \frac{1}{2}\Delta V_{c1} = 410V \qquad 6.43$$

Figure 6.12 shows the Dc link bulk capacitor that is used in first the project while figure 6.13 shows Dc bus in the integrated system.

Figure 6.12 Dc link bulk Capacitors

Figure 6.13 Integrated Systems with Dc Bus Capacitors

6.2.11 IGBT Switches

The average current rating of one inverter switch can be obtained by,

$$I_{SA,AV} = 28\text{A} \qquad 6.44$$

The peak voltage of each IGBT is 410V which is the peak Dc link voltage.
Based on these designed values, IGBTs with 600V, 50A ratings were selected from a manufacturer.

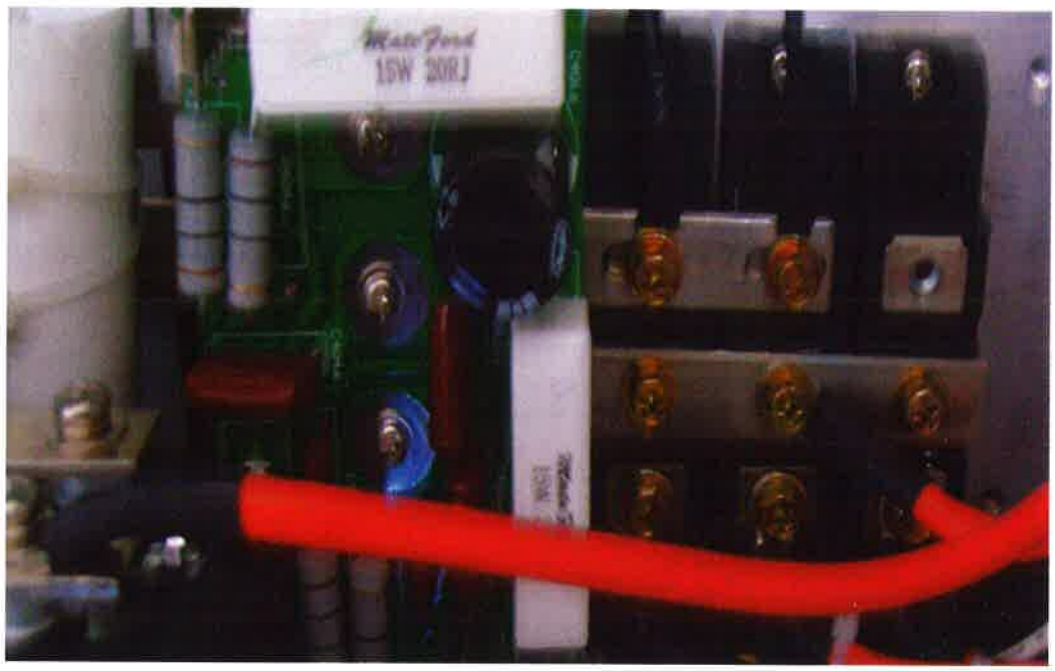

Figure 6.14 Dc-Ac Converter Switches

6.2.12 Output Filter Design

Assuming the switching frequency f_s to be 30 kHz, the frequency ratio is,

$$n = \frac{f_s}{f_1} = \frac{30000}{50} = 600 \qquad 6.45$$

An equivalent circuit for output filter design is shown in figure 6.14. The transfer function H_n for the equivalent circuit is obtained as

$$H_n = \frac{Va,n}{V_{in}} = \frac{-jX_c \times Z_{L,n}}{nX_L X_c + jZ_{L,n}\left(n^2 X_L - X_c\right)} \qquad 6.46$$

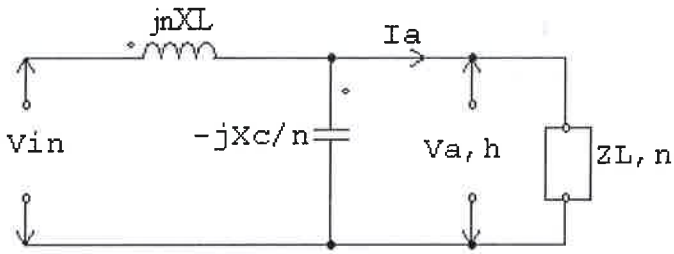

Figure 6.14 Equivalent Circuit Diagram for an LC Output Filter

The gain of the transfer function at fundamental frequency, $|H_1|$, approaches unity if

$$X_L << X_c \qquad 6.47$$

Where

V_{an}: output voltage harmonic

V_c: input voltage harmonic

X_c: impedance of capacitor

X_L: impedance of inductor

$Z_{L,n}$: impedance of load

n: harmonic due to the switching

As the load impedance $Z_{L,n}$ approaches infinity, that is , at no load condition the gain at harmonic frequency, $|H_1|$, approximates in the following

$$|H_n| = -\frac{X_c}{n^2 X_L - X_c} = \frac{1}{n^2 \frac{Z_L}{X_c} - 1} \qquad 6.48$$

Therefore, to satisfy low THD of less than 5%, only the switching frequency component is considered as,

$$\frac{1}{n^2 \frac{Z_L}{X_c} - 1} \leq 0.045 \qquad 6.49$$

To limit the ripple voltage across the filter capacitance generated from the third harmonic load current, an equivalent circuit is considered as shown in figure 6.16. The current flowing through the filter capacitor is,

$$I_c = \frac{jhX_L}{-\frac{jX_c}{h} + jhX_L} \times I_{a,h} \qquad 6.50$$

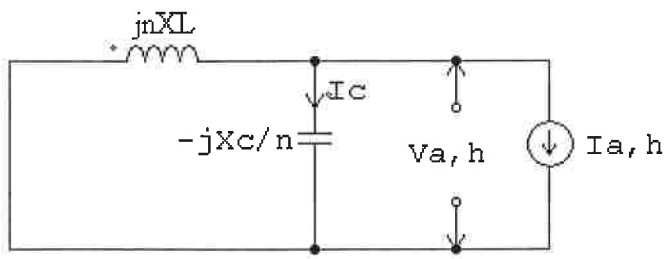

Figure 6.16 Equivalent Circuit Diagram for a Non Linear Load

Then, the voltage across the filter capacitor at a harmonic frequency becomes,

$$V_{a,h} = \frac{jhX_L}{1-h^2\frac{X_L}{X_c}} \times I_{a,h} \qquad 6.51$$

Where

$V_{a,h}$: equivalent voltage

I_h: current at harmonic

X_c: impedance of capacitor

X_L: impedance of inductor

n: harmonic due to nonlinear load

This further approximate,

$$|V_{a,h}| \leq jhX_L \times I_{a,h} \qquad 6.52$$

if

$$\frac{h^2 X_L}{X_c} << 1 \qquad 6.53$$

For the third harmonic h=3,

$$\left|\frac{V_{a,e}}{Va,1}\right| \leq \frac{3 \times X_L \times I_{a,h}}{|V_{a,1}|} \qquad 6.54$$

The capacitor ripple voltage at the third harmonic frequency is limited to 3% of the fundamental output voltage. Then, the impedance of the filter inductor is determined by,

$$X_L \geq \frac{0.03 \times |V_{a,1}|}{3 \times I_{a,3}} = \frac{0.03 \times 230}{3 \times 17.82} = 0.129\Omega \quad 6.55$$

Then, the filter inductance becomes,

$$L_f = \frac{X_L}{2\pi f_1} = \frac{0.129}{2\pi \times 50} = 411\mu H \quad 6.56$$

From equations 6.53 and 6.54, the impedance of the capacitor is obtained by,

$$X_c \leq \frac{0.129 \times 400^2}{23.22} = 888.88\Omega \quad 6.57$$

Then, the filter capacitance becomes,

$$C_f \geq \frac{1}{2\pi f X_c} \quad 6.58$$

$$C_f \geq \frac{1}{2\pi \times 50 \times 888.88} = 3.58\mu F \quad 6.59$$

6.2.13 Input Capacitor Filter

Selecting a proper input capacitor contributes to the reduction in fuel cell input current ripple. The average input current I_{avg} at full load is 238.10A. Assuming a square wave input current, for a duty ratio of 0.9 (worst-case scenario), the peak current I_{peak} is,

$$I_{peak} = 264.55A \quad 6.60$$

And the RMS current I_{RMS} is,

$$I_{c,rms} = I_{peak}\sqrt{D} \quad 6.61$$

$$I_{c,rms} = 250.97A \quad 6.62$$

Therefore the RMS capacitor current $I_{c,rms}$

$$I_{c,rms} = \sqrt{I_{rms}^2 - I_{avg}^2} = 79.34A \quad 6.63$$

Based on the rated ripple current, 4 aluminium electrolytic capacitors 22000μF, 100V each is selected.

6.2.14 Fuel Cells System

In order to design the fuel cells system that was used for the simulation of the above designed circuits, an approximate linear model of PEM fuel cells was implemented. Table 6.3 shows the voltage and current relationship of a typical PEM fuel cells system. Excel was used to obtain a linearised relationship between the voltage output and current output. This is justified as the fuel cells system mostly operates in the linear region of its polarisation curve.

Table 6.3.Voltage and Current Relationship of a Typical Fuel Cell System

Voltage	Current
41	0
38	0.01
34	27
32	44
31	64
29.5	100
29	115
28.5	132
28	142
27.5	146
27	150
22	275

A reasonable regression coefficient of 0.8786 was obtained for the simulation demonstration as show in figure 6.17. The only constraint is that the fuel cells could not be operated at the maximum voltage of 42V due to the best line of fit used. A capacitor with a very small value is connected across the fuel cells to account for slow response of the system.

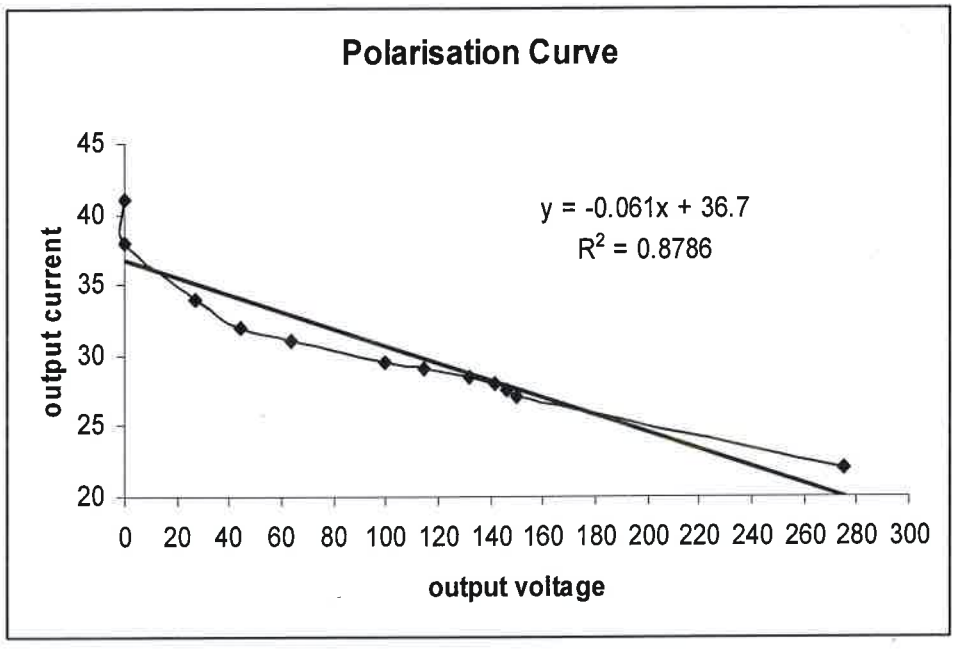

Figure 6.17 Polarisation Curve of PEM Fuel Cells System

6.3 Power Loss Budgets

With the main objective of achieving overall efficiency of 90%, only 500W of power loss is available for optimum design considerations. Components are selected based on minimum power loss so that the overall efficiency of 90% is achievable. A power loss budget of less than or equal to 150W is allocated to the first stage boost converter and 150W power loss budget to the second stage boost converter. The inverter stage power loss allocation is less than or equal to 150W.The input capacitor, Dc link capacitor, output filter as well as parasitic effects take the balance thereof.

The inductor power loss is calculated using the software provided by Micrometals Software. The copper loss is 69.24W and the core loss is 0.34W. Thus, the total power loss is 69.58W.

Figure 6.17 shows the design parameters such as inductance at maximum current, maximum Dc resistance, maximum current, peak regulator voltage, regulator Dc output voltage, core shape and winding type.

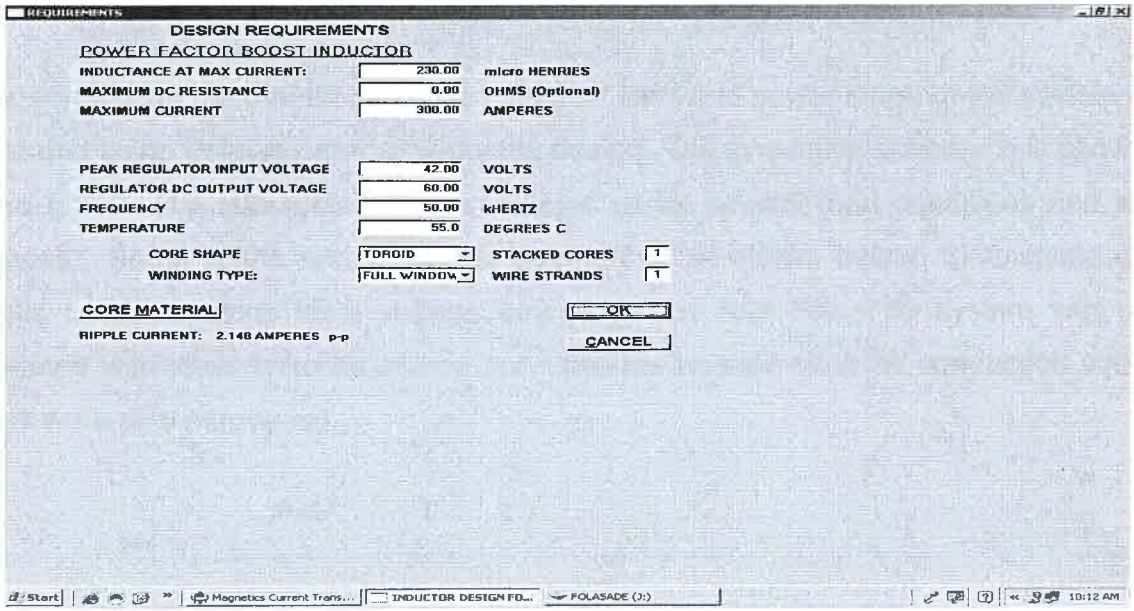

Figure 6.18 Design Parameters Input Interface

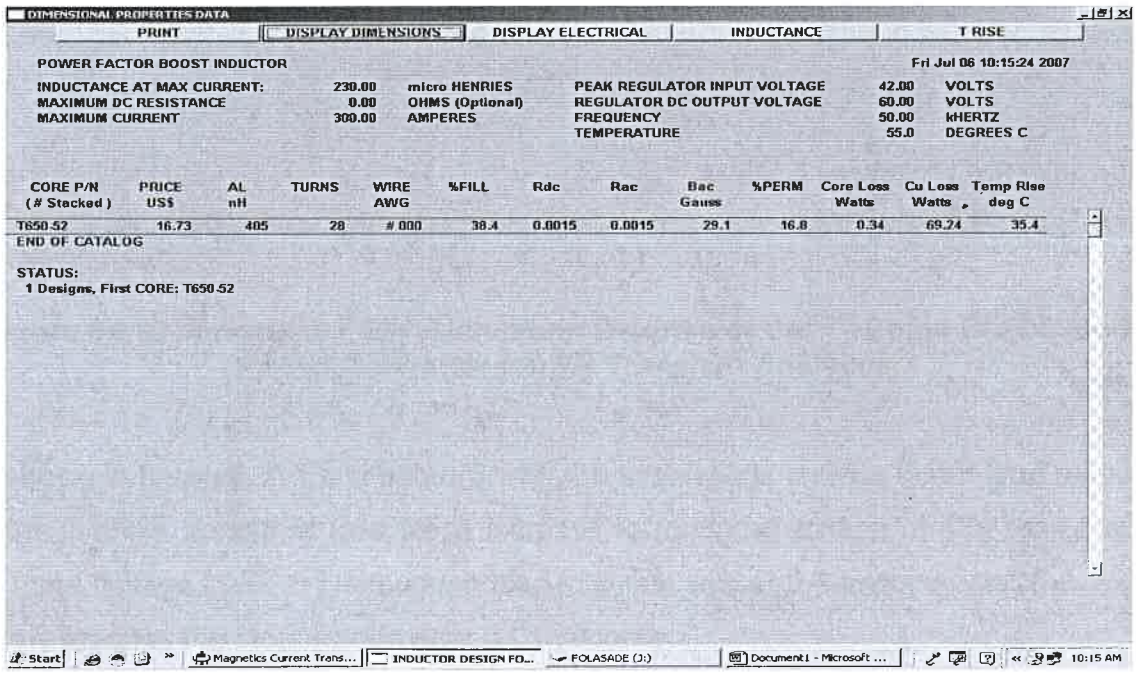

Figure 6.19 Inductor Designed Parameters and Inductor Power Loss

Figure 6.19 displays the inductor selection with power losses and other important parameters.

6.4 First Stage Dc-Dc Boost Power Converter Transient Analysis

After completing the theoretical design, the first front end power stage of the system was simulated using Psim in order to verify the design. The simulation schematic is shown in figure 6.110. The sub system was simulated under several load conditions and input voltages. Some of the system output waveforms are shown below. Simulations were results obtained using ideal voltage source as the fuel cell. The system was also simulated with ideal switches. Some non ideal parameters such as conduction voltage drops were also introduced.

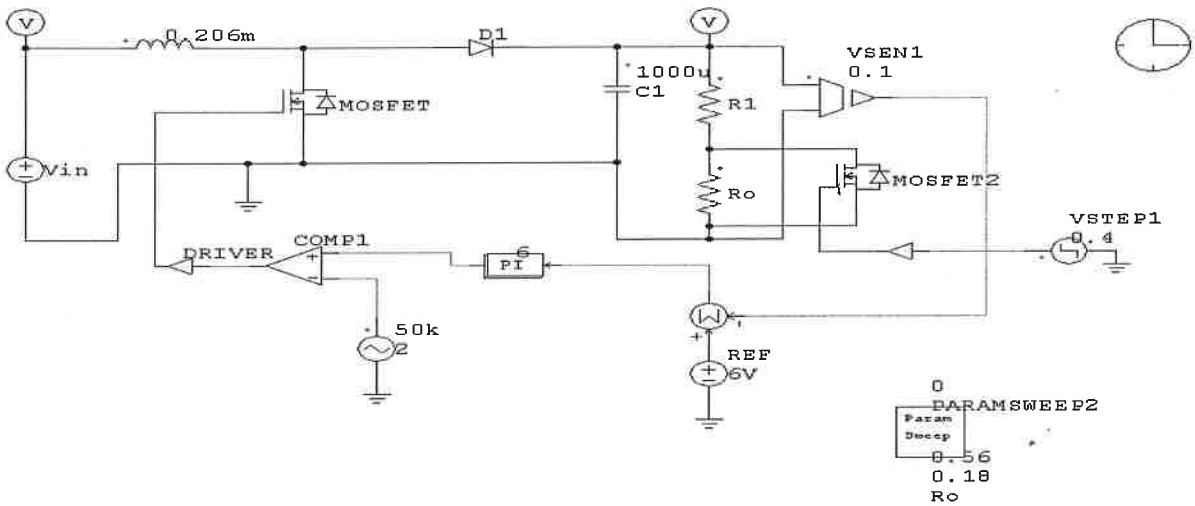

Figure 6.110 Schematic PSIM Simulation Diagram of the 1st Stage DC-DC Boost Power Converter for the Transient Analyses.

As shown in figure 6.111 and figure 6.112, the simulations show a faster time response for the fuel cell system to load steps increase for an input voltage of 42V than the fuel cell input voltage of 21V. The sudden load injection was at 0.4 seconds and the system quickly reaches the steady-state after 0.01 seconds.

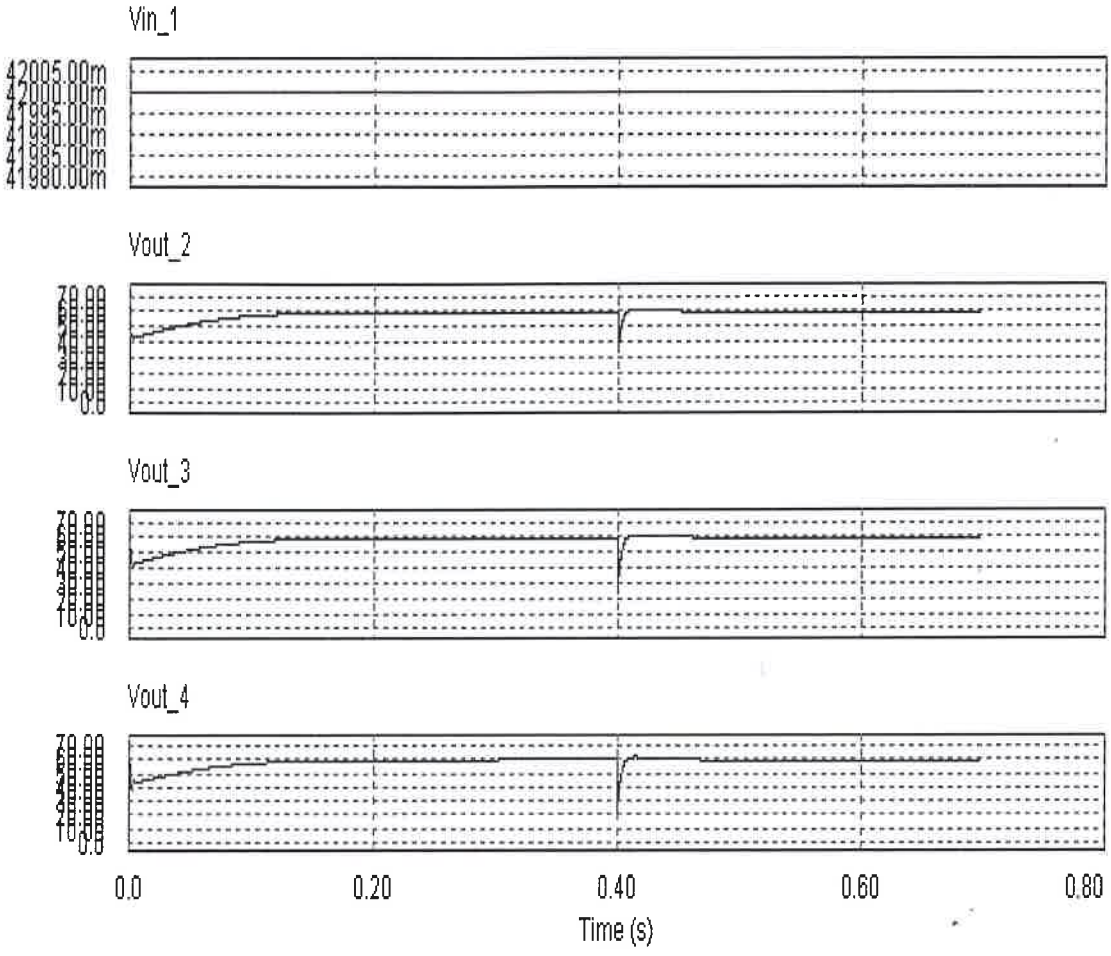

Figure 6.111 Transient Response Analyses for V_{in_max} = 42V at 50%, 75% and 100% Load Steps.

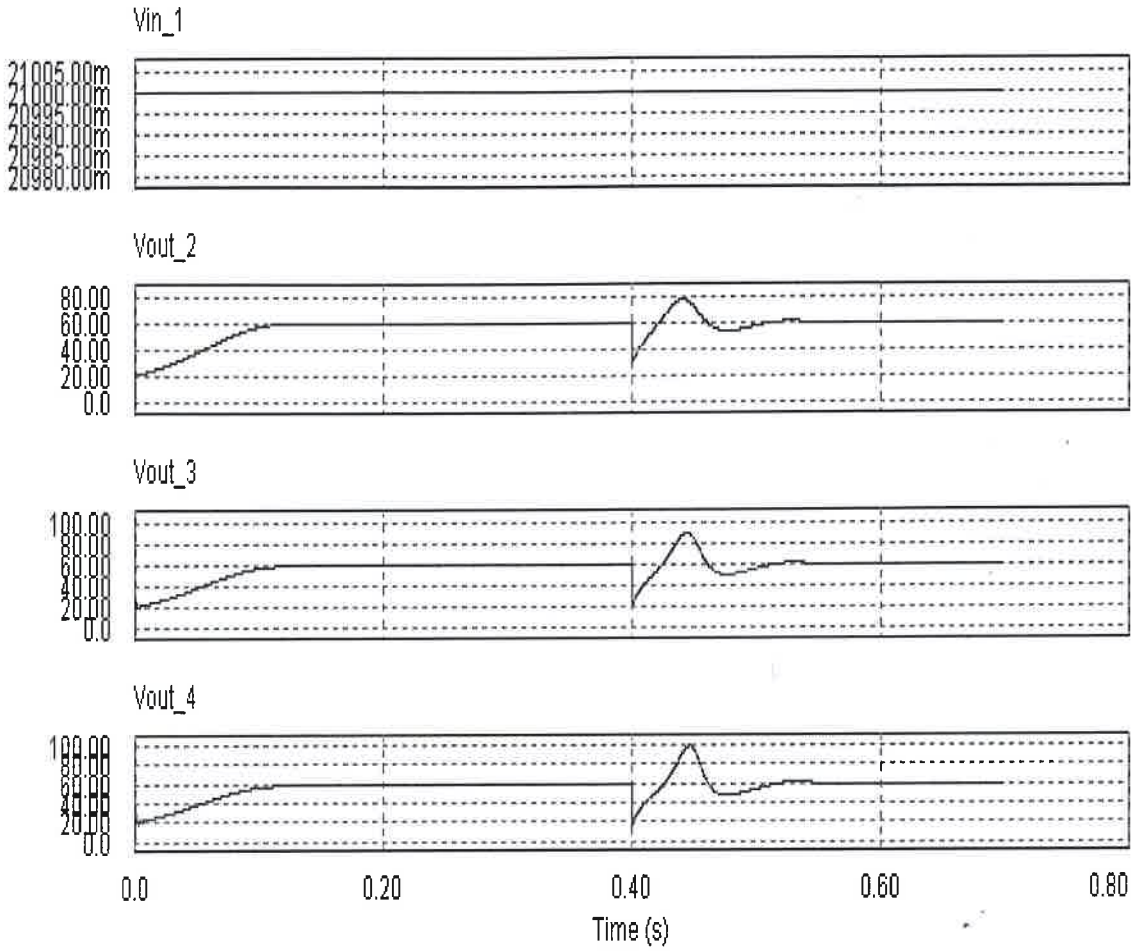

Figure 6.112 Transient Response Analyses for V_{in_min} = 21V at 50%, 75% and 100% Load Steps.

A slower time response is achieved with fuel cell input voltage of 32V which is taken as the nominal voltage but that is better minimum fuel cell input voltage of 21V. For an input voltage of 21V, the sudden load was injected into the system at 0.12 second and reaches steady-steady after 0.5 seconds Figure 6.19 shows the simulation results for the fuel cell input voltage of 21V.

An adequately sized auxiliary energy storage system with time constant less than the system response time will supply the system during this short period of time (D Candusso, I Valero, A Walter, S Bacha, E Rulliere &B Raison, 2000) .

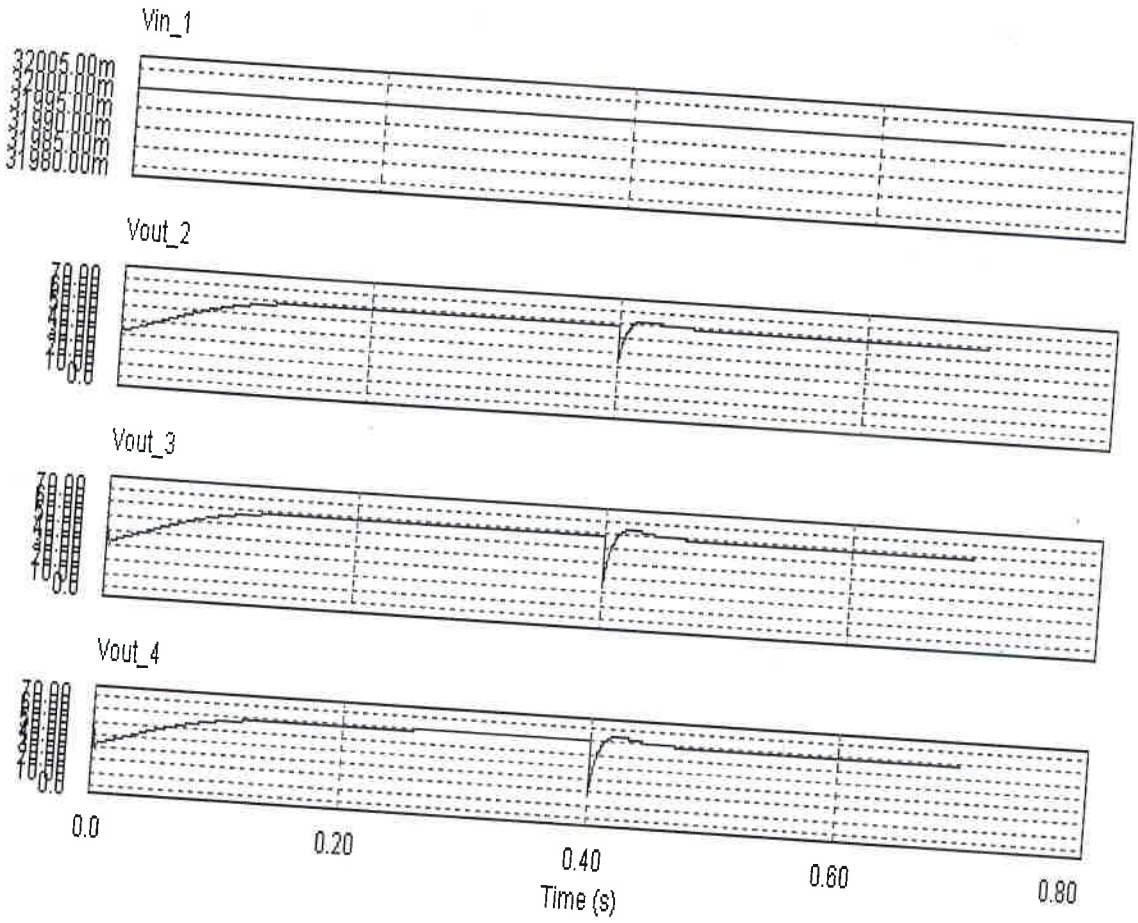

Figure 6.113 Transient Response Analyses for $V_{in\_nominal}$ = 32V at 50%, 75% and 100% Load Steps.

For an input voltage of 32V, the sudden load was injected into the system at 0.4 second and reaches steady-steady after 0.02 seconds Figure 6.113 shows the simulation results for the fuel cell input voltage of 21V.

CHAPTER 7

CONCLUSIONS AND RECOMMENDATIONS

7.1 Summary

Fuel cells can convert a remarkably high proportion of the chemical energy in a fuel to electricity. With the efficiency approaching 60%, even without co-generation, fuel cell power plants are nearly as efficient as convectional power plants. Unlike in the large steam plants, the efficiency is not a function of the plant size for the fuel cell power plants. Small-scale fuel cell plants are just as efficient as the large ones, whether they operate at full load or not. Fuel cells contribute significantly to the cleaner environment; they produce dramatically fewer polluting emissions, and their by-products are primarily hot water and electricity. Chapter two gives an overview of different types of fuel cells power converter systems already designed and developed, and other related important issues. Because of their modular nature, fuel cells systems can be located at or near load centres, resulting in savings in transmission network expansion. As a result, fuel cells systems are increasingly used for various purposes, such as in automotive, residential, and industrial applications. Chapter three was dedicated to reviewing the properties of several types of fuel cells technology.

In order to efficiently use the energy provided by a fuel cell, a typical system requires the use of a power converter system. These fuel cell power converters consist of a Dc-Dc converter coupled with a Dc-Ac converter to produce the Ac waveform suitable for residential or industrial applications. Chapter four presented a detailed modelling and control scheme that was used in this project. Important issues, such as the criteria for using the adopted new converter topology, fuel cell model were presented.

There is no ultimate Dc-Dc converter perfectly suited for all applications. For a given application with given specifications, trade off should be performed to select the converter topology. Several approaches that meet the specifications should be considered, and for each important quantity such as worst case semiconductor device RMS currents, size, component count, etc should be computed. This type of quantitative comparison can lead to the selection of the best converter topology or design of a novel power convert as for this project. Extensive review of different types of developed fuel cell systems played a very vital role in conceiving novel fuel cells off grid power converter topology system for this research project.

7.2 Future Research

The future improvements of the system will involve the use of synchronous rectifiers instead of diodes to further increase the efficiency of the power converter system. The power converter system should be tested with the real fuel cell system as the input source instead of bank of batteries so that the real time response of the system could be studied for system performance improvement and higher reliability.

7.3 Publications Related to the Thesis

Raji AK and Kahn MTE, "Overview of Energy Conversion Systems for Fuel Cell Technology: Alternative Energy Generation", Domestic Use Energy Conference, Cape Town, South Africa, 11-12 April, 2007, pp 123-128

Raji AK and Kahn MTE, "Fuel Cell Technology for Greenhouse Gas Emission Reduction: Alternative Energy Source", Botswana Institution of Engineers International Biennial Conference, 17-19 October 2007, Gaborone, pp. 13

References

Aguair A.P, Adjiman C.S and Brandon N.P.,"Anode-supported Intermediate Temperature Direct Internal Reforming Solid Oxide Fuel Cell I: model-based steady-state performance", *Journal of Power Sources*, vol. 138,

Ahmet Lokurlu, Thomas Grube, Bernd Höhlein and Detlef Stolten, "Fuel Cells for Mobile and Stationary Applications- cost Analysis for Combined Heat and Power Stations on the Basis of Fuel Cells". *International Journal of Hydrogen Energy,* vol. 28, pp.703-711, 2003

Andersen G K, Klumpner C, Kjær and Blaabjerg F, "A New Green Power Inverter for Fuel Cells", *IEEE Power Electronics Specialist Conference*, Vol. 2, pp.727-733

Andersen G K, Klumpner C, Kjær and Blaabjerg F, "A New Power Converter for Fuel Cells with High System Efficiency", *International Journal of Electronics*, 2003, Vol. 90, no. 11-12, pp. 737-750

Attansio R, Caccinato M, Consoli A, Scarcella G, Testa A and Gennaro F, "A New converter System for Fuel Cell Distributed Energy Generation", *IEEE Power Electronics Specialist Conference,* 36th Annual, pp. 1621-1627, 2005

Basu Supratim and Undeland T M, "Design Considerations for Optimizing Performance & Cost of Continuous Mode Boost PFC Circuits", *IEEE Applied Power Electronics Conference and exposition,*20th Annual, Vol. 2, pp. 1133-1138, 2005

Bohn T.P and Lorenz Robert D., 2003, "A low-cost inverter for domestic fuel cell application", *Proceedings in Fuel Cell Seminar 2003*, pp. 41-48

Bor-Ren Lin, 2001, "A single-phase three-phase pulse width modulation ac/dc converter with the function of power factor corrector and active power filter", *Electric Power System Research*, 58, pp. 157-167

Calais M, Agelidis V G and Heinhard M, "Multilevel Converter for Single-Phase Grid Connected photovoltaic Systems: An Overview", *Solar Energy*, Vol. 66, No. 5. pp. 325-335, 1999

Canales F, Barbosa P, Aguilar C and Lee F L, "A High-Power-Density Dc/Dc Converter for High-Power Distributed power Systems", *IEEE Power Electronics Specialist Conference,* 34th Annual, Vol. 1, pp. 11-18, 2003

Chen R Y, Lin R L, Liang T J, Chen J F and Tseng K C, "Current-fed Full-Bridge Boost Converter with Zero Current Switching for high Voltage Applications", *IEEE Industry applications Conference,* 40th Annual, Vol. 3, pp. 2000-2006, 2005

Choi Woojin, Howze Jo. W and Enjeti Prasad, 2006, "Fuel cell powered uninterruptible power supply system design consideration", *Journal of Power Sources*, 157, pp. 311-317

Dan Rastler and EPRISolutions, "Opportunities and Challenges for Fuel Cells in the Evolving Energy Enterprises", *Fuel Cell Bulletin,* vol. 3 (19), pp. 7-11, 2000

Denis Candusso, Ianko Valero, Aurelien Walter, Seddick Bacha, Elisabeth Rulliere and Bertrand Raison, "Modelling, Control and Simulation of a Fuel Cell Based Power supply System with Energy Management" *Industrial Electronics Society,* Vol. 2, IEEE 2002 28th Conference pp 1294-1299

Dufour A.U., "Fuel Cell - A New contributor to stationary power". *Journal of Power Sources*, vol. 71, pp.19-25, 1998

EG&G Technical Services, Parsons Inc., Science applications international corporation, *Fuel cell Handbook*, 5th ed., U.S. Department of Energy, office of fossil energy, National Energy Technology Laboratory, Virginia 2000

Ellis M.W, Von Spakovsky M.R and Nelson D.J, 2001, "Fuel cell systems: efficient, flexible energy conversion for the 21st century," *Proceedings of the IEEE*, vol. 39, no. 12, pp. 1808-1818,

Ellis M.W, Von Spakovsky M.R and Nelson D.J., "Fuel Cell Systems: Efficient, Flexible Energy Conversion for the 21st Century". *Proceedings of the IEEE*, Vol. 39 (12), pp. 1808-1818, 2001.

Ferguson J.R, Fiard J.M and Herbin R, "Three Dimensional Numerical Simulation for Various Geometries of Solid Oxide Fuel Cells", *Journal of Power Sources*, vol. 58, pp.109-122,1999

Fontes G, Turpin C, Astier S and Meynard T A, "Interactions Between Fuel Cells and Power Converters: Influence of Current Harmonics on a Fuel Cell Stack", *IEEE Transaction on Power Electronics,* Vol. 22, no. 2, March 2007

Franco L C, Pfitscher L L and Gules R, "A New Static Gain Non-Isolated Dc-Dc Converter", *IEEE Power Electronics Specialist Conference,* 34th Annual, Vol. 3, pp.1367-1372, 2003

Frank de Bruijin, "The Current Status of Fuel Cell Technology for Mobile and Stationary Applications". *Green Chem.,* vol.7, pp. 132-150, 2005.

Gang Wang, Pradeep Pant, Hasan Mohammad, Parvic Famouri and Osman Demirce, 2003, "High efficiency low cost inverter system for fuel cell application", *Proceeding in Fuel Cell Seminar 2003*, pp. 16-20

Gemmen R. "Analysis for the Effect of Inverter Ripple Current on Fuel Cell Operating Condition". *Proceedings of the ASME 2001 International Mechanical Engineering Congress and Exposition*, New York

Gopinath R, Kim S, Hahn J-H, Webster M, Burghardt, Campell S, Becker D, Enjeti P, Yeary M and Howze J, "Development of a Low Cost Fuel Cell Inverter System with DSP Control", *IEEE Power Electronics Specialist Conference*, 2002, Vol. 1, pp. 309-314

Guillaume Fontes, Christophe Turpin, Stephan Astier and Thierry A Meynard, "Interaction Between Fuel Cells and Power Converters: Influence of Current Harmonics on a Fuel Cell Stack" *IEEE Transaction on Power Electronics,* March 2007 Vol. 22, no. 2, pp 670-678.

Haiping Xu, Li Kong and Xuhui Wen, " Fuel Cell Power System and Hidg Power DC-DC Converter" *IEEE Transaction on Power Electronics,* Vol. 19, no. 5, September 2004, pp. 1250-1956

Hernando M, Villegas P, Fernández, Sebastián and Corral J, "Design Considerations for a 48V to ± 400VDC Converter for UPS Applications", *Power Electronics Specialist Conference*, 2003, Vol. 4, pp.1924-1928

Hirschenhofer J. "How the Fuel Cell Produces Power". *IEEE AES Systems Magazine,* vol. 7 (11), pp.24-25, 1992

J. Padulles G.W, Ault, and J. R. McDonald, "An Integrated SOFC Plant Dynamic Model for Power Systems Simulation" *Journal of Power Sources*, vol. 86, pp. 495-500, 2000

Jin Wang, Fang Z. Peng, Joel Anderson, Alan Joseph and Ryan Buffenbarger, 2003, "A new low cost inverter system for 5 kW fuel cell", *Proceedings in Fuel Cell Seminar 2003*, pp. 1-7

Jinhee Lee, Jinsang Jo and Sewan Choi, Soobin Han, 2003 "A 10 kW SOFC low Voltage battery hybrid power processing unit for residential use", *Proceedings in Fuel Cell Seminar 2003*, pp. 33-40

John K., "Fuel Cells-a 21st Century Power System". *Journal of Power Sources*, vol. 71, pp. 12-18, 1998.

Ka Leug & Don Alfano, "Design and Implementation of a Practical Digital PWM Controller" IEEE APEC, 2006, pp.1437-1442

Klaus Tüber, Marco Zobel, Heribert Schmidt and Christopher Hebling, "A polymer Electrolyte Membrane Fuel Cell System for Powering Portable Computers". *Journal of Power Sources*, vol. 122, pp.1-8, 2003.

Krein P T and Balog R, "Low Cost Inverter Suitable for Medium-Power Fuel Cell Sources", *IEEE Power Electronics Specialist Conference*, 2002, Vol. 1, pp. 321-326

Lai J-S, "A High-Performance V6 Converter for Fuel Cell Power Conditioning System", *Vehicle Power and Propulsion, IEEE conference*, 2005, pp 642-630

Lehman P.A and Chamberlin C.E., 1991, "Design of a photovoltaic-hydrogen-fuel cell energy system", *International Journal of Hydrogen Energy*, vol. 16, no. 5, pp. 349-352

Lesster L.E., "Fuel cell power electronics- managing a variable-voltage dc source in a fixed-voltage ac world", *Fuel Cell Bulletin*, 2000, vol. 3, no. 25, pp. 5-9

Lipman T.E, Edward J.L and Kammen D.M., "Fuel Cell System Economics: Comparing the Costs of Generating Power with Stationary and Motor Vehicle PEM Fuel Cell Systems". *Energy Policy*, vol. 32, pp.101-125, 2004.

Lynch J., "The Rise of MicroGrid Power Networks - Next Generation DG Architecture for the New Energy Landscape". *Northern Power Systems, Energy and Power Management,* pp. 16-19, February 1st 2006.

Magadza, C.H.D., "Climate Change: Some Likely Multiple Impacts in Southern Africa". *Food Policy,* vol. 19 (2), pp. 165-191, 1994

Martina Calais, Vassilios G. Agelidis and Mike Meinhardt, "Multilevel Converters for Single-Phase Grid Connected Photovoltaic Systems: Overview", *Solar Energy,* Vol. 66, no. 5, pp. 325-335, 1999

Mason A J and Jain P K, "New ZVS-PS-PB DC/DC Converters with Adaptive Energy Storage for High Power SOFC Application", *IEEE Industrial Applications Conference*, 2005, Vol.1, Oct 2-6, pp 607-613

Mazundar J, Batarseh I, Kutkut N and Demirci O, "High Frequency Low Cost DC-AC Inverter Design with Fuel Cell Source for Home applications", *IEEE Industry Applications Conference*, 2002, Vol. 2, pp. 789-794

Nergaard T A, Ferrell J F, Leslie L G and Lai J-S, "Design Considerations for a 48V Fuel Cell to Split Single Phase Inverter System with Ultracapacitor Energy Storage", *IEEE Power Electronics Specialist Conference*, 2002, Vol. 4, pp. 2007-2012

Novaes Y. R and Barbi I., "Low frequency ripple current elimination in fuel cell systems", *Proceedings in Fuel Cell Seminar 2003*, pp. 21-26

Onovwiona H.I and Ugursal V.I., "Residential Cogeneration Systems: Review of the Current Technology". *Renewable and Sustainable Energy Reviews,* vol. 10, pp. 389-431, 2006.

Puttgen H.B., MacGrego P.R and Lambert F.C., "Distributed generation: Semantic hype or the down of a new era" *Power and Energy Magazine IEEE*, 2002, vol. issue 1, pp. 22-29

Puttgen H.B., MacGrego P.R and Lambert F.C., "Distributed Generation: Semantic Hype or the Down of a New Era". *Power and Energy Magazine IEEE*, 2002, vol. issue 1, pp. 22-29.

Raji A.K. and Kahn M.T.E, "Overview of Energy Conversion Systems for Fuel Cell Technology: Alternative Energy Generation", *Proc. 15th International Domestic Use of Energy Conference,* Cape Town, South Africa, pp. 123-128, 11-12 April, 2007.

Rashid M.E., 2004, *Power Electronics: Circuits, Devices and Applications,* 3rd edn. Pearson Education, Inc. Upper Saddle River, USA, p. 226

Rashid M.E., 2004, *Power Electronics: Circuits, Devices and Applications,* 3rd edn. Pearson Education, Inc. Upper Saddle River, USA, p.810

Rashid M.E., 2004, *Power Electronics: Circuits, Devices and Applications,* 3rd edn. Pearson Education, Inc. Upper Saddle River, USA, p.827

Rashid M.E., 2004, *Power Electronics: Circuits, Devices and Applications,* 3rd edn. Pearson

Rekha T.J and G. Radman, "Modelling and Control of Distributed Generation Systems including PEM fuel Cell and Gas Turbine", *Electric Power Systems Research*, vol. 77, pp. 83-92, 2007.

Roderick W.S and Coors W.G, "Large Limits of Electrical Efficiency in Hydrocarbon Fuelled SOFCs", *Journal of Power Sources*, vol. 143, pp. 166-172, 2005

Sharma R and Gao H, "A new DC-DC Converter for Fuel Cell Powered Distributed Residential Power Generation Systems", *IEEE Applied Power Electronics Conference and Exposition*, APEC 06, pp. 1014-1018

Shi Jianjiang, Pan X, Chen L, Hu L and He X, "Development of A Novel Combined Converter with Low-Voltage and High-Current Input, High Power and High-Voltage Output", *Industry Applications Conference*, 2005, Vol. 1, pp. 620-624

Shin H.-B, Park J.-G, Chang S.-D and Choi, "Generalized Analysis of Multi-Phase Interleaved Boost Converter", *International Journal of Electronics*, Vol. 92, no.1, Jan. 2005, pp 1-20

Shireen W, Kulkarni R.A and Arefeen M, "Analysis and Minimization of Input Ripple Current in PWM Inverters for Designing Reliable Fuel Cell Power Systems", *Journal of Power Sources*, vol. 156, pp.448-454, 2006

Smith Chris, Gillion Mike, Urciuoli Darmian, Mclandrich Andy, Pepa Elton and Lai Jin-Sheng, "low-cost Solid Oxide fuel cell power conditioning with bidirectional charging", *Proceeding in Fuel Cell Seminar 2003*, pp. 8-15

Sung-Jun Park, Feel-Soon Kang, Su Eog Cho, Chae-Joo Moon, Hae-kon Nam and Toshifumi Ise, , "New parallel driving strategy based on modified converters and peak current mode control for photovoltaic power generation systems". *Solar Energy*, 2006, vol. 80, pp. 524-534

Thounthong Phatiphat, Rael Stephane and Davat Bernard, "Test of a PEM fuel cell with low-voltage static converter", *Journal of Power Sources*, 2006,153, pp. 145-150

TIHANYI T., *Electromagnetic compatibility in power electronics*, New York: Butterworth-Heinemann, 1995

Todorovic Maja Haarfman, Palma Leorardo, Choi Woojin, Dowling Cody, Humphrey Daniel, Tarbel David , Enjeti Prasad and Howze Jo , "Development of a low cost fuel cell inverter system with DSP control for residential use", *Proceedings in Fuel Cell Seminar 2003*, pp. 27-32

Tofoli Fernando Lessa and Gallo Carlos Alberto, "A High Power Factor Symmetrical Switched Mode Power Supply", *Rev. TecnoL, Fortaleza*, June2005, Vol.26, no. 1, pp. 12-20,

Turkey A M and Krase J N, "A Low-Cost Inverter for Domestic Fuel Cell Applications", *IEEE Power Electronics Specialist Conference,* 33rd Annual, Vol. 1, pp. 339-346, 2002

Wai R-J and Duan R-G, "High-Efficiency Power Conversion for Low Power Fuel Cell Generation System", *IEEE Transactions on Power Electronics*, Vol. 20, no. 4, 2005

Wajiha Shireen, Kulkani Rahul A & Arefeen M., "Analysis and minimization of input ripple current in PWM inverter for designing reliable fuel cell power systems", *Journal of Power Sources*, 2006, vol. 156, issue 2, pp. 257-264

Wei Chen, "High Efficiency, High Density, Polyphase Converters", *Linear Technology*, 1999, Application Note 77,

Xue X.D, Cheng K.W.E and Saatanto D, "Unified Mathematical Modelling of Steady-state and Dynamic-state Voltage-current Characteristics for Fuel Cells", *Electrochimica Acta*, vol. 52, pp. 1135-1144, 2006

Yamamoto, O, "Solid Oxide Fuel Cells: Fundamental Aspects and Prospects". *Electrochimica Acta*, vol. 45, pp.2423-2435, 2000.

Yuvarajan S, Dachuan Yu and Shanguang Xu, "A Novel Power Converter for Photovoltaic Applications". *Journal of Power Sources*, Vol. 135 pp. 327-331, 2004

Zhu X, Xu D, Shen G, Xi D, Mino K and Umida H, "Current-Fed DC/DC Converter with Reverse Block IGBT for Fuel Cell Distributing(sic) Power System", *Industry Applications conference*, 2005, Vol. 3, pp. 2043-2048

Vutrax, 1998, 'Vutrax Technical Database, Aspect of Track Widths', www.vutrax.co.uk/trackwidth.htm (10 August, 2007)

United State Department of Energy: Energy efficiency and renewable energy, [On-line] www.eere.energy.gov/consumer/information_resources [22 June 2007]

Wikipedia, The free encyclopedia, Fuel Cells. [On-line]. Available from: www.en.wikipedia.org/wiki/fuel_cells, [03 October 2006]

Gangi J. Worldwide Fuel Cell Installations, updated October 2005. [On-line]. Available: www.//fuelcells.org/info/charts/FCInstallationChart.pdf

Worldwide Fuel Cell Installations, updated June 2007. [On-line]. Available: www.//fuelcells.org/info/charts/h2fuelingstations.pdf

Wikipedia, The free encyclopedia; "Fuel Cells" [online]. Available from: www.en.wikipedia.org/wiki/fuel_cells [03 October 2006]

Wikipedia, The free encyclopedia; History of Fuel Cell. [On-line]. Available from: www.en.wikipedia.org/wiki/fuel_cells [04 March 2007]

Appendices

Appendix A: Transformer Core Selection by Area Product Distribution

[Design Application Notes, MAGNETIC Inc]

WaAc* (cm^4)	PC	RS,DS,HS	RM, EP	RM SOLID	PQ	EE LAM	EE,EEM,EFD	EE,EI PLANAR	UU, UI	ETD, EER	EC	TC
See Section	6	7	8/9	8	10	11	11	11	11	12	12	13
0.001	40704							41309 (EE)				40601
0.002	40905		40707 (EP)				40904 40906					40603
0.004												
0.007	41107		41110(RM)									40705
0.010		41408 (RS,DS)	41010(EP)			41203			41106 (UI)		41003	41005
0.020	41408		41510(RM) 41313(EP)	41510		41205	41208 41209 41515 41707		41106(UU)		40907	41303
0.040			41812(RM)	41812			41709 42110					41206 41305
0.070	41811	42311 (RS,DS,HS)	41717(EP)		42610	41808						41306 41605
0.100	42213	42318 (HS)	42316(RM)	42316	42016 42614	41810 42510		42216(EE)				
0.200	42616	42318 (RS,DS) 42616 (RS,DS,HS)	42819(RM) 42120(EP)		42020 42620 43214		42211 42810 43009 42523	43618(EI) 43208(EI)	42515 (UI)			41809 42206
0.400		43019 (RS,DS,HS)		42819	42625	42520	42515 43007	43618(EE) 43208(EE)				42207
0.700	43019		43723(RM)		43220	43515	43013		42220(UU) 42512(UU) 42515(UU)	43517		42507
1.00	43622	43622 (RS,DS,HS)		43723	43230	44317	43520 43524 44011	44308(EI)	42530(UU)	44119	43434 43521(EER)	42908
2.00	44229 44529	44229 (RS,DS,HS)			43535	44721	44020 44924	44308(EE) 45810(EI)	44119(UU) 44121(UU)	45224 44216(EER)	43939 43615 44444 45032	43610 43813
4.00					44040	45724	44022 45021	46410(EI)	44125(UU) 44130(UU)	44949	44416	
7.00							45528 46016	45810(EE) 46409(EE)				
10.00							45530	46410(EE)		47035 47228		44916 44925 46113
20.00							48020				47054	47313 47325
40.00								49938(EE)				48613
100							49928		49925(UU) 49925(UI)			

*Bobbin window and core area product. For bobbins other than those in this catalog, WaAc may need to be recalculated.

Appendix B: 47054-EC Magnetic Data (MAGNETIC Inc)

Core Data (ungapped)

Any practical gap available. See pages 1.8-1.11

			MECHANICAL DIMENSIONS (mm)							
PART	CORE TYPE	FIG.	A	B	C	D	E	F	S	T
0_43517EC	EC 35	1	34.5 ± .8	17.3 ± .15	9.5 ± .3	12.3 ± .4	22.75 ± .55	9.5 ± .3	2.75 ± .25	28.5 ± .8
0_44119EC	EC41	1	40.6 ± 1.0	19.5 ± .15	11.6 ± .3	13.9 ± .4	27 + .7	11.6 ± .3	3.25 ± .25	33.6 ± 1
0_45224EC	EC52	1	52.2 ± 1.3	24.2 ± .15	13.4 ± .35	15.9 ± .4	33 ± .9	13.4 ± .35	3.75 ± .25	44 ± 1.3
0_47035EC	EC70	1	70 ± 1.7	34.5 ± .15	16.4 ± .4	22.75 ± .45	44.5 ± 1.2	16.4 ± .4	4.75 ± .25	59.6 ± 1.7

To order, add material code to part number.

	A_L (mH/1000T) min					MAGNETIC DATA					
	POWER MATERIALS			HIGH PERMEABILITY MATERIALS							
PART	R	P	F*	J	W	l_e (mm)	A_e (mm^2)	A min (mm^2)	V_e (mm^3)	CORE WEIGHT (grams per set)	WaAc (cm^4)
0_43517EC	1,660	1,800	3,000	-	-	77.4	84.3	71	6,530	36	0.833
0_44119EC	2,605	2,400	3,700	-	-	89.3	121	106	10,800	52	1.67
0_45224EC	2,900	3,150	5,040	-	-	105	180	141	18,800	111	3.87
0_47035EC	3,310	3,600	5,760	-	-	144	279	211	40,100	253	13.4

* F material nominal ± 25%

Appendix C: American Wire Gauge (AWG) and Metric Wire Gauge Wire Sizes Table

AWG gauge	Diameter Inches	Diameter mm	Ohms per 1000 ft	Ohms per km	Max amps for chassis wiring	Max amps for power transmission
0000	0.4600	11.6840	0.0490	0.160720	380	302
000	0.4096	10.40384	0.0618	0.202704	328	239
00	0.3648	9.26592	0.0779	0.255512	283	190
0	0.3249	8.25246	0.0983	0.322424	245	150
1	0.2893	7.34822	0.1239	0.406392	211	119
2	0.2576	6.54304	0.1563	0.512664	181	94
3	0.2294	5.82676	0.1970	0.646160	158	75
4	0.2043	5.18922	0.2485	0.815080	135	60
5	0.1819	4.62026	0.3133	1.027624	118	47
6	0.1620	4.11480	0.3951	1.295928	101	37
7	0.1443	3.66522	0.4982	1.634096	89	30
8	0.1285	3.26390	0.6282	2.060496	73	24
9	0.1144	2.90576	0.7921	2.598088	64	19
10	0.1019	2.58826	0.9989	3.276392	55	15
11	0.0907	2.30378	1.2600	4.132800	47	12
12	0.0808	2.05232	1.5880	5.208640	41	9.3
13	0.0720	1.82880	2.0030	6.569840	35	7.4
14	0.0641	1.62814	2.5250	8.282000	32	5.9
15	0.0571	1.45034	3.1840	10.44352	28	4.7
16	0.0508	1.29032	4.0160	13.17248	22	3.7
17	0.0453	1.15062	5.0640	16.60992	19	2.9
18	0.0403	1.02362	6.3850	20.94280	16	2.3
19	0.0359	0.91186	8.0510	26.40728	14	1.8
20	0.0320	0.81280	10.150	33.29200	11	1.5
21	0.0285	0.72390	12.800	41.98400	9	1.2
22	0.0254	0.64516	16.140	52.93920	7	0.92
23	0.0226	0.57404	20.36	66.78080	4.7	0.729
24	0.0201	0.51054	25.67	84.19760	3.5	0.577
25	0.0179	0.45466	32.37	106.1736	2.7	0.457
26	0.0159	0.40386	40.81	133.8568	2.2	0.361
27	0.0142	0.36068	51.47	168.8216	1.7	0.288
28	0.0126	0.32004	64.9	212.8720	1.4	0.226
29	0.0113	0.28702	81.83	268.4024	1.2	0.182
30	0.0100	0.254	103.2	338.4960	0.86	0.142
31	0.0089	0.22606	130.1	426.7280	0.700	0.1130
32	0.0080	0.2032	164.1	538.2480	0.530	0.0910
Metric 2.0	0.00787	0.200	169.39	555.6100	0.510	0.0880
33	0.00710	0.18034	206.9	678.6320	0.430	0.0720
Metric 1.8	0.00709	0.18000	207.5	680.5500	0.430	0.0720
34	0.00630	0.16002	260.9	855.7520	0.330	0.0560
Metric 1.6	0.00630	0.16002	260.9	855.7520	0.330	0.0560
35	0.00560	0.14224	329.0	1079.120	0.270	0.0440
Metric 1.4	0.00551	0.14000	339.0	1114	0.260	0.0430
36	0.00500	0.12700	414.8	1360	0.210	0.0350
Metric 1.25	0.00492	0.12500	428.2	1404	0.200	0.0340
37	0.00450	0.11430	523.1	1715	0.170	0.0289
Metric 1.12	0.00441	0.11200	533.8	1750	0.163	0.0277
38	0.00400	0.10160	659.6	2163	0.130	0.0228
Metric 1.0	0.00394	0.10000	670.2	2198	0.126	0.0225
39	0.00350	0.08890	831.8	2728	0.110	0.0175
40	0.00310	0.07874	1049	3440	0.090	0.0137

Appendix D: Tabulated Designed Components Values

RATINGS OF THE POWER SEMICONDUCTOR SWITCHING DEVICES

SELECTION	COMPONENTS	DESIGNED VALUES	
FIRST STAGE BOOST DC-DC CONVERTER	MOSFET	Vpeak (V)	42V
		Irms (A)	239.10A
	DIODES	Vpeak (V)	60V
		Irms (A)	83.3A
SECOND STAGE DC-DC BOOST CONVERTER	MOSFET	Vpeak (V)	60V
		Irms (A)	42.21A
	DIODES	Vpeak (V)	600V
		Irms (A)	4.69A
DC-AC CONVERTER	IGBT	Vpeak (V)	410V
		Irms (A)	21.74A

RATINGS OF THE INPUT CAPACITOR

SELECTION	CURRENT DESIGNED VALUE	VOLTAGE DESIGNED VALUE	DESIGNED CAPACITANCE VALUE
CAPACITOR	79.34A	42V	22000μF

RATINGS OF THE HIGH VOLTAGE DC BUS CAPACITOR

SELECTION	CURRENT DESIGNED VALUE	VOLTAGE DESIGNED VALUE	DESIGNED CAPACITANCE VALUE
CAPACITOR	25.46A	410V	2315μF

RATINGS OF THE HIGH FREQUENCY TRANSFORMER

SELECTION	PRIMARY CURRENT DESIGNED VALUE	SECONDARY CYRRENT DESIGNED VALUE	POWER DESIGNED VALUE	EFFICIENCY
HIGH FREQUENCY TRANSFORMER	30A	3.125A	1.25 kW	> 90%